An overview of the petroleum systems of the northern deep-water Gulf of Mexico

Paul Weimer, Renaud Bouroullec, James Adson, and Stephen P. J. Cossey

ABSTRACT

The northern deep-water Gulf of Mexico is one of the most active deep-water petroleum provinces in the world. This paper introduces the regional geologic setting for the northern deep-water Gulf of Mexico and briefly discusses the importance of technology in developing the area's resources. Exploration has focused on four major geologic provinces: Basins, Subsalt, Fold Belt, and Abyssal Plain. These provinces formed from the complex interactions between Mesozoic–Cenozoic sedimentation and tectonics. Improved understanding of the geology of these provinces has largely been accomplished by improvements in seismic acquisition and processing. In addition, advances in drilling technology have permitted drilling and field development in increasingly greater water depths.

The 226 oil and gas fields and discoveries in the northern deep-water Gulf of Mexico are summarized in terms of their exploration and development history, producing facility, ages of reservoirs (Upper Jurassic, upper Paleocene–lower Eocene, Oligocene, lower Miocene–upper Pleistocene), and trap type (structural, combined structural-stratigraphic, and stratigraphic). In addition, the interpreted regional distribution of Upper Jurassic and possible Lower Cretaceous source, source rocks is shown, in part based on the 26 wells that have penetrated these source rocks.

The eight papers in this special issue review the geology of the Mississippi Canyon and northern Atwater Valley protraction areas. The first five papers review the subregional structural setting and the evolution of its tectonics and petroleum systems. The final three papers summarize the geologic evolution of two economically important intraslope basins—Thunder Horse and Mensa—in terms of their stratigraphy, structural evolution, and petroleum

Copyright ©2017. The American Association of Petroleum Geologists. All rights reserved.

Manuscript received October 18, 2008; provisional acceptance February 9, 2009; revised manuscript received May 14, 2015; revised manuscript provisional acceptance April 23, 2015; 2nd revised manuscript received May 5, 2015; final acceptance September 1, 2016.
DOI:10.1306/09011608136

AUTHORS

PAUL WEIMER ~ *Energy and Applied Minerals Research Center, Department of Geological Sciences, University of Colorado, Boulder, Colorado 80309; paul.weimer@colorado.edu*

Paul Weimer holds the Bruce D. Benson Endowed Chair in the Department of Geological Sciences at the University of Colorado and serves as the director of the Energy and Minerals Applied Research Center. His recent research activities include the study of the petroleum systems of deep-water margins, creating animations for public outreach, and co-chairing the 100th AAPG Anniversary Committee.

RENAUD BOUROULLEC ~ *Petroleum Geosciences, TNO, Princetonlaan 6, 3584 CB Utrecht, The Netherlands; renaud.bouroullec@tno.nl*

Renaud Bouroullec received his B.Sc. degree from the Université de Bretagne Occidentale, Brest, France (1994); his M.Sc. degree from the Université de Rennes 1, France (1996); and his Ph.D. from Imperial College, London (2001). After graduation, he conducted postdoctoral research at the Energy and Minerals Applied Research Center at the University of Colorado, Boulder, and then joined the Bureau of Economic Geology at The University of Texas at Austin, where he was principal investigator of the Laser-Assisted Analogs for Siliciclastic Reservoirs Consortium. He then joined the Chevron Center of Research Excellence, Department of Geology, Colorado School of Mines, as a research assistant professor. Currently, he is a senior researcher and Basin Analysis Team coordinator at TNO, the Netherlands Organisation for Applied Scientific Research.

JAMES ADSON ~ *Energy and Applied Minerals Research Center, Department of Geological Sciences, University of Colorado, Boulder, Colorado 80309; present address: Level 3 Communications, 1025 Eldorado Boulevard, Broomfield, Colorado 80021; james.adson@colorado.edu*

Jim Adson works as a senior Internet security analyst at Level 3 Communications. He received his B.A. from Temple University in

Tokyo in 2010 in Far East languages. He worked as an animator of Colorado geology from 2011 to 2016 at the Interactive Geology Project at the University of Colorado.

Stephen P. J. Cossey ~ *Cossey and Associates, Inc., P.O. Box 1510, Durango, Colorado 81302; cosseygeo@aol.com*

Stephen P. J. Cossey is a geologist with over 37 years of experience with Conoco (1978 to 1983) and with Sohio/BP (1983 to 1995). From 1990 to 1992, he was at BP Research in Sunbury, United Kingdom, and helped to start their deep-water research program. In 1995, he started the consulting company Cossey and Associates, Inc., specializing in the exploration, development, and modeling of deep-water clastic reservoirs, with emphasis on the Gulf of Mexico.

ACKNOWLEDGMENTS

We thank AAPG Editor Mike Sweet and past elected editors Gretchen Gillis and Steve Laubach for their support in assembling this issue. This *AAPG Bulletin* issue includes many of the research results from the University of Colorado Gulf of Mexico Research Consortium Phase III. Work was done from late 1999 to early 2005; 12 M.S. degrees were awarded for the research, and 3 research scientists were supported. Our sincerest thanks go to the following companies for their support and technical input: AEC, Agip, Amerada Hess, Anadarko, BP, Burlington, Chevron, Conoco, Devon, Dominion, Enterprise, ExxonMobil, Helis, Kerr McGee, Maersk, Marathon, Maxus, Murphy, Nexen, Norsk Hydro, Ocean Energy, Occidental, PanCanadian, Pemex, Petrobras, Phillips, Shell, Texaco, Total, Unocal, Vastar, and Woodside. Members of the sponsoring companies have given us input that has improved some of the interpretation.

We thank the following companies and individuals who made this study possible. Seismic data have been kindly provided by WesternGeco Geophysical (Jerry Peterson), now Schlumberger (Ian Bryant, Daniel Domeracki); PGS Geophysical (Mark Wilkinson); and TGS Geophysical (John Adamick). Bob Wentland was essential in helping to arrange the donation of some of these data sets. Software donations were from IHS (Petra, SMT), Landmark Graphics

systems. These two basins contain two of the larger oil and gas fields, respectively, in the northern deep-water Gulf of Mexico.

INTRODUCTION

The northern deep-water Gulf of Mexico (i.e., >457 m [1500 ft] water depth) is one of the most active deep-water areas in the world for petroleum exploration and development (Figure 1). The geology of the area is extremely complex, comprising a thick Cenozoic sedimentary fill (>15,000 m [50,000 ft]) and a structural setting including multilevel allochthonous salt systems, extensional and contractional faults, and large, salt-cored fold belts. In the early 1980s, only a few wells in this area had been drilled in water depths greater than 457 m (1500 ft); 30 yr later, there are 226 discoveries and fields in these depths (Tables 1–5).

The northern deep-water Gulf of Mexico is noteworthy for three reasons. First, its petroleum is an important part of the US energy supply. In 2015, the US Energy Information Administration predicted daily oil production of 1.52 million bbl, approximately 16% of the daily production in the United States (Yen, 2016). Production is expected to increase to approximately 1.9 million BOE/day by 2016 and then stay at that level for the next 5 yr (Beaubouef, 2015; Yen, 2016). Second, the northern deep-water Gulf of Mexico serves as a geologic analog to help us understand other deep-water basins. Third, its geologic complexity spurred many technological advances; workers have had to invent new techniques in seismic imaging, drilling, and development.

This theme issue of the *AAPG Bulletin* consists of eight papers that address the different components of the petroleum systems for one part of the northeastern deep-water Gulf of Mexico—specifically in the Mississippi Canyon and Atwater Valley protraction areas. This introductory paper is intended for geoscientists who are not familiar with the details of the northern Gulf of Mexico. We explain the advances in technology that have led to economic success. We also summarize the area's geology, exploration provinces, and exploration plays to give the regional context of the seven following papers that focus on the eastern part of the northern Gulf of Mexico.

IMPROVING TECHNOLOGY FOR EXPLORATION AND DEVELOPMENT

Drilling in Deep Water

Two geologic attributes found in the north-central deep-water Gulf of Mexico and only a few other deep-water basins create significant challenges in drilling. First, overpressured sediments

occur directly below the sea floor and continue downward in the shallow subsurface (Day-Stirrat et al., 2012). These shallow, overpressured sediments are likely caused by clay, specifically smectite (N. Braunsdorf, 2015, personal communication). Second, the sand-bearing, near-surface sedimentary section (upper 1000 m [3300 ft]) can be out of equilibrium with the surrounding overpressured muds. Undercompacted, near-surface sands, deposited late in the basin's history (in some cases during the past few tens of thousands of years), create flow problems during drilling (i.e., large volumes of water released into the well bore from overpressured sands, termed "shallow-water flow"). Other shallow drilling problems include overpressured gas-charged sands and near-surface faults. All of these shallow-subsurface drilling challenges, when identified, can often be avoided or at least mitigated.

Deep-water exploration and development have many challenges, which have been addressed by innovative drilling technology. These challenges include (1) routine drilling in water depths 458 to 3050 m (1650 to 10,000 ft) and beyond; (2) safely securing development platforms during hurricanes and storms; (3) adapting for high-velocity loop and eddy currents that induce vortex vibration and motion to marine risers; (4) near-surface drilling hazards; (5) drilling through thick, allochthonous salt masses (up to 3 km [9840 ft] thick) with unpredictable layers of enclosed nonsalt sediments; (6) abrupt and unpredictable pressure changes at the base of salt, which are extremely difficult to predict and remediate; (7) underpressured porous and permeable sands (i.e., thief zones), with a loss of circulation leading to a significant loss of drilling fluid; (8) high temperatures, high pressures, and low permeability in ultradeep reservoirs; and (9) biodegraded oil, creating asphaltenes and waxes that impede drilling circulation in pipes.

With successful exploration in increasing water depths, drilling and development facilities have evolved from simple jackup rigs to tension-leg platforms, floating production storage offloading units (FPSOs), floating platforms, and subsea tiebacks (Figure 2). The vast amount of drilling in the northern deep-water Gulf of Mexico has led to several record-breaking achievements for exploration and production (Figure 2). Exploration drilling is becoming more common in ultradeep water, where 40 fields and discoveries have been drilled in water depths greater than 2135 m (7000 ft) (Table 1). Long-distance subsea tiebacks, a technology first developed in the North Sea, are now common in some areas of the northern deep-water Gulf of Mexico; 143 of the 226 fields and discoveries are or will be produced by subsea tiebacks (Tables 2–5), and this technology will increasingly be used. The deepest subsea tieback is the Tobago field in 2945 m (9656 ft) of water for the Perdido SPAR hub in Alaminos Canyon; two separate fields have been tied back to one production facility (Figure 2; Table 4). With ongoing development, these water-depth records for development are broken every few years. The deepest water depth for

(Connie Johnson, Bill Keach), Paradigm (Duane Dopkins), and Platte River (China and Jay Leonard). Digital wire-line logs were donated from A2D (Bill Ross, Linda Santiago). Art Waterman (PaleoData, Inc.) kindly allowed the use of his proprietary biostratigraphic data. A special thanks to IHS and Pete Stark for creating the graph in Figure 23. Finally, we are indebted to Norman Rosen, executive director of the Gulf Coast Section SEPM Foundation; Kate Kipper, executive director of the Gulf Coast Association of Geological Societies; ION Geophysical; Springer-Verlag; and CGG (Mathhew Bognar) for their permission to reprint their figures.

The input from the following colleagues was absolutely essential to the completion of this paper: Jon Blickwede, Mary Broussard, Robin Broussard, Steve Burt, Andrew Cook, Richard Denne, Scott Douglas, Shirley Dutton, Mike Fauquier, Mike Fein, Chelsea Fenn, Ted Godo, Alfredo Guzman, Sverre Henricksen, Peter Etherman, Dan Huffman, Mike Jobe, Ian Kane, Jack Leedy, Ann Marchand, Tim McGinty, Alonso Navarro, Henry Pettingill, Andy Pulham, David Reiter, Toby Roesler, Kurt Rovang, Kris Schwendeman, Colin Stabler, Cheree Stover, John Wagner, Art Waterman, Paul Wieg, Larry Zarra, and Eric Zimmerman. To all of them, we express our sincerest gratitude.

The inclusion of two sections above was only possible with the input of Rick Lindsey, who patiently walked us through the discussion of seismic acquisition and processing, and Larry Zarra and Tim Diggs, who helped us summarize the reservoir quality accurately. For all three of them, 100,000 thanks.

We thank the following individuals for their careful reviews, which greatly improved the final content: Shirley Dutton, Laurie Lamar, Mike Leibovitz, Rick Lindsay, Robert Loucks, Ira Pasternak, David Sawyer, Kris Schwendeman, Craig Shipp, Derek Smalls, M. S. Wacker, and Larry Zarra. We alone are responsible for the interpretation presented here.

EDITOR'S NOTE

Color versions of Figures 1–24 can be seen in the online version of this paper.

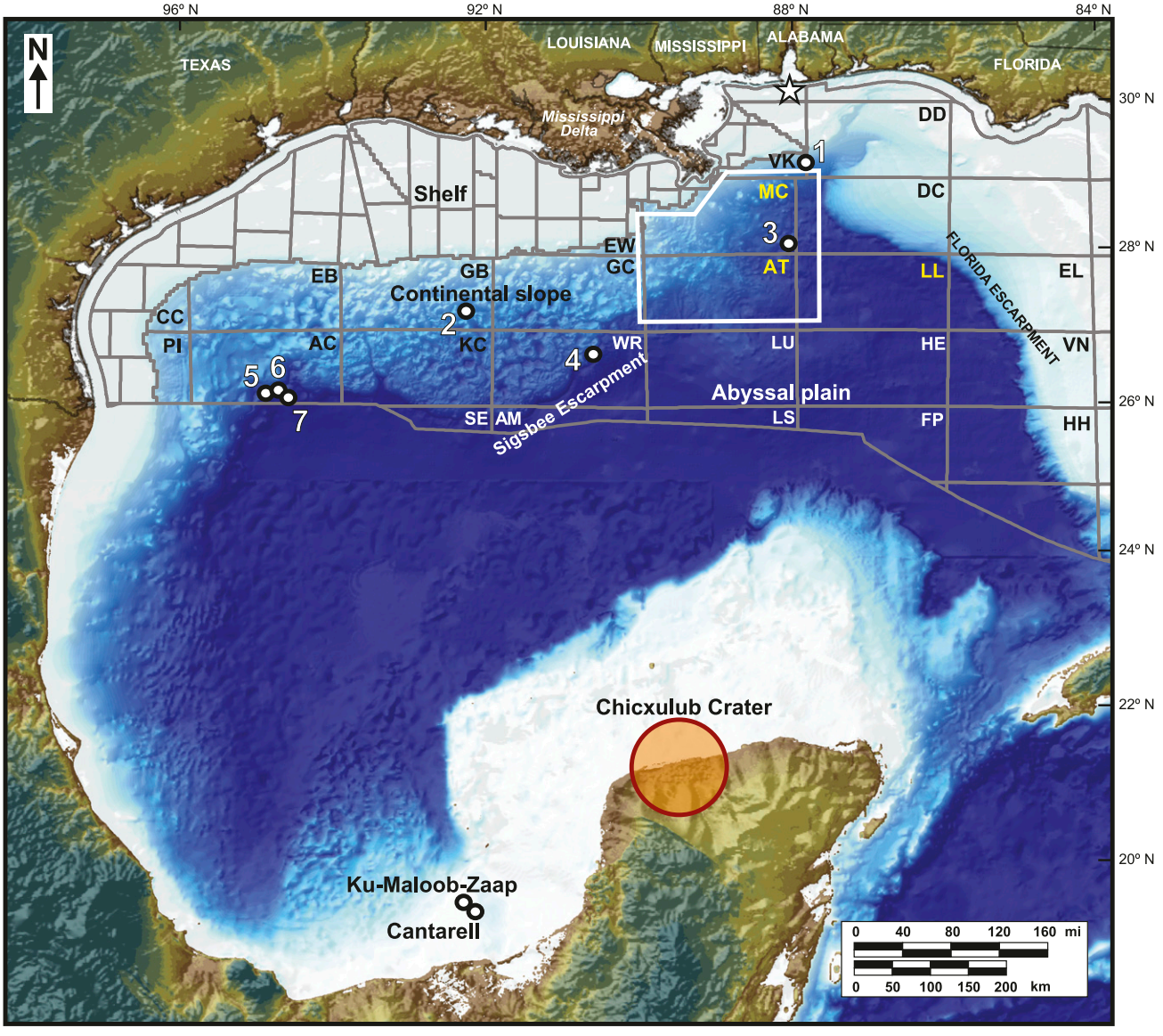

Figure 1. Regional shaded bathymetric map of the Gulf of Mexico, with protraction boundaries. Outline of study area is shown by a white polygon. Circles indicate wells discussed in the text and shown in Figure 2. The location of the Fairway field in Mobile Bay is shown by a white star. Locations of Chicxulub crater and the supergiant Cantarell and Ku-Maloob-Zaap fields are shown. Base map is courtesy of Trey Meckel and Wayne Clark. Abbreviations for protraction areas: AC = Alaminos Canyon; AM = Amery Terrace; AT = Atwater Valley; CC = Corpus Christi; DC = DeSoto Canyon; DD = Destin Dome; EB = East Breaks; EL = Elbow; EW = Ewing Bank; FP = Florida Plain; GB = Garden Banks; GC = Green Canyon; HE = Henderson; HH = Howell Hook; KC = Keathley Canyon; LL = Lloyd Ridge; LS = Lund South; LU = Lund; MC = Mississippi Canyon; PI = Post Isabel; SE = Sigsbee Escarpment; VK = Viosca Knoll; VN = Vernon; WR = Walker Ridge.

exploration drilling in the Gulf of Mexico was 3300 m (10,010 ft) in Alaminos Canyon 951 in 2003.

The technology for the new deep-water floating rigs (semisubmersible or drillship) has continued to improve to address the upcoming challenges. Many of the newest deep-water rigs have two independently operated drill floors on the rig (termed dual activity), with more capability to drill deeper, allowing a total drill-string length of 12,200 m (40,000 ft) in water depths up to 3660 m (12,000 ft). Although commonly used in many deep-water basins globally, only two FPSOs in the Gulf of Mexico have been used in the development of the Cascade and Chinook fields in Walker Ridge (8877 ft [2706 m]) and the Stones field (9576 ft [2919 m]) in Walker Ridge 508. These fields are also the deepest water for FPSOs in the world (Offshore Technology, 2015).

Table 1. Fields and Discoveries in Water Depths Greater Than 7000 ft (2134 m), Northern Deep-Water Gulf of Mexico

Field Number in Figure 5A	Field Name	Location Abbreviation	Discovery Year	Water Depth (ft [m])	Operator
216	Maximino DL	Mexico	2014	9984 (3043)	Pemex
203	Tobago	AC 859	2004	9636 (2937)	Shell
195	Stones	WR 508	2005	9576 (2919)	Shell
215	Maximino	Mexico	2012	9574 (2918)	Pemex
217	Supremus	Mexico	2013	9426 (2873)	Pemex
201	Silvertip	AC 815	2004	9356 (2852)	Shell
219	Cratos	Mexico	2015	9213 (2808)	Pemex
224	Atlas	LL 50	2003	9000 (2743)	Anadarko
226	Cheyenne	LL 399	2004	8987 (2739)	Anadarko
213	Chinook	WR 469	2003	8826 (2690)	Petrobras
223	Atlas NW	LL 5	2004	8810 (2685)	Anadarko
221	Jubilee	AT 349	2003	8800 (2682)	Anadarko
225	Jubilee Extension	LL 309	2005	8774 (2674)	Anadarko
189	Phobos	SE 39	2013	8500 (2591)	Anadarko
214	Exploratus	Mexico	2014	8488 (2587)	Pemex
220	Vortex	AT 261	2002	8340 (2542)	Anadarko
222	Mondo NW Extension	LL 1	2005	8340 (2542)	Anadarko
218	Trion	Mexico	2012	8304 (2531)	Pemex
212	Cascade	WR 206	2002	8203 (2500)	Petrobras
10	Spiderman	DC 621	2003	8100 (2469)	Anadarko
202	Great White	AC 857	2002	8009 (2441)	Shell
211	Q	MC 961	2005	7925 (2415)	Statoil
204	Merganser	AT 37	2002	7900 (2408)	Anadarko
9	San Jacinto	DC 618	2004	7850 (2393)	ENI
136	Callisto	MC 876	2001	7800 (2377)	Anadarko
200	Logan	WR 969	2011	7750 (2362)	Statoil
119	Na Kika–Coulomb	MC 657	1988	7600 (2316)	Shell
114	Rydberg	MC 525	2014	7479 (2279)	Shell
8	Vicksburg	DC 353	2007	7457 (2273)	Shell
122	Troubadour	MC 699	2013	7438 (2267)	Noble
169	Hadrian–Hadrian South	KC 919	2009	7425 (2263)	ExxonMobil
101	Appomattox	MC 392	2010	7290 (2222)	Shell
99	Camden Hills	MC 348	1999	7213 (2198)	ATP
121	Big Bend	MC 698	2012	7200 (2194)	Noble
168	Lucius	KC 875	2009	7100 (2164)	Anadarko
197	Julia	WR 627	2007	7087 (2159)	ExxonMobil
98	Aconcagua	MC 305	1999	7039 (2145)	ATP
112	Na Kika–Fourier	MC 522	1989	7000 (2134)	BP
118	Na Kika–East Anstey	MC 607	1998	7000 (2134)	BP
199	Jack	WR 759	2004	7000 (2134)	Chevron

Locations of fields are shown in Figures 5, 10, and 11.

Abbreviations: AC = Alaminos Canyon; AT = Atwater Valley; DC = DeSoto Canyon; KC = Keathley Canyon; LL = Lloyd Ridge; MC = Mississippi Canyon; SE = Sigsbee Escarpment; WR = Walker Ridge.

Table 2. Fields and Discoveries in Basins Province, Northern Deep-Water Gulf of Mexico

Field Number	Field Name	Location Abbreviation	Discovery Year	Water Depth (ft [m])	Operator	Status	Onstream	Production Type	Age of Reservoir	Trap Type(s)
1	Madison	AC 24	1998	4854 (1479)	ExxonMobil	Producing	2002	SS	l. Pliocene	Three-way closure against salt flank
2	Hoover	AC 25	1997	4806 (1465)	ExxonMobil	Producing	2000	SPAR	l. Pliocene	Four-way closure (compactional drape)
3	Diana South	AC 65	1996	4679 (1426)	ExxonMobil	Abandoned, 2015	2000	SS	l. Pliocene	Three-way closure against salt flank
4	Dalmatian North	DC 4	2008	5876 (1791)	Murphy	Producing	2014	SS	m. Miocene	Stratigraphic
5	Dalmatian	DC 48	2008	5876 (1791)	Murphy	Producing	2014	SS	m. Miocene	Stratigraphic
6	Dalmatian South	DC 134	2012	6394 (1949)	Murphy		2016	SS	l. Miocene	Stratigraphic
7	Shiloh	DC 269	2003	7509 (2289)	Shell	Appraisal	Projected 2020	SS	L. Jurassic	Three-way closure against salt flank
8	Vicksburg	DC 353	2007	7457 (2273)	Shell	Appraisal	Projected 2020	SS	L. Jurassic	Three-way closure against salt flank
9	San Jacinto	DC 618	2004	7850 (2393)	ENI	Abandoned, 2011	2007	SS	l. Miocene	Four-way closure (compactional drape)
10	Spiderman	DC 621	2003	8100 (2469)	Anadarko	Abandoned, 2015	2007	SS	l. Miocene	Four-way closure (compactional drape)
11	Lost Ark	EB 421	2001	2740 (1749)	Noble	Abandoned, 2009	2002	SS	l. Pliocene	Three-way closure against fault–stratigraphic
12	SW Horseshoe	EB 430	2000	2285 (696)	Walter	Producing	2005	SS	l. Pliocene	Three-way closure against fault
13	Balboa	EB 597	2001	3373 (1028)	Apache	Producing	2010	SS	l. Pliocene	Two-way closure between faults–onlap
14	North Boomvang	EB 599	2001	3153 (961)	Anadarko	Producing	2007	SS	l. Pliocene–e. Pleistocene	Three-way closure against fault
15	Nansen	EB 602	1999	3686 (1123)	Anadarko	Producing	2002	SPAR	l. Pliocene–e. Pleistocene	Three-way closure against fault
16	Tomahawk	EB 623	2003	3514 (1071)	Marubeni	Producing	2004	SS	m. Miocene	Three-way fault closure against fault–stratigraphic
17	Boomvang	EB 643	1997	3539 (1079)	Anadarko	Producing	2002	SPAR	l. Pliocene–e. Pleistocene	Faulted high over salt ridge

(*continued*)

Table 2. Continued

Field Number	Field Name	Location Abbreviation	Discovery Year	Water Depth (ft [m])	Operator	Status	Onstream	Production Type	Age of Reservoir	Trap Type(s)
18	Navajo–Northwest	EB 646	2001	4114 (1254)	Anadarko	Producing	2002	SS	l. Pliocene–e. Pleistocene	Three-way closure against fault
19	Diana	EB 945	1990	4670 (1423)	ExxonMobil	Abandoned, 2015	2000	SS	l. Pliocene	Three-way closure against salt flank–stratigraphic
20	Marshall	EB 949	1998	4376 (1334)	ExxonMobil	Producing	2001	SS	e. Pliocene	Three-way closure against salt flank–stratigraphic
21	Rockefeller	EB 992	1996	4872 (1424)	ExxonMobil	Abandoned 2015	2009	SS	e. Pliocene	Four-way closure (compactional drape)
22	Ewing Bank 878	EW 878	2000	1523 (464)	Walter	Producing	2001	SS	e. Pliocene	Three-way closure against fault
23	Morpeth–Klamath	EW 921	1992	1747 (532)	ENI	Producing	1998	TLP	l. Miocene–e. Pliocene	Three-way closure against fault–stratigraphic
24	Prince	EW 958	1994	1502 (457)	Enven	Producing	2001	SS	e. Pliocene	Stratigraphic
25	Arnold	EW 963	1996	1752 (534)	Marathon	Producing	1998	SS	e. Pleistocene	Three-way closure against fault
26	Black Widow	EW 966	1998	1840 (560)	Apache	Producing	2000	SS	e. Pleistocene	Three-way closure fault–dip
27	Manta Ray	EW 1006	2003	1854 (565)	Walter	Abandoned, 2003	1999	SS	e. Pleistocene	Three-way closure against salt flank
28	Northwestern	GB 200	1998	1750 (533)	Hess	Producing	2000	SS	l. Pliocene–e. Pleistocene	Three-way closure against salt flank
29	Cottonwood	GB 244	2001	2000 (610)	Petrobras	Producing	2007	SS	e. Pliocene	Three-way closure against fault
30	Power Play	GB 258–302	2006	2310 (704)	W&T	Producing	2008	SS	l. Pliocene	Three-way closure against salt–fault
31	Baldpate	GB 260	1991	1650 (502)	Hess	Producing	1998	FP	e. Pliocene–e. Pleistocene	Three-way closure against salt
32	Pyrenees	GB 293	2009	2100 (640)	W&T	Abandoned, 2015	2012	SS	e. Pliocene	Three-way closure against salt
33	Sargent	GB 339	2008	2240 (683)	Deep Gulf Energy	Producing	2010	SS	l. Pleistocene	Stratigraphic
34	Habanero	GB 341	1999	2001 (610)	Shell	Producing	2003	SS	e. Pliocene	Three-way closure against salt

(*continued*)

Table 2. Continued

Field Number	Field Name	Location Abbreviation	Discovery Year	Water Depth (ft [m])	Operator	Status	Onstream	Production Type	Age of Reservoir	Trap Type(s)
35	Llano	GB 386	1989	2294 (699)	Shell	Producing	2004	SS	l. Miocene–e. Pliocene	Three-way closure against salt
36	Auger	GB 426	1987	2863 (873)	Shell	Producing	1994	TLP	e. Pliocene–e. Pleistocene	Three-way closure against fault–stratigraphic
37	Cardamom	GB 427	1995	2873 (876)	Shell	Producing	2014	SS	l. Pliocene–e. Pleistocene	Three-way closure against fault–stratigraphic
38	Geauxpher–Noonan	GB 462–506	2008	2820 (859)	ERT	Producing	2009	SS	e. Pleistocene	Three-way closure against fault
39	Bushwood	GB 463	2009	2700 (823)	Apache	Appraisal	Projected 2017		e. Pleistocene	Three-way closure against fault
40	Danny	GB 506	2007	2700 (823)	ERT	Producing	2010	SS	e. Pliocene	Three-way closure against fault
41	Ozona Deep	GB 515	2001	3280 (999)	Marathon	Development	Projected 2017	SS	l. Miocene	Three-way closure against salt flank
42	Serrano	GB 516	1996	3400 (1036)	Shell	Abandoned, 2004	2001	SS	e. Pliocene–e. Pleistocene	Stratigraphic
43	Oregano	GB 559	1999	3400 (1036)	Shell	Producing	2001	SS	e. Pliocene–e. Pleistocene	Three-way closure against fault–stratigraphic
44	Macaroni	GB 602	1995	3700 (1128)	Shell	Producing	1999	SS	e. Pliocene–e. Pleistocene	Three-way closure against fault–stratigraphic
45	Winter	GB 605	2009	3400 (1036)	W&T	Appraisal			l. Pleistocene	Stratigraphic
46	Dawson Deep	GB 625	2004	2900 (884)	Anadarko	Producing	2006	SS	l. Pliocene–e. Pleistocene	Faulted closure against salt overhang
47	Durango	GB 667	2001	3150 (960)	Anadarko	Producing	2004	SS	e. Pleistocene	Three-way closure against salt flank–fault–stratigraphic
48	Gunnison	GB 668	2000	3131 (954)	Anadarko	Producing	2003	SPAR	e. Pleistocene	Three-way closure against salt flank–fault–stratigraphic
49	Dawson	GB 669	2001	3000 (914)	Anadarko	Producing	2004	SS	e. Pleistocene	Three-way closure against salt flank–fault–stratigraphic

(*continued*)

Table 2. Continued

Field Number	Field Name	Location Abbreviation	Discovery Year	Water Depth (ft [m])	Operator	Status	Onstream	Production Type	Age of Reservoir	Trap Type(s)
50	Magnolia	GB 783	1999	4700 (1432)	ConocoPhillips	Producing	2004	TLP	e. Pleistocene	Three-way closure against fault–stratigraphic
51	Katmai	GC 40	2014	2100 (640)	Noble	Appraisal			e.–m. Miocene	Four-way closure against faults
52	Rocky	GC 110	1987	1785 (544)	Marubeni	Producing	1995	SS	l. Pliocene?	Three-way closure against salt flank
53	Angus	GC 113	1997	2000 (610)	Marubeni	Producing	1999	SS	e. Pleistocene	Three-way closure against salt flank
54	Popeye	GC 116	1985	2067 (630)	Shell	Producing	1996	SS	e. Pleistocene	Three-way closure against fault
55	Manatee	GC 155	1998	1940 (591)	Marubeni	Producing	2002	SS	l. Pliocene	Three-way closure against salt–stratigraphic
56	Brutus–Ru	GC 158	1989	2985 (910)	Shell	Producing	2001	TLP	l. Pliocene–e. Pleistocene	Three-way closure against salt–fault–stratigraphic
57	Jolliet	GC 184	1981	1750 (533)	MC Offshore	Producing	1989	TLP	Pleistocene	Three-way closure against fault
58	Lorien	GC 199	2003	2179 (664)	Noble	Producing	2006	SS	l. Miocene	Stratigraphic
59	Genesis	GC 205	1988	2628 (801)	Chevron	Producing	1999	FPS	e. Pleistocene	Three-way closure against salt–stratigraphic
60	Phoenix	GC 236	1998	1969 (600)	Helix (ERT)	Producing	2010	FPU	e. Pliocene	Three-way closure against salt flank
61	Aspen	GC 243	2001	3063 (934)	Walter	Producing	2002	SS	l. Miocene	Three-way closure against salt weld
62	Droshky	GC 244	2007	2900 (884)	Marathon	Producing	2010	SS	l. Miocene	Three-way structural-stratigraphic against salt
63	Troika–Wasatch	GC 244	1994	2679 (816)	Marathon	Producing	1997	SS	e. Pliocene	Three-way closure against salt flank
64	Glider	GC 248	1996	3300 (1006)	Shell	Producing	2004	SS	Pliocene	Three-way pinchout against salt–stratigraphic faults
65	Allegheny	GC 254	1992	3225 (983)	ENI	Producing	1999	TLP	e. Pliocene	Three-way closure against fault–weld

(*continued*)

Table 2. Continued

Field Number	Field Name	Location Abbreviation	Discovery Year	Water Depth (ft [m])	Operator	Status	Onstream	Production Type	Age of Reservoir	Trap Type(s)
66	Allegheny South	GC 298	2005	3280 (999)	ENI	Producing	2005	SS	l. Pliocene–e. Pleistocene	Three-way closure against salt–stratigraphic
67	Clipper	GC 300	2005	3452 (1052)	Bennu	Producing	2013	SS	e. Pleistocene	Three-way closure against salt–stratigraphic
68	Front Runner	GC 338	2000	3500 (1067)	Murphy	Producing	2004	SPAR	Pliocene	Three-way closure against salt–stratigraphic
69	Front Runner South	GC 339	2001	3500 (1067)	Murphy	Producing	2005	SS	Pliocene	Three-way closure against fault–stratigraphic
70	Quatrain	GC 382	2002	3500 (1067)	Murphy	Producing	2005	SS	Pliocene	Three-way closure against fault–stratigraphic
71	Pegasus	GC 385	2005	3491 (1064)	ENI	Producing	2008	SS	e. Pleistocene	Three-way closure against fault–stratigraphic
72	Samurai	GC 432	2009	3400 (1036)	Murphy	Appraisal			e.–m. Miocene	Four-way closure (faulted)
73	Condor	GC 448	2008	3266 (995)	Deep Gulf Energy	Producing	2011	SS	e. Pleistocene	Three-way closure against salt–faults
74	King Kong	GC 472	1989	3799 (1158)	ENI	Abandoned, 2005	2002	SS	e. Pliocene	Three-way closure against fault
75	Wide Berth	GC 490	2009	3700 (1128)	Apache	Producing	2012		e. Pleistocene	Two-way fault–stratigraphic–dip
76	Ness Deep	GC 507	2001	3950 (1204)	Hess	Appraisal		SS	l. Miocene	Three-way closure against salt weld
77	Yosemite	GC 516	2001	4452 (1357)	ENI	Abandoned, 2012	2002	SS	l. Pliocene	Three-way closure against fault–stratigraphic
78	K2 North–K2	GC 518–562	2004	4000 (1219)	Anadarko	Producing	2006	SS	e.–m. Miocene	Three-way closure against salt–stratigraphic
79	Marco Polo	GC 608	2000	4300 (1311)	Anadarko	Producing	2004	TLP	Pliocene	Three-way closure against fault–salt flank
80	Holstein	GC 644	1999	4292 (1308)	Plains E&P	Producing	2004	SPAR	l. Pliocene to e. Pleistocene	Three-way closure against faults–stratigraphic
81	Daniel Boone	GC 646	2004	4230 (1289)	W&T	Abandoned, 2015	2009	SS	Pliocene	Three-way closure against fault–salt flank

(*continued*)

Table 2. Continued

Field Number	Field Name	Location Abbreviation	Discovery Year	Water Depth (ft [m])	Operator	Status	Onstream	Production Type	Age of Reservoir	Trap Type(s)
82	Constitution	GC 680	2003	5100 (1554)	Anadarko	Producing	2006	SPAR	e. Pliocene–l. Pliocene	Three-way closure against salt–fault
83	Ticonderoga	GC 768	2004	5250 (1600)	Anadarko	Producing	2006	SS	e. Pliocene-l. Pliocene	Three-way closure against salt–fault
84	Pompano II	MC 28	1986	1864 (568)	Stone	Producing	1996	SS	l. Miocene–Pliocene	Three-way closure against fault and stratigraphic traps
85	Cardona–Cardona South	MC 29	2014	2135 (651)	Stone	Producing	2014	SS	l. Miocene	Three-way closure against salt flank
86	Mississippi Canyon 72	MC 72	2008	2013 (613)	LLOG	Producing	2009	SS	l. Miocene	Stratigraphic
87	Otis	MC 79	2014	3950 (1204)	LLOG	Producing	2016	SS	l. Miocene	Stratigraphic
88	King–King West	MC 84	1993	5386 (1642)	BP	Producing	2002	SS	l. Miocene	Three-way closure against fault
89	Horn Mountain	MC 126	1999	5400 (1646)	Plains E&P	Producing	2002	SPAR	l. Miocene	Three-way closure against fault
90	Mississippi Canyon 161	MC 161	2005	2924 (800)	Stone	Producing	2008	SS	e. Pliocene	Three-way closure against fault
91	Mandy	MC 199	2010	2096 (639)	LLOG	Producing	2012	SS	e. Pliocene	Four-way closure against fault
92	King's Peak 1	MC 217	1992	6541 (1994)	BP	Producing	2002	SS	l. Miocene	Stratigraphic
93	Matterhorn	MC 243	1991	2862 (872)	W&T	Producing	2003	TLP	e. Pliocene	Three-way closure along salt flank
94	Rigel	MC 252	1999	5200 (1585)	ENI	Abandoned, 2011	2006	SS	l. Miocene	Stratigraphic
95	Neidermeyer	MC 253	2013	3400 (1036)	LLOG	Producing	2015	SS	m. Miocene	Four-way closure (extensional–turtle)
96	Seventeen Hands	MC 299	2000	5400 (1646)	ENI	Abandoned, 2011	2006	SS	l. Miocene	Stratigraphic
97	Marmalard	MC 300	2012	5781 (1762)	LLOG	Producing	2015	SS	m. Miocene	Three-way closure against fault
98	Aconcagua	MC 305	1999	7039 (2145)	ATP	Abandoned, 2013	2002	SS	l. Miocene	Three-way closure against fault

(*continued*)

Table 2. Continued

Field Number	Field Name	Location Abbreviation	Discovery Year	Water Depth (ft [m])	Operator	Status	Onstream	Production Type	Age of Reservoir	Trap Type(s)
99	Camden Hills	MC 348	1999	7213 (2198)	ATP	Abandoned, 2010	2002	SS	l. Miocene	Stratigraphic
100	Na Kika–Kepler	MC 383	1987	5800 (1768)	BP	Producing	2004	SS	l. Miocene	Stratigraphic
101	Appomattox	MC 392	2010	7290 (2222)	Shell	Appraisal	Projected 2020	SS	L. Jurassic	Three-way closure against fault
102	La Femme	MC 427	2004	5800 (1768)	LLOG	Appraisal			l. Miocene	Stratigraphic
103	Na Kika–Ariel	MC 429	1995	6200 (1890)	BP	Producing	2004	SS	l. Miocene	Stratigraphic
104	Son of Bluto II	MC 431	2012	5013 (1528)	LLOG	Producing	2015	SS	l. Miocene	Stratigraphic
105	Appaloosa	MC 459	2008	2500 (762)	ENI	Producing	2011	SS	l. Pliocene	Three-way closure against salt flank
106	Zia	MC 496	1997	1800 (549)	Marubeni	Producing	2003	SS	l. Miocene	Three-way closure against fault–stratigraphic
107	Longhorn	MC 502–546	2006	2461 (750)	ENI	Producing	2009	SS	e. Pliocene	Four-way closure against fault
108	Who Dat	MC 503	2007	3099 (944)	LLOG	Producing	2011	FPS	l. Miocene–e. Pliocene	Three-way closure against salt flank
109	Wrigley	MC 506	2005	3700 (1128)	W&T	Producing	2007	SS	l. Miocene	Stratigraphic
110	Santiago-Santa Cruz	MC 519–563	2011	6500 (1981)	Noble	Producing	2012	SS	m. Miocene	Three-way closure against fault
111	Na Kika–Herschel	MC 520	1997	6800 (2073)	BP	Producing	2004	SS	l. Miocene	Three-way closure against fault
112	Na Kika–Fourier	MC 522	1989	7000 (2134)	BP	Producing	2004	SS	l. Miocene	Stratigraphic
113	Rydberg	MC 525	2014	7479 (2279)	Shell	Appraisal	Projected 2020	SS	L. Jurassic	Three-way closure against fault
114	Medusa North	MC 538	2003	2185 (666)	Murphy	Producing	2005	SS	e. Pliocene	Three-way closure against salt flank
115	Isabela	MC 562	2007	6500 (1981)	BP	Producing	2012	SS	m. Miocene	Four-way dosure against fault
116	Medusa	MC 582	1999	2125 (648)	Murphy	Producing	2002	SPAR	e. Pliocene	Three-way closure against salt flank
117	Ulysses	MC 583	2002	2487 (758)	ENI	Producing	2005	SS	e. Pliocene	Stratigraphic
118	Na Kika–East Anstey	MC 607	1998	7000 (2134)	BP	Abandoned, 2010	2004	SS	l. Miocene	Three-way closure against salt flank

(*continued*)

Table 2. Continued

Field Number	Field Name	Location Abbreviation	Discovery Year	Water Depth (ft [m])	Operator	Status	Onstream	Production Type	Age of Reservoir	Trap Type(s)
119	Na Kika–Coulomb	MC 657	1988	7600 (2316)	Shell	Producing	2004	SS	m. Miocene	Three-way closure against salt flank
120	Blind Faith	MC 696	2001	6900 (2103)	Chevron	Producing	2008	Semi	m. Miocene	Four-way closure (extensional–turtle)
121	Big Bend	MC 698	2012	7200 (2194)	Noble	Producing	2015	SS	m. Miocene	Three-way closure against salt flank
122	Troubadour	MC 699	2013	7438 (2267)	Noble	Appraisal	Projected 2017		l. Miocene	Stratigraphic
123	Biddy Ball	MC 705	1999	1000 (305)	LLOG	Producing	Restart–2015	SS	l. Pleistocene	Three-way closure against fault
124	Valley Forge	MC 707	2004	1538 (469)	LLOG	Producing	2008	SS	e. Pliocene	Three-way closure against salt flank
125	Pluto–BS&T	MC 718	1995	2748 (837)	Mariner	Abandoned, 2008	1999	SS	m. Miocene	Three-way closure against fault
126	Mensa	MC 731	1986	5300 (1615)	Shell	Producing	2000	SS	l. Miocene	Four-way closure (faulted)
127	Goose	MC 751	2003	1548 (472)	LLOG	Producing	Restart–2015	SS	e. Pliocene	Three-way closure against salt flank
128	Anduin West	MC 754	2008	2696 (822)	ATP	Abandoned, 2012	2010	SS	l. Miocene	Three-way closure against fault
129	Anduin	MC 755	2005	2400 (731)	ATP	Abandoned, 2013	2007	SS	l. Miocene	Three-way closure against fault
130	Goldfinger	MC 771	2004	5423 (1653)	ENI	Producing	2005	SS	l. Miocene	Stratigraphic
131	Triton	MC 772	2002	5610 (1710)	ENI	Producing	2005	SS	l. Miocene–e. Pliocene	Three-way closure against fault
132	Devils Tower	MC 773	1999	5607 (1709)	ENI	Producing	2004	SPAR	l. Miocene–e. Pliocene	Three-way closure against salt flank
133	Dantzler	MC 782	2013	6613 (2016)	Noble	Producing	2015	SS	l. Miocene	Three-way closure against salt flank
134	Gladden	MC 800	2008	3116 (950)	LLOG	Producing	2011	SS	e. Pliocene	Three-way closure against salt flank
135	Mississippi Canyon 837	MC 837	2001	1520 (463)	Walter	Producing	2003	SS	e. Pleistocene	Three-way closure against fault

(*continued*)

Table 2. Continued

Field Number	Field Name	Location Abbreviation	Discovery Year	Water Depth (ft [m])	Operator	Status	Onstream	Production Type	Age of Reservoir	Trap Type(s)
136	Callisto	MC 876	2001	7800 (2377)	Anadarko	Abandoned, 2015	2007	SS	l. Miocene	Three-way closure against fault
137	Europa	MC 935	1994	3900 (1189)	Shell	Producing	2000	SS	l. Miocene–e. Pliocene	Three-way closure against salt flank
138	Tahoe–SE Tahoe	VK 783–827	1984	1500 (457)	W&T	Producing	1994	SS	m. Miocene	Three-way closure against fault
139	Petronius	VK 786	1995	1754 (535)	Chevron	Producing	2000	CT	m. Miocene	Three-way closure against fault
140	Neptune–Thor	VK 826	1984	1866 (569)	Anadarko	Producing	1997	SPAR	m. Miocene	Three-way closure against fault
141	Perseus	VK 830	2003	3376 (1029)	Chevron	Producing	2005	DT	m. Miocene	Stratigraphic
142	Einset	VK 873	1998	3500 (1067)	Shell	Producing	2002	SS	l. Miocene	Stratigraphic
143	Nile	VK 914	1997	3534 (1077)	BP	Producing	2001	SS	m. Miocene	Stratigraphic
144	Dorado	VK 915	2002	4023 (1226)	BP	Producing	2009	SS	m. Miocene	Four-way closure over salt (compactional drape)
145	Marlin	VK 915	1993	3384 (1031)	Plains E&P	Producing	1999	TLP	m. Miocene	Four-way closure over salt (compactional drape)
146	South Dorado	VK 915	2003	3494 (1065)	BP	Producing	2004	SS	m. Miocene	Four-way closure over salt (compactional drape)
147	Ram–Powell	VK 956	1985	3214 (980)	Shell	Producing	1997	TLP	m. Miocene	Stratigraphic
148	Swordfish	VK 961	2001	4677 (1425)	Noble	Producing	2005	SS	m. Miocene	Stratigraphic
149	Fastball	VK 1003	1999	3000 (914)	W&T	Abandoned, 2014	2009	SS	m. Miocene	Three-way closure against fault–stratigraphic

Locations of fields are shown in Figures 5, 10, and 11.

Location abbreviations: AC = Alaminos Canyon; DC = DeSoto Canyon; EB = East Breaks; EW = Ewing Bank; GB = Garden Banks; GC = Green Canyon; MC = Mississippi Canyon; VK = Viosca Knoll. Production type abbreviations: CT = compliant tower; DT = dry tree; FP = floating production; FPS = floating production storage; FPU = floating production unit; Semi = semisubmersible; SS = subsea tieback; TLP = tension leg platform. Age of reservoir abbreviations: e. = early; l./L. = late/Late; m. = middle.

Table 3. Fields and Discoveries in the Subsalt Province, Northern Deep-Water Gulf of Mexico

Field Number	Field Name	Location Abbreviation	Discovery Year	Water Depth (ft [m])	Operator	Status	Onstream	Production Type	Age of Reservoir	Trap Type(s)
150	Telemark	AT 63	2000	4385 (1336)	Bennu	Development	2010	MinDOC	e.–m. Miocene	Three-way closure against base of salt
151	North Platte	GB 959	2012	4871 (1485)	Cobalt	Appraisal			l. Paleocene–e. Eocene	Four-way closure (contractional fold)
152	Boris	GC 282	2001	2393 (729)	ERT	Producing	2003	SS	e. Pliocene	Three-way closure against base of salt
153	Stampede	GC 468	2005	3440 (1048)	Hess	Development	Projected 2018	TLP	m. Miocene	Four-way closure (extensional fold–turtle)
154	Tahiti	GC 640	2002	4017 (1224)	Chevron	Producing	2009	SPAR	e.–m. Miocene	Three-way closure against base of salt
155	Holstein Deep	GC 643	2006	3830 (1167)	Plains E&P	Producing	2016	FPS	e. Miocene	Three-way closure against base of salt
156	Genghis Khan	GC 652	2005	4300 (1311)	BHP Billiton	Producing	2007	SS	e.–m. Miocene	Three-way closure against base of salt
157	West Tonga–Caesar	GC 726	2007	4700 (1432)	Anadarko	Producing	2012	SS	m. Miocene	Three-way closure against base of salt
158	Anchor	GC 807	2014	5183 (1580)	Chevron	Appraisal			l. Paleocene–e. Eocene	Three-way closure against base of salt
159	Heidelberg	GC 903	2009	5000 (1524)	Anadarko	Producing	2016		m. Miocene	Three-way closure against base of salt
160	Guadalupe	KC 10	2014	3992 (1217)	Chevron	Appraisal			l. Paleocene–e. Eocene	Four-way closure (contractional fold)
161	Gila	KC 93	2013	4900 (1493)	BP	Appraisal			l. Paleocene–e. Eocene	Four-way closure (contractional fold)
162	Tiber	KC 102	2009	4155 (1266)	BP	Appraisal			l. Paleocene–e. Eocene	Four-way closure (contractional fold)
163	Kaskida	KC 292	2006	5860 (1786)	BP	Appraisal		FPS	l. Paleocene–e. Eocene	Three-way closure against base of salt
164	Leon	KC 642	2014	6117 (1864)	Repsol	Appraisal			l. Paleocene–e. Eocene	Four-way closure (contractional fold)
165	Moccasin	KC 736	2011	6739 (2054)	Chevron	Appraisal			l. Paleocene–e. Eocene	Four-way closure (contractional fold)

(*continued*)

Table 3. Continued

Field Number	Field Name	Location Abbreviation	Discovery Year	Water Depth (ft [m])	Operator	Status	Onstream	Production Type	Age of Reservoir	Trap Type(s)
166	Sicily	KC 814	2015	6716 (2047)	Chevron	Appraisal			l. Paleocene–e. Eocene	Four-way closure (contractional fold)
167	Buckskin	KC 872	2009	6920 (2109)	Chevron	Appraisal			l. Paleocene–e. Eocene	Four-way closure (contractional fold)
168	Lucius	KC 875	2009	7100 (2164)	Anadarko	Producing	2015	SPAR	l. Miocene–e. Pliocene	Three-way closure against salt keel
169	Hadrian–Hadrian South	KC 919	2009	7425 (2263)	ExxonMobil	Producing	2015	SS	l. Miocene–e. Pliocene	Three-way closure against salt keel
170	Mica–Mickey	MC 211	1990	4314 (1315)	ExxonMobil	Producing	2001	SS	l. Miocene	Four-way closure (fault bounded)
171	Raton–Raton South–Gemini	MC 248–292	2006	3400 (1036)	Noble	Producing	2008	SS	l. Miocene	Stratigraphic
172	Tubular Bells	MC 725	2003	4300 (1311)	Hess	Producing	2014	FPS	m. Miocene	Three-way closure against base of salt
173	Thunder Hawk	MC 734	2004	5724 (1745)	Murphy	Producing	2009	Semi	m. Miocene	Three-way closure against base of salt
174	West Boreas	MC 762	2004	3112 (948)	Shell	Producing	2014	SS	l. Miocene	Three-way closure against base of salt
175	King	MC 764	1997	2940 (896)	Shell	Producing	2000	SS	l. Miocene	Three-way closure against base of salt
176	Princess	MC 765	2000	3650 (1112)	Shell	Producing	2002	SS	l. Miocene	Three-way closure against base of salt
177	Kodiak	MC 771	2008	5000 (1524)	Deep Gulf Energy II	Producing	2016	SS	m. Miocene	Four-way closure (extensional fold–turtle)
178	Thunder Horse North	MC 776	2000	5640 (1719)	BP	Producing	2009	SS	m. Miocene	Three-way closure against base of salt
179	Thunder Horse	MC 778	1999	6103 (1860)	BP	Producing	2008	Semi	m. Miocene	Four-way closure (extensional fold–turtle)
180	Deimos	MC 806	2002	3000 (914)	Shell	Producing	2005	SS	m.–l. Miocene	Three-way closure against fault
181	Mars	MC 807	1989	2990 (911)	Shell	Producing	1996	TLP	l. Miocene	Three-way closure against base of salt

(*continued*)

Table 3. Continued

Field Number	Field Name	Location Abbreviation	Discovery Year	Water Depth (ft [m])	Operator	Status	Onstream	Production Type	Age of Reservoir	Trap Type(s)
182	Ursa	MC 810	1991	3800 (1158)	Shell	Producing	1999	TLP	l. Miocene	Three-way closure against base of salt
183	Crosby	MC 899	1997	4400 (1341)	Shell	Producing	2001	SS	l. Miocene	Three-way closure against base of salt
184	Mirage	MC 941	1991	3914 (1193)	Bennu	Producing	2010	MinDOC	m. Miocene	Three-way closure against base of salt
185	Morgus	MC 942	1999	3937 (1200)	Bennu	Producing	2012	SS	m. Miocene	Three-way closure against base of salt
186	Gunflint	MC 948	2008	6100 (1859)	Noble	Appraisal	2016	SS	m. Miocene	Four-way closure (extensional fold–turtle)
187	Vito	MC 984	2009	4038 (1231)	Shell	Appraisal			e. Miocene	Four-way closure (extensional fold–turtle)
188	Power Nap	MC 986	2015	4200 (1280)	Shell	Appraisal			e. Miocene	Three-way closure against base of salt
189	Phobos	SE 39	2013	8500 (2591)	Anadarko	Appraisal			l. Paleocene–e. Eocene	Four-way closure (contractional fold)
190	Big Foot	WR 29	2005	5330 (1624)	Chevron	Producing	2015	TLP	l. Paleocene–e. Eocene-m. Miocene	Three-way closure against base of salt
191	Shenandoah	WR 52	2009	5750 (1753)	Anadarko	Appraisal			l. Paleocene–e. Eocene	Four-way closure against salt keel
192	Yucatan	WR 95	2015	5945 (1812)	Chevron	Appraisal			l. Paleocene–e. Eocene	Three-way closure against salt weld
193	Coronado	WR 98	2008	5722 (1744)	Chevron	Appraisal			l. Paleocene–e. Eocene	Three-way closure against base of salt
194	Yeti	WR 160	2015	5924 (1806)	Statoil	Appraisal			m. Miocene	Three-way closure against base of salt
195	Stones	WR 508	2005	9576 (2919)	Shell	Producing	2016	FPS	l. Paleocene–e. Eocene	Four-way closure (contractional fold)
196	Tucker	WR 543	2006	6778 (2066)	Statoil	Appraisal			l. Paleocene–e. Eocene	Three-way closure against fault–salt
197	Julia	WR 627	2007	7087 (2157)	ExxonMobil	Appraisal	2016	SS, FPS	l. Paleocene–e. Eocene	Four-way closure (contractional fold)

(*continued*)

Table 3. Continued

Field Number	Field Name	Location Abbreviation	Discovery Year	Water Depth (ft [m])	Operator	Status	Production Onstream	Production Type	Age of Reservoir	Trap Type(s)
198	St. Malo	WR 678	2003	6900 (2103)	Chevron	Producing	2014	FPS	l. Paleocene–e. Eocene	Four-way closure (contractional fold)
199	Jack	WR 759	2004	7000 (2134)	Chevron	Producing	2014	FPS	l. Paleocene–e. Eocene	Four-way closure (contractional fold)
200	Logan	WR 969	2011	7750 (2362)	Statoil	Appraisal			l. Paleocene–e. Eocene	Four-way closure (contractional fold)

Locations of fields are shown in Figures 5, 10, and 11.

Location abbreviations: AT = Atwater Valley; GB = Garden Banks; GC = Green Canyon; KC = Keathley Canyon; MC = Mississippi Canyon; SE = Sigsbee Escarpment; WR = Walker Ridge. Production type abbreviations: FPS = floating production storage; MinDOC = Minimum Deep-Water Operating Concept; Semi = semisubmersible; SS = subsea tieback; TLP = tension leg platform. Age of reservoir abbreviations: e. = early; l. = late; m. = middle.

Future challenges in deep-water technology must address routine development in water depths greater than 2745 m (9000 ft). To operate economically in these water depths, companies must have reliable production facilities and systems. For example, fluids in pipelines must flow continuously, which is an extremely challenging problem, because pipeline blockages can be caused by waxes, asphaltenes, and gas hydrates at the lower temperatures of deep water. Another ongoing problem is dealing with the separation and sequestration of CO_2 gas, which will be a major challenge in the future.

Seismic Acquisition and Processing

Improvements in both seismic acquisition and processing have been crucial to the continued successful exploration and development in the northern deep-water Gulf of Mexico. The improved seismic imaging has allowed for more accurate definition of the structure and stratigraphy below shallow allochthonous salt and has opened an entire new exploration province. Shallow allochthonous salt presents major challenges for seismic imaging, primarily because the long offset seismic signals do not penetrate through salt. The critical angle is reached at relatively low incidence angles, typically little more than 30°, at the top of salt. Consequently, seismic energy gets refracted along the salt–sediment interface. Imprecise knowledge of depth of base of salt also results in imaging problems. The result is that a limited range of receivers collect seismic wavelets that have passed through the salt. Fewer active reflections result in noisier data. That is, the effective "fold" of the data is less than the acquisition geometry predicts.

Because of the strong velocity contrast of salt (~14,600 ft/s [4790 m/s]) with subjacent and overlying sediments (6000–8000 ft/s [1970–2625 m/s]), the seismic wavefront travels almost twice as fast in the salt as in the surrounding sediment. That phenomenon causes the wavelet to change shape as it travels through the salt. Different ray paths through the salt, as demanded by different shot and receiver locations, cause the signal to exit the base of salt at different times and at different places. Unless the signals are corrected perfectly for the different ray paths, which would require a priori knowledge of the salt body geometry, wavelets of different shapes and

times are summed together. The result is destructive interference, which translates to a reduction in high frequencies, and therefore, lower resolution.

There has been a distinct evolution in improved acquisition and updated streamer technologies. Initially, narrow azimuth towed streamer (NAZ) data with prestack depth migration (PSDM) processing were used for imaging the geology below salt; NAZ typically uses one boat (source of sound) towing 6-km (3.7-mi)–long streamers. A typical crossline aperture is 0.5 km (0.3 mi), with an inline aspect ratio of 1:16 and typically 60-fold data. By 2006, wide azimuth towed streamer (WAZ) became common in multiclient acquisition; WAZ may use up to four source boats with multiple streamer arrays. Typical crossline aperture is 4 km, with an inline aspect ratio of 1:2 and 160-fold data. The increase in spatial distribution of the data improves the signal-to-noise ratio, provides natural attenuation of some multiples, and potentially allows oblique ray paths unavailable with NAZ acquisition. Additionally, new streamer technologies are being introduced to reduce noise, provide deeper penetration, and sharpen imaging of the subsurface. However, the tradeoff is that WAZ data tend to have poorer resolution in the shallower part of the subsurface.

Seismic surveys are now routinely processed to depth with the multiple processing algorithms available. Each processing algorithm has different strengths and different levels of resolution. Wave equation migration (WEM) is current technology. Reverse time migration (RTM) is a special kind of WEM requiring a more precise velocity model; RTM can produce excellent results when a better velocity model is known. It is primarily used for imaging the structural geology below salt at depth; RTM can preserve lower frequencies than other processing. Kirchoff PSDM is older technology but is considered to better retain the amplitude information than other processing. Beam migration is perhaps state of the art, because it combines the better features of the earlier algorithms and, possibly, better images the steeper dips of salt edge and sediment. The latest versions of modern migration algorithms include anisotropic parameters. These data are closer to true depth and accurate geometric shapes—assuming that the anisotropy model, like the velocity model, is correct.

Finally, WAZ data can be processed into multiple output volumes, relating to the source-receiver azimuth. These products are the equivalent of multiple shoots in varying azimuths. And, as such, they image complex structures differently. Where one azimuth may image the dipping base of salt, another might better image a steep salt face not in the plane of the first azimuth.

REGIONAL SETTING

Geology as an Analog

The northern deep-water Gulf of Mexico serves as a crucial geologic analog for the exploration and development of many other deep-water basins. To date, approximately 70% of the deep-water reserves in the world are found in sedimentary basins with mobile substrates (i.e., salt, shale), similar to the Gulf of Mexico (updated from Worrall et al., 2001). These basins have four salient characteristics: (1) numerous extensional and contractional structures creating potential traps, (2) drainage of moderate to large areas of continents so that there is abundant overburden and vast volumes of sand for reservoirs, (3) stacked reservoir sands that are deposited in intraslope basins or at the base of slope, and (4) a petroleum system characterized by older, deeper source rocks, whose generation and migration are a fairly recent phenomenon geologically.

The continental slope and abyssal plain of the northern deep-water Gulf of Mexico were developed by the complex set of interacting processes that create a suite of unique features. A bathymetric map of the slope shows highly irregular topography in the central and western part of the continental slope (Figure 1). The slope has a more uniform bathymetry to the northeast, and the gradient increases substantially to the southeast along the Florida Escarpment, where slope gradients range from 10° to 40° (locally 90°).

Two factors are critical in understanding the geology of the northern deep-water Gulf of Mexico and the controls on its petroleum systems: (1) major siliciclastic sedimentation during the Cenozoic (Figures 3–5) and (2) complex tectonics caused by high sedimentation rates and the mobile substrates (Figure 3). The interaction of these two factors has created complex petroleum systems, where migration pathways are constantly evolving and changing because of the ongoing deformation (McBride et al., 1998a;

Table 4. Fields and Discoveries in Fold Belt Province, Northern Deep-Water Gulf of Mexico

Field Number	Field Name	Location Abbreviation	Discovery Year	Water Depth (ft [m])	Operator	Status	Onstream	Production Type	Age of Reservoir	Trap Type(s)
201	Silvertip	AC 815	2004	9356 (2852)	Shell	Producing	2010	SS	Oligocene	Four-way closure (contractional fold)
202	Great White	AC 857	2002	8009 (2441)	Shell	Producing	2010	SPAR	l. Paleocene–e. Eocene, Oligocene	Four-way closure (contractional fold)
203	Tobago	AC 859	2004	9636 (2937)	Shell	Producing	2011	SS	l. Paleocene–e. Eocene, Oligocene	Four-way closure (contractional fold)
204	Merganser	AT 37	2002	7900 (2408)	Anadarko	Abandoned, 2014	2007	SS	l. Miocene	Three-way closure against flank of salt
205	Bass Lite	AT 426	2001	6623 (2019)	Apache	Producing	2008	SS	l. Pleistocene	Three-way closure against salt–fault–stratigraphic
206	Neptune	AT 575	1995	6162 (1878)	BHP	Producing	2008	TLP	e.–m. Miocene	Four-way closure (contractional fold)
207	Shenzi	GC 654	2002	4400 (1341)	BHP	Producing	2009	TLP	e. Miocene	Four-way closure (contractional fold)
208	Atlantis	GC 699	1998	6133 (1869)	BP	Producing	2007	Semi	e.–m. Miocene	Four-way closure (contractional fold)
209	Parmer	GC 823	2004	4130 (1259)	Stone	Appraisal	Projected 2016	FPS	e.–m. Miocene	Four-way closure (contractional fold)
210	Mad Dog	GC 826	1999	4400 (1341)	BP	Producing	2005	SPAR	e.–m. Miocene	Four-way closure (contractional fold)
211	Q	MC 961	2005	7925 (2415)	Statoil	Abandoned, 2010	2007	SS	m. Miocene	Three-way closure against fault
212	Cascade	WR 206	2002	8203 (2500)	Petrobras	Producing	2012	FPSO	l. Paleocene–e. Eocene	Four-way closure (contractional fold)
213	Chinook	WR 469	2003	8826 (2690)	Petrobras	Producing	2012	SS	l. Paleocene–e. Eocene	Four-way closure (contractional fold)
214	Exploratus	Mexico	2014	8488 (2587)	Pemex	Appraisal			l. Paleocene–e. Eocene	Four-way closure (contractional fold)
215	Maximino	Mexico	2012	9574 (2918)	Pemex	Appraisal			l. Paleocene–e. Eocene	Four-way closure (contractional fold)
216	Maximino DL	Mexico	2014	9984 (3043)	Pemex	Appraisal			l. Paleocene–e. Eocene	Four-way closure (contractional fold)

(*continued*)

Table 4. Continued

Field Number	Field Name	Location Abbreviation	Discovery Year	Water Depth (ft [m])	Operator	Status	Onstream	Production Type	Age of Reservoir	Trap Type(s)
217	Supremus	Mexico	2013	9426 (2873)	Pemex	Appraisal			Oligocene	Four-way closure (contractional fold)
218	Trion*	Mexico	2012	8304 (2531)	Pemex	Appraisal			l. Paleocene–e. Eocene	Four-way closure (contractional fold)
219	Cratos	Mexico	2015	9213 (2808)	Pemex	Appraisal			l. Paleocene–e. Eocene	Four-way closure (contractional fold)

Locations of fields are shown in Figures 5, 10, and 11.
Location abbreviations: AC = Alaminos Canyon; AT = Atwater Valley; GC = Green Canyon; MC = Mississippi Canyon; WR = Walker Ridge. Production type abbreviations: FPS = floating production storage; FPSO = floating production storage offloading; Semi = semisubmersible; SS = subsea tieback; TLP = tension leg platform. Age of reservoir abbreviations: e. = early; l. = late; m. = middle.
*The Trion discovery is not technically in the Fold Belt province (see Figure 18), but it is included here because of its proximity.

Colling et al., 2001; Stover et al., 2001; Mount et al., 2006; Pilcher et al., 2011; Gibson, 2012).

Geologic Evolution of the Northern Deep-Water Gulf of Mexico

The geologic evolution of the northern deep-water Gulf of Mexico is illustrated in regional seismic profiles (Figures 3, 6), a series of chronostratigraphic and tectonic charts (Figures 7–9), and seven sequential maps that show the regional distribution of reservoirs in producing fields and discoveries by their ages (Figure 10).

Rifting developed during the Bajocian–Bathonian, and Louann Salt was deposited during the Middle Jurassic (Callovian) (Figures 6–8). During the Late Jurassic, the modern, deep northern Gulf of Mexico subsided rapidly during sea-floor spreading (Figure 8). Locally, in the northeastern deep-water Gulf of Mexico, the Norphlet Formation, an eolian sandstone, developed across the Middle Ground arch before the regional subsidence (Figures 7, 8, 10A). Two of the major source rocks in the deep water were deposited during this period: Oxfordian and Tithonian source rock (Figures 7, 8). The first allochthonous salt was initially emplaced during the Kimmeridgian in the northwest in the present area of the Perdido fold belt (D. Worrall, 2012, personal communication; Figure 8).

During the Berriasian–Valanginan, a third possible source rock was deposited locally in the eastern Gulf of Mexico (Figure 7). From the latest Valanginian through the Barremian, a major allochthonous salt layer was rafted basinward and translated the original Upper Jurassic and lowermost Cretaceous strata (Hudec et al., 2013). The initial contractional folds in the Keathley–Walker and Mississippi Fan fold belts developed within the downdip parts of this allochthonous salt layer (Figures 5, 6, 8). The Early Cretaceous emplacement of this salt layer is significant, because much of the subsequent Cenozoic salt tectonics were related to its initial deformation. Regionally, it is likely that this allochthonous salt emplacement continued later in time, possibly into the Late Cretaceous.

The Upper Cretaceous strata are dominated by interbedded, fine-grained shales and carbonates to the northeast; they are more shale rich centrally and to the northwest (Weimer et al., 2016a). One major

Table 5. Fields and Discoveries in Abyssal Plain Province, Northern Deep-Water Gulf of Mexico

Field Number	Field Name	Location Abbreviation	Discovery Year	Water Depth (ft [m])	Operator	Status	Onstream	Production Type	Age of Reservoir	Trap Type(s)
220	Vortex	AT 261	2002	8340 (2542)	Anadarko	Abandoned, 2011	2007	SS	l. Miocene	Four-way closure (compactional drape)
221	Jubilee	AT 349	2003	8800 (2682)	Anadarko	Abandoned, 2015	2007	SS	l. Miocene	Four-way closure (compactional drape)
222	Mondo NW Extension	LL 1	2005	8340 (2542)	Anadarko	Abandoned, 2015	2007	SS	l. Miocene	Four-way closure (Fault bounded)
223	Atlas NW	LL 5	2004	8810 (2685)	Anadarko	Abandoned, 2009	2007	SS	l. Miocene	Four-way closure (compactional drape)
224	Atlas	LL 50	2003	9000 (2743)	Anadarko	Abandoned, 2009	2007	SS	l. Miocene	Four-way closure (compactional drape)
225	Jubilee Extension	LL 309	2005	8774 (2674)	Anadarko	Abandoned, 2015	2007	SS	l. Miocene	Four-way closure (compactional drape)
226	Cheyenne	LL 399	2004	8987 (2739)	Anadarko	Abandoned, 2015	2007	SS	l. Miocene	Four-way closure (compactional drape)

Locations of fields are shown in Figures 5, 10, and 11.
Location abbreviations: AT = Atwater Valley; LL = Lloyd Ridge. Production type abbreviation: SS = subsea. Age of reservoir abbreviation: l. = late.

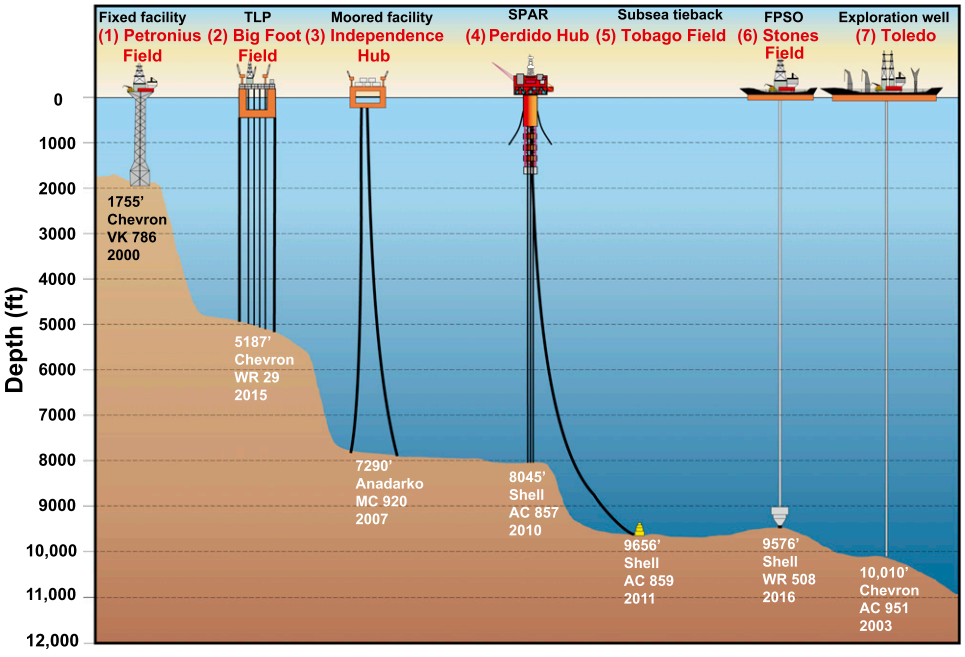

Figure 2. Schematic diagram showing the world-record water depths for exploration and development facilities. See Figure 1 for location of facilities. Note that the deepest water exploration well in the Gulf of Mexico is (7) Toledo, Alaminos Canyon (AC) block 951 (10,010 ft [3051 m]). Globally, the deepest water exploration well is the Raya-1 well in 11,191 ft (3411 m), Pelotas Basin, Uruguay. A SPAR is a type of floating oil platform typically used in very deep waters and is named for logs used as buoys in shipping that are moored in place vertically. Updated from Weimer and Pettingill (2007). FPSO = floating production storage offloading; MC = Mississippi Canyon; TLP = tension-leg platform; VK = Viosca Knoll; WR = Walker Ridge.

sandstone unit, the downdip equivalent to the productive, updip shallow-marine Tuscaloosa sandstone, was deposited during the Cenomanian to earliest Turonian (Figures 7, 8). This sandstone has been penetrated in two wells: Tiber (WR 102) and Baha 2 (AC 600) (Figure 7; Horn, 2011; Scott et al., 2012, 2014).

A unique geologic event at the end of the Cretaceous, the meteorite impact at Chicxulub in the northwestern Yucatan platform to the south in Mexico, had a major effect on the geologic evolution of the Gulf of Mexico. The Yucatan platform was a carbonate province, and the bolide impact generated an instantaneous, extensive collapse of the platform margin and created carbonate-rich debris flows, which form some of the reservoirs for the supergiant Cantarell and Ku-Maloob-Zaap Complexes (Figure 1; Magoon et al., 2001; Ricoy, 2005; Mitra et al., 2006).

Regionally, extensive carbonate debris flows and turbidity flows were generated and transported across the northern deep-water Gulf of Mexico onto the slope. The seismic stratigraphic expression of the

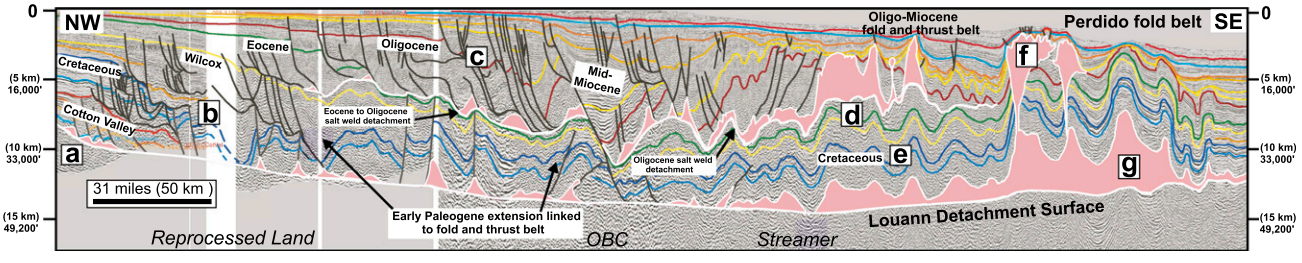

Figure 3. Regional seismic profile (in depth) from the Texas coastal plain (left) across shelf, slope, and abyssal plain, showing the complexity of the Mesozoic–Cenozoic strata of the northwestern Gulf of Mexico. Marine data were collected from ocean bottom cables (OBC). The profile crosses the four deep-water provinces: Basins, Subsalt, Fold Belt, and Abyssal Plain. From the north (left), note the (a) original level of autochthonous (Middle Jurassic) salt, (b) different level of normal faults, (c) expansion of Oligocene–Miocene sediments, (d) Oligocene salt-weld detachment and associated structures, (e) extensive structures interpreted below the salt and salt weld, (f) shallow allochthonous salt in lower slope, and (g) Perdido fold belt with early allochthonous salt. See Figure 5B for location of the profile. After Radovich et al. (2007). Reproduced with permission of Barbara Radovich, Ion Geophysical, and the Gulf Coast Section SEPM Foundation, and any other use requires their permission.

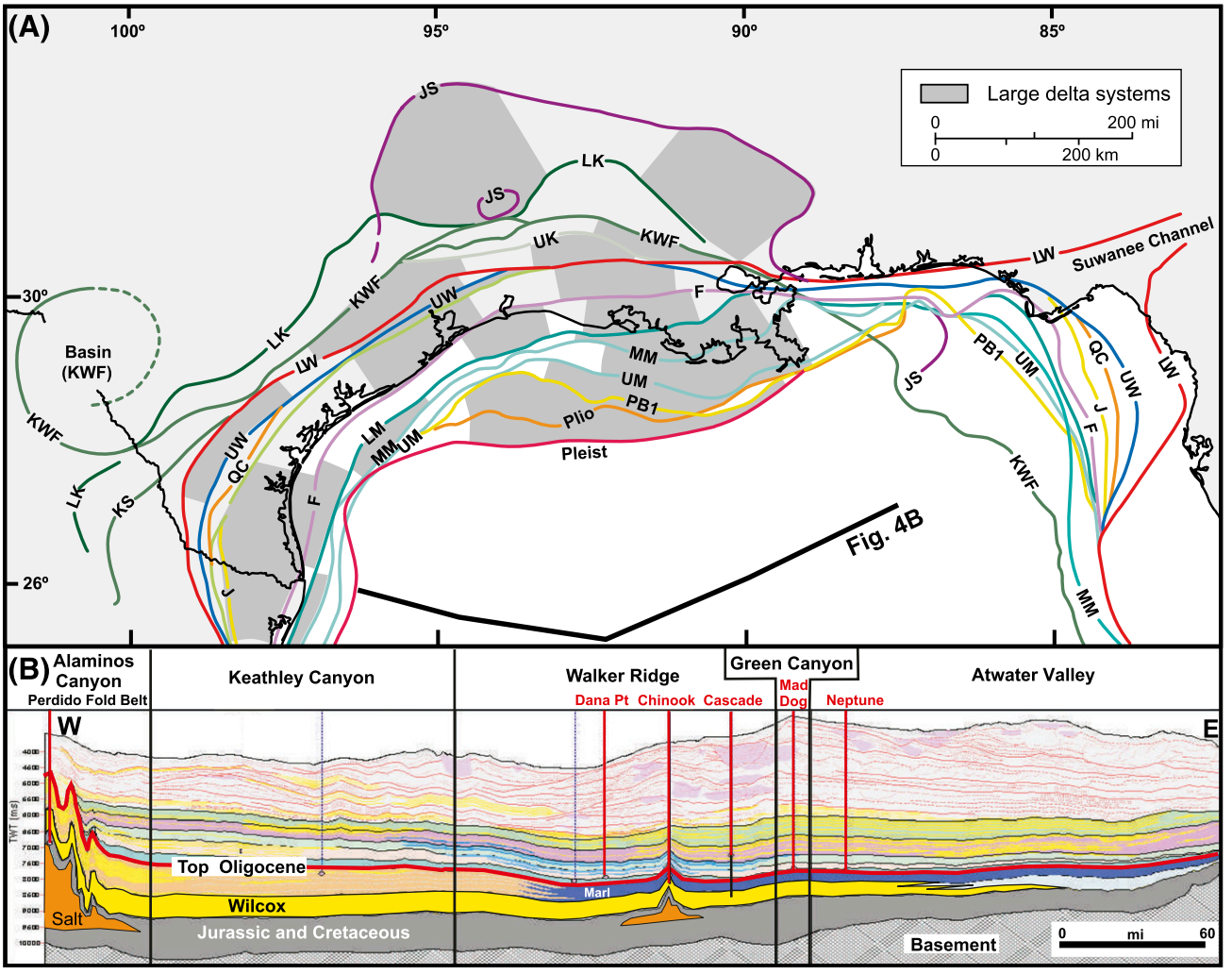

Figure 4. (A) Map showing the distribution of large Mesozoic and Cenozoic deltas and shelf margins, northern Gulf of Mexico (GOM). After Galloway (2008). Approximate location of (B) is shown. Reprinted with permission of Springer-Verlag. (B) Regional seismic profile basinward of the Sigsbee Escarpment in the Abyssal Plain province, showing the regional distribution of sediments in deep water. Distinct wedges of the Cenozoic strata can be seen. Paleogene strata are largely present in the western deep GOM, whereas the Neogene depocenter sits to the center and east. These depocenters mirror the locations of the shallow-marine depocenters preserved in the present onshore and shelf. After Zarra (2007a). Reprinted with permission of the Gulf Coast Section SEPM Foundation, and any other use requires their permission. F = Frio; J = Jackson; JS = Jurassic Smackover; KS = Sligo; KWF = Washita–Fredericksburg; LK = Lower Cretaceous = Hosston; LM = lower Miocene; LW = lower Wilcox; MM = middle Miocene; PB1 = *Buliminella* 1; Pleist = Pleistocene; Plio = Pliocene; Pt = Point; QC = Queen City; TWT = two-way traveltime; UK = Upper Cretaceous; UM = upper Miocene; UW = upper Wilcox.

impact on the deep-water strata has been documented by Scott et al. (2012, 2014) and Sanford (2015), and the wireline characteristics for all penetrations are shown in Weimer et al. (2016b); 58 wells have penetrated this deposit and have found a variable thickness (0 to 204 m [0 to 669 ft]) of the deposit (Tables 6–8). Scott et al. (2012, 2014) noted that this deposit eroded significant parts of the underlying strata. The minimum stratigraphic level of erosion across the northern deep-water Gulf of Mexico was at the mid Campanian level (Richard Denne, 2014, personal communication). The greatest amount of eroded section penetrated in wells was in the Atwater Valley 336 well, where erosion extended down to the Upper Jurassic strata, which overlie the Lower Cretaceous allochthon (Weimer et al., 2016b).

This impact deposit likely affected the stratigraphic evolution of the area for several million years. The deposit possibly affected the evolution of the salt, which in turn affected the distribution of the

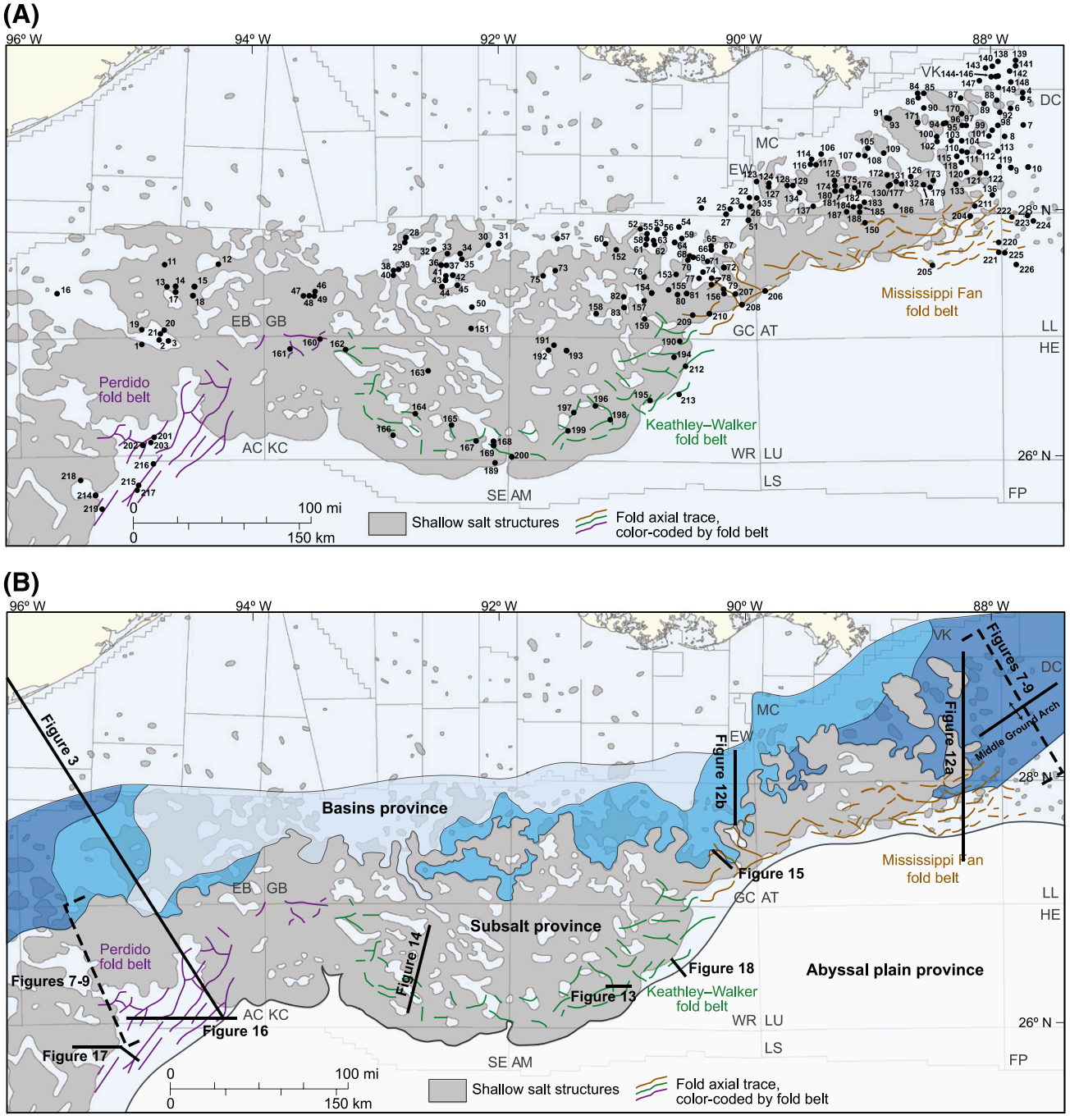

Figure 5. (A) Regional map of the northern deep-water Gulf of Mexico showing the protraction boundaries, locations of major structural features, and the 226 fields and discoveries (black dots) in greater than 1500-ft (457-m) water depth. Numbers correspond to fields listed in Tables 2–5. (B) Regional map of the northern deep-water Gulf of Mexico showing the protraction boundaries, locations of major structural features, tectonic-exploration provinces (Basins, Subsalt, Fold Belt, and Abyssal Plain), and age of stratigraphic fill in the Basins province: dark blue = Miocene; medium blue = Pliocene; light blue = Pleistocene. Area used for the schematic cross sections in Figures 7–9 is shown by the dashed brackets. Locations are shown for Figures 3 and 12–18. Provinces and ages are modified from Zarra (2007a). Base map is adapted from Hudec et al. (2013), including distribution of shallow salt and trends for the Perdido, Keathley–Walker Ridge, and Mississippi Fan fold belts. Trends of fold axes for Perdido fold belt in Mexican water is adapted from Figure 17. Abbreviations for protraction areas: AC = Alaminos Canyon; AM = Amery Terrace; AT = Atwater Valley; DC = DeSoto Canyon; EB = East Breaks; EW = Ewing Bank; FP = Florida Plain; GB = Garden Banks; GC = Green Canyon; HE = Henderson; KC = Keathley Canyon; LL = Lloyd Ridge; LS = Lund South; LU = Lund; MC = Mississippi Canyon; SE = Sigsbee Escarpment; VK = Viosca Knoll; WR = Walker Ridge. Note: A color version can be seen in the online version.

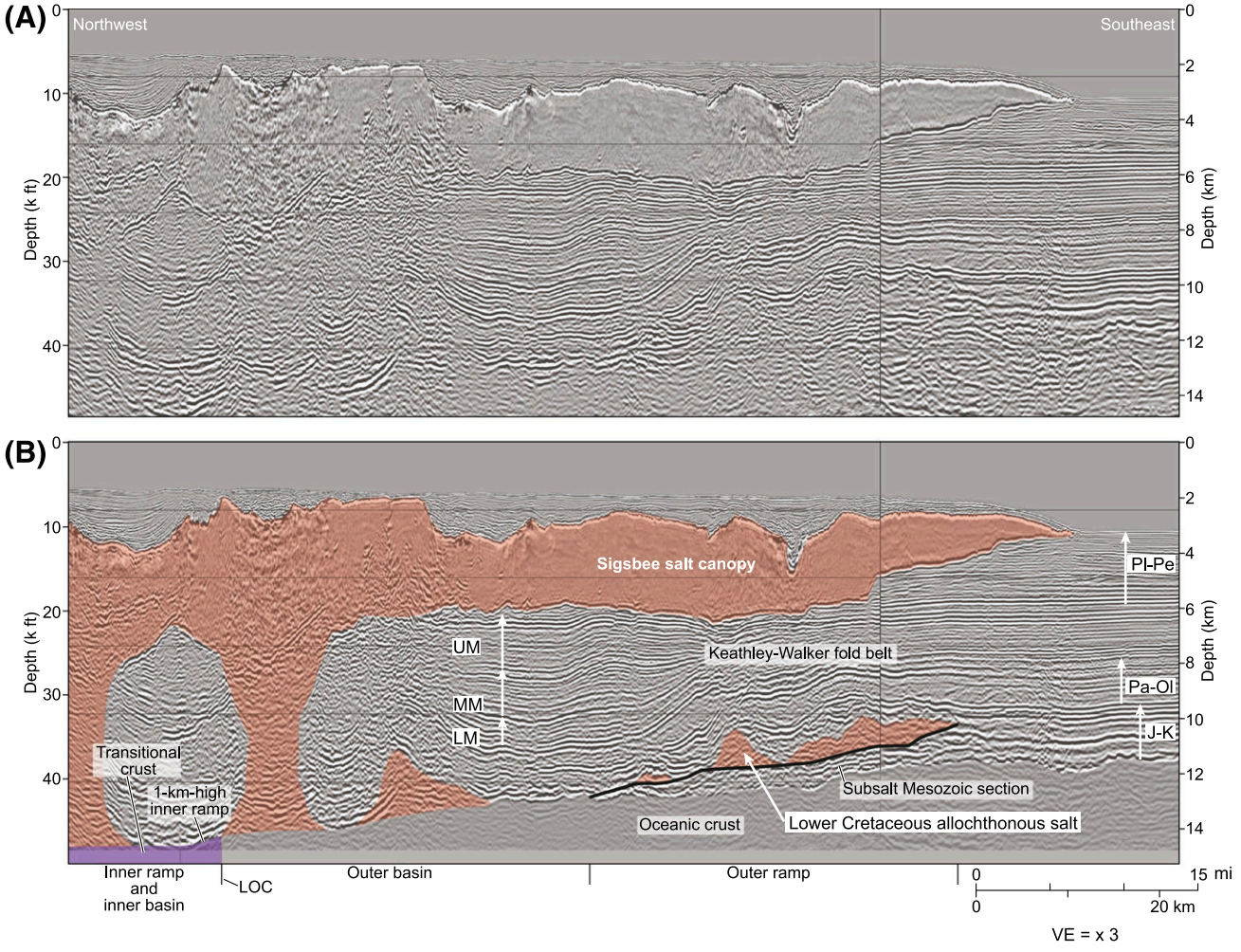

Figure 6. Regional seismic profile across Walker Ridge–Keathley Canyon: (A) uninterpreted; (B) interpreted. Shallow allochthonous salt overlies the Lower Cretaceous allochthonous level. Approximate ages of key horizons are shown. See text for detail. Modified from Hudec et al. (2013). Seismic data image proprietary to and provided courtesy of CGG. Reprinted with permission of CGG and Matthew Bognar. J = Jurassic; K = Cretaceous; LM = lower Miocene; LOC = limit of normal oceanic crust; MM = middle Miocene; Ol = Oligocene; Pa = Paleogene; Pe = Pleistocene; Pl = Pliocene; UM = upper Miocene; VE = vertical exaggeration.

overlying Wilcox sandstones across the entire area (Scott et al., 2012, 2014).

During the Paleocene, there was a marked increase in rates of sedimentation in the northern deep-water Gulf of Mexico (Figures 4, 9, 10A). Siliciclastic sediments were derived from highlands created from the Laramide orogeny in the Rocky Mountains to the northwest and deposited in a series of sand-rich shorelines during the Paleogene (Figure 4). Two major deep-water reservoir deposits are equivalent to the petroleum-productive shallow-marine sandstones. First, the Wilcox Formation (upper Paleocene–lower Eocene) forms the reservoir in 23 fields and discoveries in the United States and 5 additional discoveries in Mexico (Figures 9, 10A; Tables 3, 4). Second, the Frio Formation (Oligocene) forms the reservoir in the two fields in the United States (Great White, Silvertip) and one in the Mexican area (Supremus) (Figure 10A; Table 4).

At the beginning of the Miocene, two significant events affected the regional sedimentation. First, the drainage area for sediment expanded to the east and included the western Appalachian Mountains. These additional drainages caused the shallow-marine depocenters to shift to the east into the central Gulf of Mexico (Figures 4, 10B). Second, the rates of sedimentation greatly increased, causing large volumes of sediment to be deposited overlying the deeper salt. This extensive loading of sediment significantly impacted the tectonics in two ways: (1) the Lower

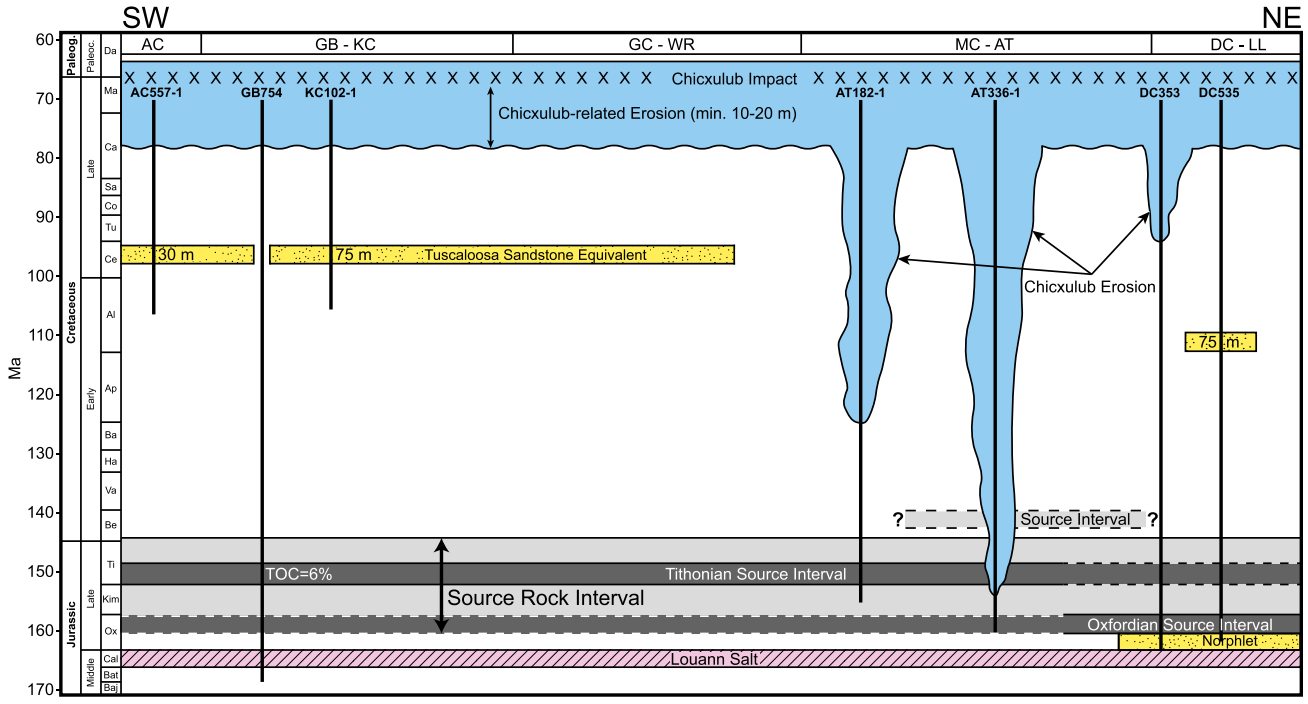

Figure 7. Regional chronostratigraphic chart across the northern deep-water Gulf of Mexico showing the stratigraphic evolution of the Middle Jurassic through Upper Cretaceous section. See Figure 5B for general area included in the cross section. Seven key wells and their depths of penetration are projected onto the section. Norphlet eolian sandstone is penetrated in the DeSoto Canyon (DC) 353 Vicksburg discovery well and three additional discoveries. Two main source intervals, centered on the Tithonian (Ti) and Oxfordian (Ox), are shown in dark gray; light gray shows other possible source intervals. The dashed lines indicate where the lithofacies of the source intervals may not contribute to oil generation. Total organic carbon (TOC) values for the source intervals of the Garden Banks (GB) 754 well are plotted (adapted from Cole et al., 2001b). Note that considerable thickness variation exists in the Upper Jurassic and Lower Cretaceous sections resulting from salt tectonics. The DC 535 well penetrated Albian sandstone unit, and two wells (Alaminos Canyon [AC] 557 and Keathley Canyon [KC] 102) that penetrate the deep-water Tuscaloosa (and their thickness at penetration) are shown. The X's at the top Cretaceous indicate the instantaneous gravity-flow deposit layer deposited from the Chicxulub meteorite in Mexico. Blue (in online version) indicates the depth of erosion from the Chicxulub gravity-flow deposit at the top Cretaceous, as indicated by the wells that penetrated the section (Denne et al., 2013). Protraction area abbreviations: AT = Atwater Valley; GC = Green Canyon; LL = Lloyd Ridge; MC = Mississippi Canyon; WR = Walker Ridge. Geologic age abbreviations: Al = Albian; Ap = Aptian; Ba = Barremian; Baj = Bajocian; Bat = Bathonian; Be = Berriasian; Ca = Callovian; Ce = Cenomanian; Co = Coniacian; Da = Danian; Ha = Hauterivian; Kim = Kimmeridgian; Ma = Maestrichtian; Paleoc. = Paleocene; Paleog. = Paleogene; Sa = Santonian; Tu = Turonian; Va = Valanginian.

Cretaceous allochthon began to deform, creating the emplacement of the shallow-salt features present in the slope (Figures 3, 6), such as extensive series of salt diapirs and intraslope basins developed, and where many reservoir sands were deposited, and (2) the associated salt migration downdip resulted in increased deformation in the Keathley–Walker and Mississippi Fan fold belts (Figure 6). During the middle to late Miocene, numerous fold-belt structures developed, and fold limbs steepened considerably, increasing the structural closures that are now being explored and developed (see below). Finally, continued sediment loading at high depositional rates throughout the Neogene–Pleistocene created the irregular bathymetry on the slope that we see today in shallow allochthonous salt features (bathymetric highs) and intraslope basins (bathymetric lows) (Figure 1).

The evolution of the shallow-marine and downdip deep-marine depocenters during the Neogene is shown in Figures 4, 9, and 10B–G. The location of the fields and discoveries is only a general proxy for the location of the deep-marine depocenters (Figure 10). During the early Miocene, the shallow-marine depocenter was in the north-central Gulf of Mexico (Figure 4); the downdip-equivalent deep-water reservoir sands are primarily located in southern Green Canyon (Figure 10B). During the middle to

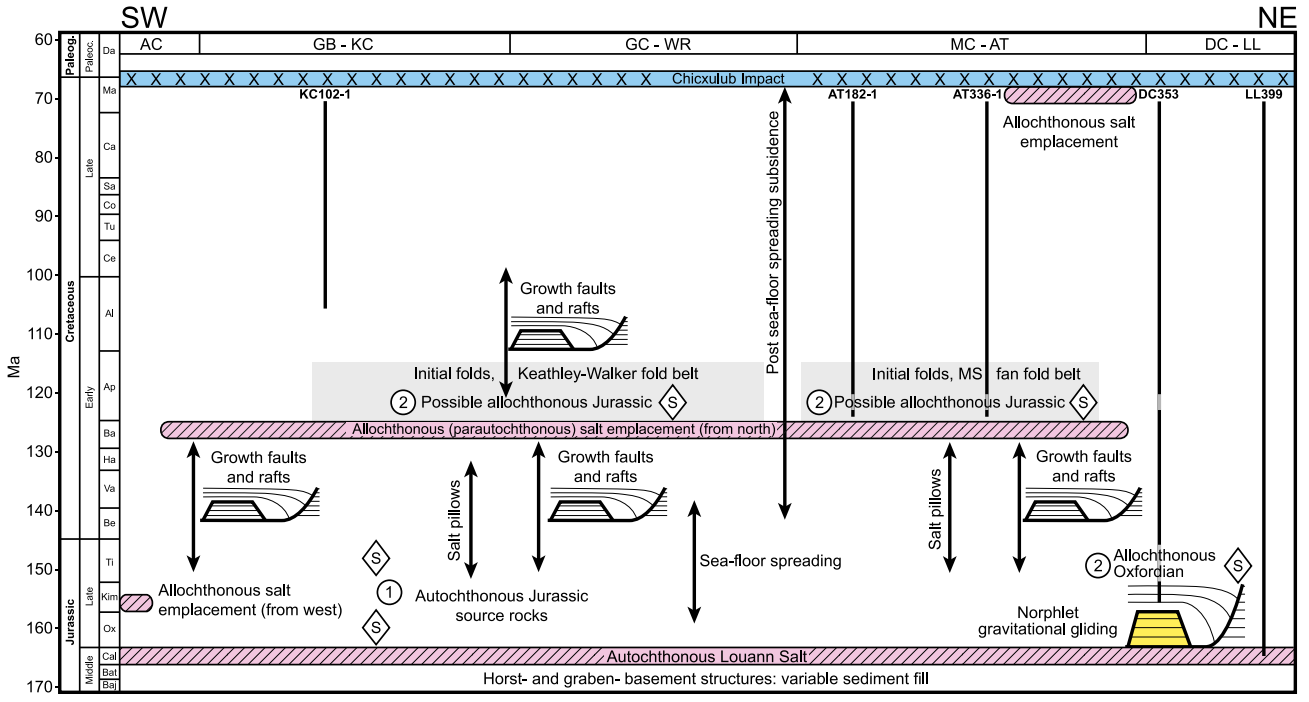

Figure 8. Tectonic events chart for the Jurassic and Cretaceous section shown in the chronostratigraphic chart in Figure 7. Five key wells and their depths of penetration are projected onto the section. Bajocian and Bathonian strata are present in the inherited rift topography, below the Callovian autochthonous Louann salt. Emplacement of allochthonous salt happened at three discrete times: Kimmeridgian (Kim) (western Gulf of Mexico [GOM]), Early Cretaceous (regional in GOM), and locally at the top Cretaceous in the eastern GOM. Early salt pillows, growth faults, and raft systems developed during the Late Jurassic and continued during the Cretaceous. The initial stages of deformation of the Keathley–Walker fold belt and Mississippi Fan fold belt occurred on top of the Lower Cretaceous allochthonous salt layer. Source intervals (shown by numbers in circles) are indicated by diamonds (with S). To the east, the Oxfordian (Ox) source interval was translated laterally on top of the Norphlet sandstone raft (e.g., DeSoto Canyon [DC] 353). The Norphlet sandstone was not present in the Lloyd Ridge (LL) 399 well, which did penetrate Louann salt. The Ox and Kim source intervals were emplaced on top of the Lower Cretaceous nappe and provide much of the oil in the deep water. Note that the Atwater Valley (AT) 182 and 336 wells penetrate the Jurassic source intervals where they overlie the Lower Cretaceous allochthonous salt. Protraction area abbreviations: AC = Alaminos Canyon; GB = Garden Banks; GC = Green Canyon; KC = Keathley Canyon; MC = Mississippi Canyon; WR = Walker Ridge. Geologic age abbreviations: Al = Albian; Ap = Aptian; Ba = Barremian; Baj = Bajocian; Bat = Bathonian; Be = Berriasian; Ca = Callovian; Ce = Cenomanian; Co = Coniacian; Da = Danian; Ha = Hauterivian; Ma = Maestrichtian; Paleoc. = Paleocene; Paleog. = Paleogene; Sa = Santonian; Ti = Tithonian; Tu = Turonian; Va = Valanginian.

late Miocene, the main shallow-marine depocenter shifted to the east, and the downdip-equivalent reservoirs are primarily found in Mississippi Canyon, eastern Green Canyon, Viosca Knoll, and eastern DeSoto Canyon protraction areas (Figures 9; 10C, D). During the early Pliocene, the shallow-marine depocenter shifted westward to the central part of the northern Gulf of Mexico, and deep-water reservoirs are primarily found in Green Canyon, western Garden Banks, and western Mississippi Canyon protraction areas (Figures 9; 10E, F). During the late Pliocene, the shallow-marine depocenter continued to shift westward, with the deep-water reservoirs found in East Breaks, Garden Banks, and Green Canyon (Figures 9, 10G). During the early Pleistocene, reservoir sands are primarily East Breaks, Garden Banks, and Green Canyon. Only a few reservoirs produce from the upper Pleistocene sediments (Figures 9, 10G).

EXPLORATION AND TECTONIC PROVINCES

The distribution of the general geologic and exploration provinces of the northern deep-water Gulf of Mexico is shown in Figure 5. Zarra (2007a) defined four main provinces based on the ages of strata and styles of deformation: Basins, Subsalt, Fold Belt, and Abyssal Plain (Figure 5B). The geology of each province is summarized here, including a summary of the fields, the ages of the reservoirs (Figure 10; Tables

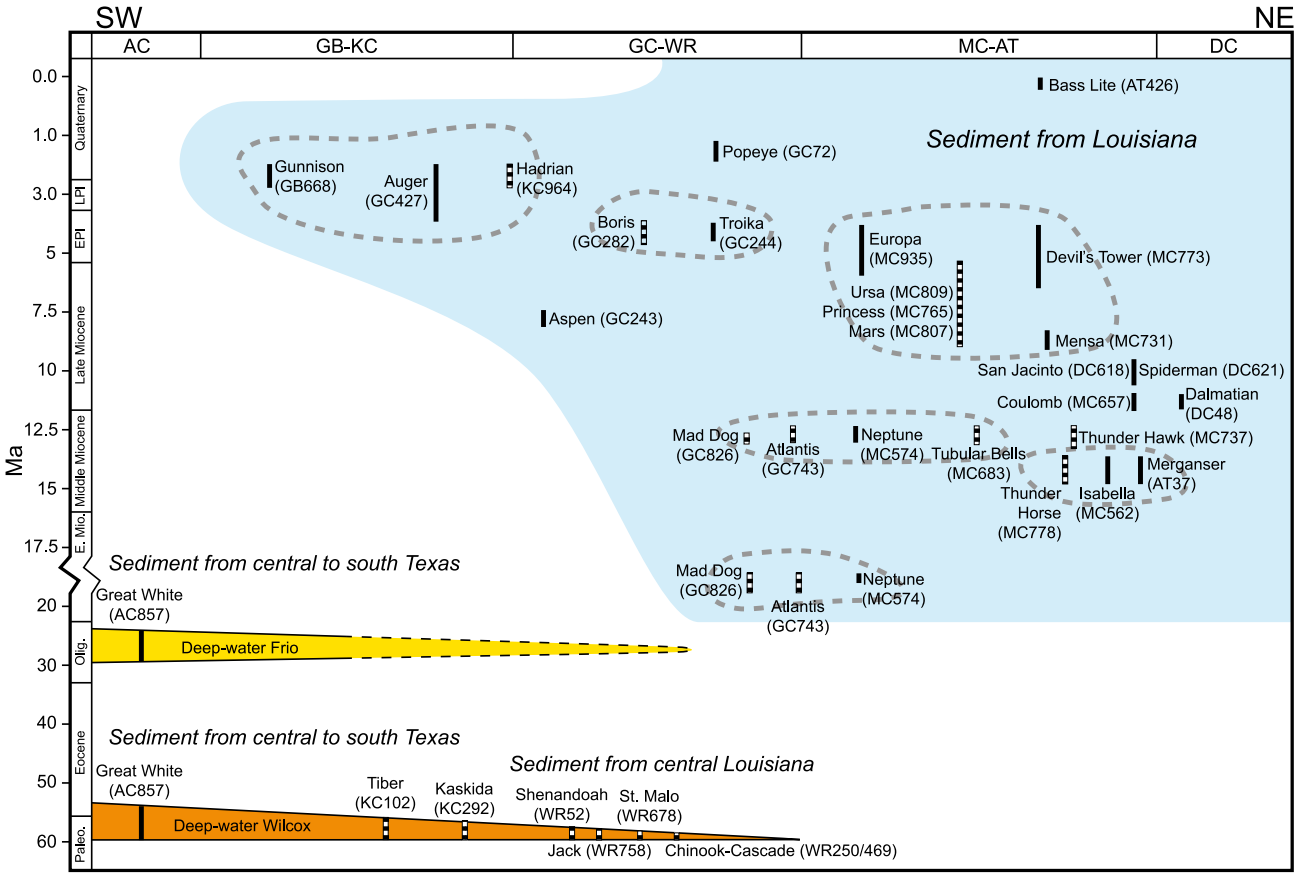

Figure 9. Regional chronostratigraphic chart across the northern deep-water Gulf of Mexico showing the stratigraphic evolution of the Cenozoic. Note the change in scale at 20 Ma. See Figure 5B for the general area included in the cross section and wells. The changing locations of the depocenters are highlighted by the ages of the reservoirs in different key fields; subsalt fields are shown by dashed lines, and suprasalt fields are shown by solid lines. See Figure 4 for detailed distribution of sediment in deep water in the abyssal plain. Protraction area abbreviations: AC = Alaminos Canyon; AT = Atwater Valley; DC = DeSoto Canyon; GB = Garden Banks; GC = Green Canyon; KC = Keathley Canyon; MC = Mississippi Canyon; WR = Walker Ridge. Geologic age abbreviations: E. Mio. = Early Miocene, EPl = Early Pliocene; LPl = Late Pliocene; Olig. = Oligocene; Paleoc. = Paleocene.

2–5), the trap type of each field (Figure 11; Tables 2–5), and representative seismic profiles (Figures 12–18). In classifying the traps, it is important to note that nearly all fields in the northern deep-water Gulf of Mexico have a stratigraphic component to their trap, including those fields with four-way closure.

In addition, because of the structural complexity, some of these provinces overlap, making this classification difficult. For example, the Mississippi Fan fold belt extends below the salt in southeastern Green Canyon where four fields are present (Figures 5, 11). In this case, we included these fields in the Fold Belt province (Table 4). In contrast, all discoveries in the Keathley–Walker fold belt are included in the Subsalt province, except for Chinook and Cascade fields, which lie basinward of the Subsalt province (Figures 5, 11; Table 4). Those fields that sit below salt but are immediately adjacent to the Basins province are included in the Subsalt province (Figures 5, 11; Table 3).

Basins Province

The Basins province (Table 2) rests in the modern upper to middle slope and largely consists of thick Neogene suprasalt sediments that overlie shallow allochthonous salt or have been welded to strata that once underlaid the welded-out basins (Figures 3, 5, 12). To the northeast, the original sedimentary basins are largely undeformed in the slope, indicating relatively thinner original salt thickness and decreased subsequent related deformation.

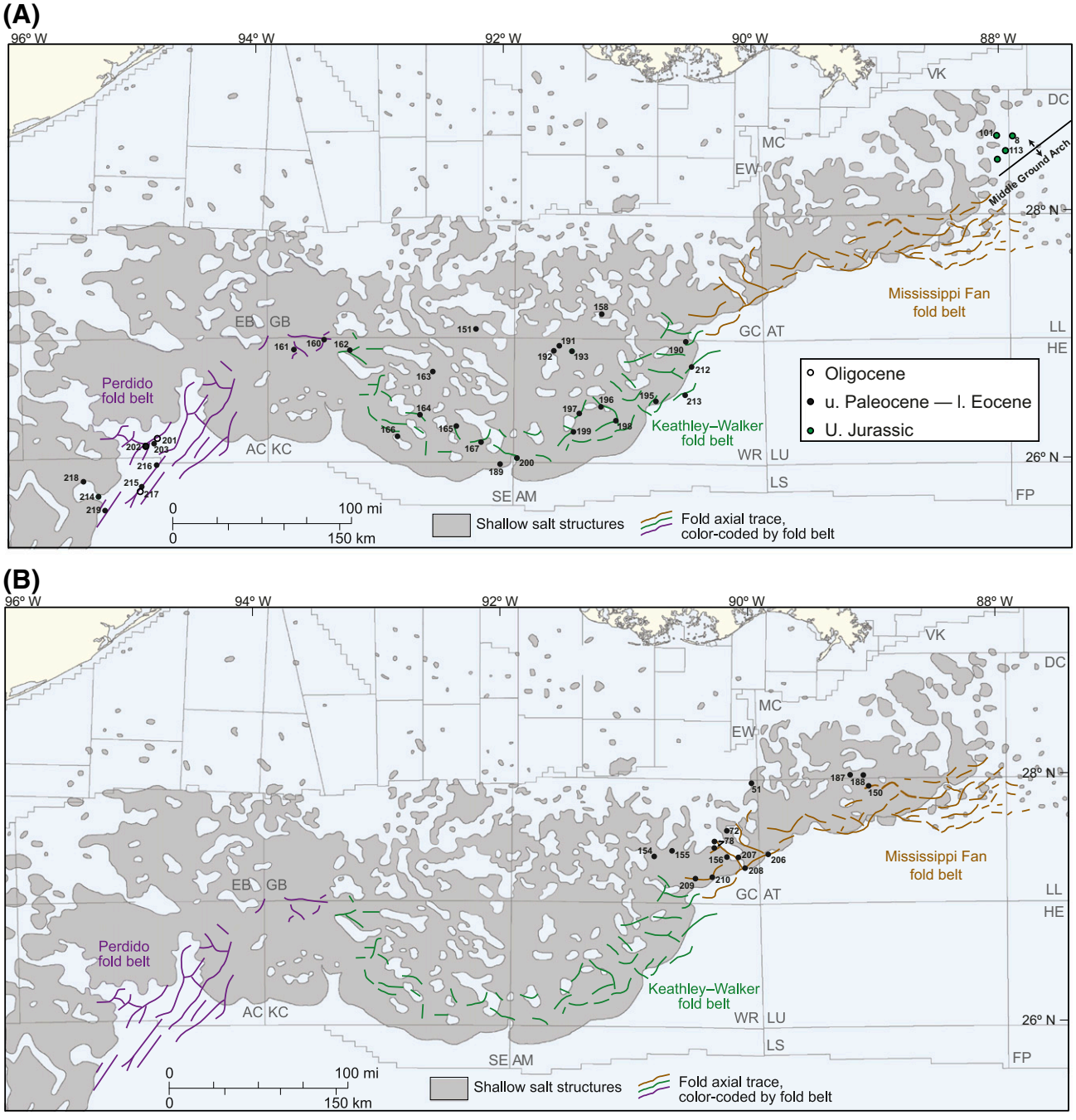

Figure 10. Sequential maps showing the distribution of reservoir ages for fields and discoveries in the northern deep-water Gulf of Mexico for (A) Late Jurassic (Oxfordian; 163.5 to 157.3 Ma), late Paleocene–early Eocene (60.0 to 51.8 Ma), and Oligocene (29 to 27 Ma); (B) early Miocene (23.0 to 16.0 Ma); (C) middle Miocene (16.0 to 11.6 Ma); (D) late Miocene (11.6 to 5.3 Ma); (E) early Pliocene (5.3 to 3.6 Ma); (F) late Pliocene (3.6 to 2.6 Ma); and (G) Quaternary (2.6 to 0.0 Ma). Black dots show locations of fields and discoveries. Numbers correspond to fields listed in Tables 2–5. Abbreviations of protraction area boundaries: AC = Alaminos Canyon; AM = Amery Terrace; AT = Atwater Valley; DC = DeSoto Canyon; EB = East Breaks; EW = Ewing Bank; FP = Florida Plain; GB = Garden Banks; GC = Green Canyon; HE = Henderson; KC = Keathley Canyon; LL = Lloyd Ridge; LS = Lund South; LU = Lund; MC = Mississippi Canyon; SE = Sigsbee Escarpment; VK = Viosca Knoll; WR = Walker Ridge. Geologic age abbreviations: l. = late; u./U. = upper/Upper.

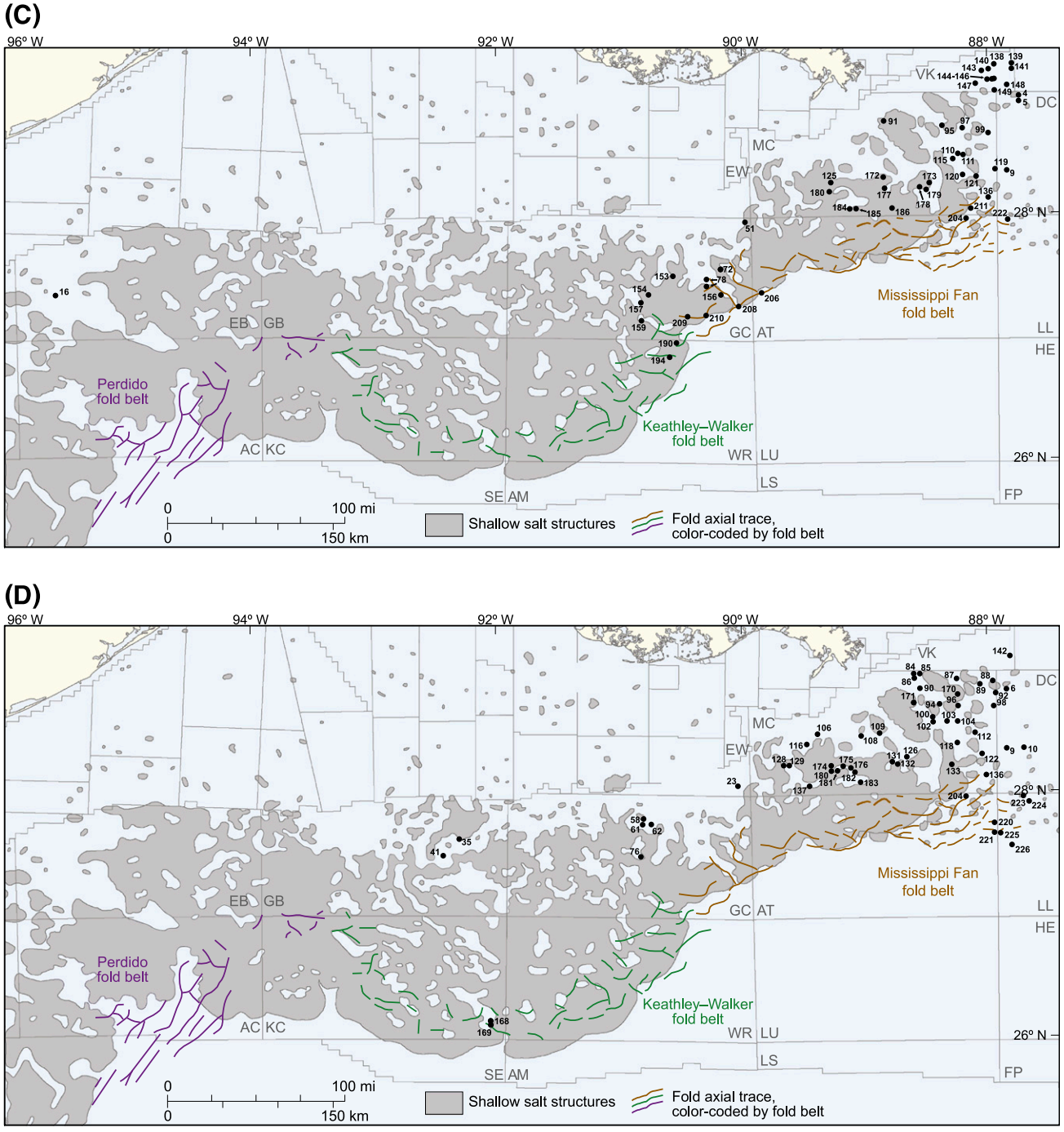

Figure 10. Continued.

The Neogene sedimentary fill is younger in the central part of the province and older to the east and west, as indicated by the different shades of blue in Figure 5B. These different ages of sedimentary fill are caused by the regional shifting of the shallow-marine depocenters during the Cenozoic (Galloway et al., 2000, 2011; Galloway, 2008; Figures 4, 10). The structural geology varies regionally, ranging from little to no deformation to the northeast to areas of extensive salt migration and intraslope basin formation in the central upper slope (Figure 5B). Salt structures vary as well, including diapirs, shallow tongues, and deep remnants such as pillows and rollers. Finally, both normal and reverse faulting is present in the

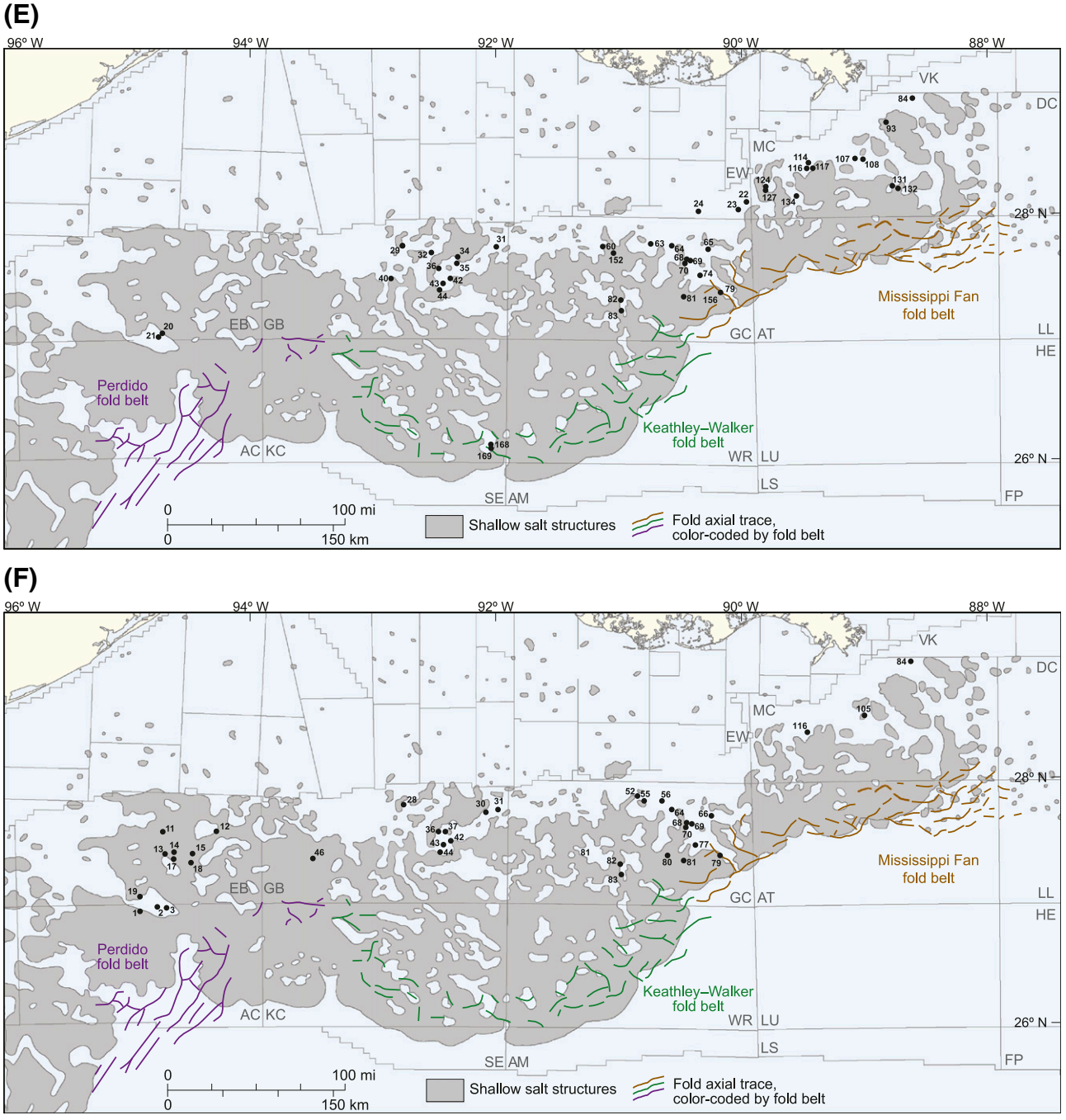

Figure 10. Continued.

upper slope (Figure 12; McBride et al., 1998a; Mount et al., 2006, 2007; Pilcher et al., 2011).

The Basins province includes 149 fields (Figures 5, 10, 11; Table 2). Most of the traps developed in association with sediment loading and salt deformation, primarily on the salt-diapir flanks and/or associated with salt-related faults. Three broad trap types are recognized (Figure 11). First, four-way closure exists in 15 fields: (1) extensional anticline turtles (2 fields), (2) fault bounded (6 fields), and (3) compactional drape overlying a deeper structure (7 fields). Second, 103 fields have three-way closures with combined structural-stratigraphic traps, which include (1) termination against a fault (51 fields) and (2) reservoir onlap pinchout along the flanks of salt bodies (52 fields). (In fact, many of the fields have

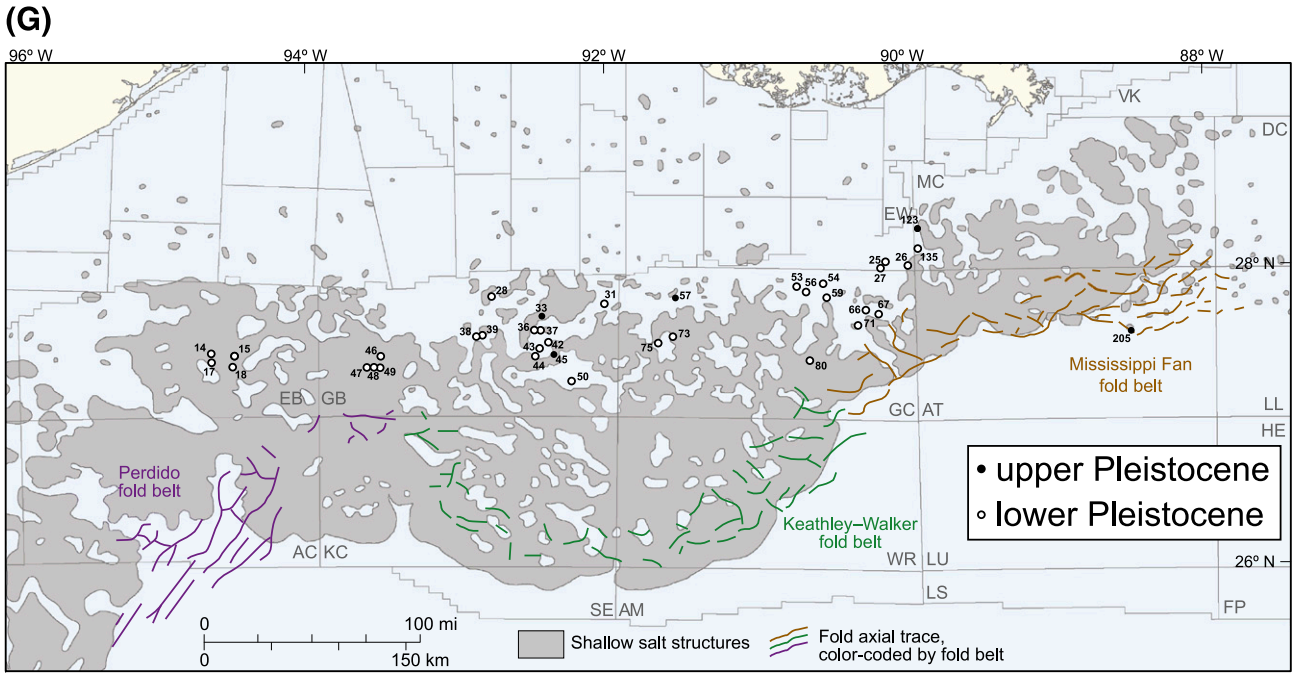

Figure 10. Continued.

multiple trapping elements, e.g., dominantly pinchout against salt flanks with minor faulting.) Third, 28 fields have stratigraphic traps that consist of onlap onto the slope or salt (Table 2). Note that nearly all of the fields (27 of 28) with stratigraphic traps in the northern deep-water Gulf of Mexico are present in the Basins province, and the fields are primarily Miocene in age. One field produces from a trap that is a fault-bounded two-way closure.

Reservoirs are primarily middle Miocene through Pleistocene in age (Figures 10C–G; Table 2). Reservoirs primarily consist of single to multistory channel-fill sands, amalgamated and layered sheet sands, and, to a lesser degree, thin-bedded sands in levees. Note that 105 of the 151 fields and discoveries produce or will produce by subsea tieback to nearby permanent facilities (see figure 2 in Weimer et al., 2017d, this issue).

To the northeast, four fields contain Upper Jurassic (Oxfordian) eolian sandstone reservoirs (Appomattox, Fort Sumter, Vicksburg [A, B] Rydberg; Figure 10A; Tables 2, 6). The reservoirs are equivalent to the producing eolian sandstone reservoirs in the Mobile Bay area near the present-day shoreline (Figure 1; Story, 1998). The fields overlie rafted stratal blocks over the Louann salt (Godo et al., 2011; Godo, in press; Pilcher et al., 2014; Figure 8), and traps consist of three-way closure against faults and four-way closure (Figures 7, 11; Table 2). These discoveries indicate that this particular area remained a relative high along the Middle Ground arch immediately after oceanic spreading began, in contrast to surrounding areas. This area then subsided rapidly during the late Oxfordian. Appraisal drilling of these discoveries for possible field development is ongoing. These four discoveries open up the possibility of exploration in Upper Jurassic shallow-marine to continental reservoirs as well as in Upper Triassic rift-related strata.

Subsalt Province

The Subsalt province (Table 3) contains shallow allochthonous salt bodies, most of which have bathymetric expression (Figures 1, 3, 5). The term primarily refers to "subsalt" prospects that are imaged below the allochthonous salt and thus present significant challenges in seismic imaging. Substantial resources have been dedicated to the acquisition and processing for higher-resolution seismic data for exploration.

The Subsalt province is simplistically viewed as a nearly continuous shallow-salt feature (Figure 5). In actuality, allochthonous salt has considerable variation in its thickness, styles, and timing of formation (Hudec

Table 6. Wells That Penetrated Upper Jurassic Strata, Northern Deep-Water Gulf of Mexico: Exploration Target, Thickness of Top Cretaceous–Paleogene Deposit, (after Denne et al., 2013), Well Status

Well Number in Figure 19	Location Abbreviation	Field, Well Name	Exploration Target	Approximate Top Cretaceous Erosion (m [ft]) or Thickness of KPg Deposit (After Denne et al., 2013)	Status
1	AT 26	Big Horn	MS Fan fold belt	0	Dry hole
2	AT 182-1	Sturgis-1	MS Fan fold belt	0	Noncommercial
3	AT 336	Showboat	MS Fan fold belt	23 (75)	Dry Hole
4	DC 178	Titan	Norphlet	6 (20)	Dry Hole
5	DC 231	Perseus	Norphlet	NA	Dry Hole
6	DC 268	Antietam	Norphlet	13 (43)	Noncommercial
7	DC 269	Shiloh	Norphlet	21 (69)	Noncommercial
8	DC 353	Vicksburg B	Norphlet	20 (66)	Development
9	DC 353	Vicksburg A	Norphlet	NA	Tight Hole
10	DC 398	Gettysburg	Norphlet	NA	Dry Hole
11	DC 486	Fredricksburg	Norphlet	20 (66)	Dry Hole
12	DC 529	Petersburg	Norphlet	NA	Dry hole
13	DC 535	Raptor	Norphlet	9 (29)	Dry hole
14	DC 726	Sake	Smackover	NA	Dry Hole
15	DC 757	Madagascar	Norphlet	NA	Dry Hole
16	DC 843	Swordfish	Norphlet	9 (29)	Dry Hole
17	DC 927	Coral	Smackover	12 (39)	Dry Hole
18	EW 922	Wrigley	Salt weld (Overturned)	67 (220)	Dry hole
19	GB 754	Norton	Shallow salt	21 (69)	Dry Hole
20	LL 399	Cheyenne-deep	Smackover	16 (52)	u. Mio-produced 2007–2015
21	MC 348	Appomattox 3, 3ST	Norphlet	NA	Development
22	MC 391	Appomattox 1, 1ST	Norphlet	NA	Development
23	MC 392	Appomattox 1A/1S	Norphlet	27 (88)	Development
24	MC 393	Corinth	Norphlet	12 (39)	Dry Hole
25	MC 525	Rydberg	Norphlet	NA	Development
26	MC 566	Fort Sumter	Norphlet	NA	Appraisal

Abbreviations: AT = Atwater Valley; DC = DeSoto Canyon; EW = Ewing Bank; GB = Garden Banks; KPg = top Cretaceous–Paleogene; LL = Lloyd Ridge; MC = Mississippi Canyon; MS = Mississippi; u. Mio = upper Miocene; NA = not available.

et al., 2013). These extensive salt features have often merged through time but originally developed from different types of salt structures. Strata below the shallow salt are Middle Jurassic through early Pleistocene in age, depending on the timing of the development of the allochthonous salt systems. The subsalt sediments were originally deposited into the relatively unconfined abyssal plain or into intraslope fairways formed during salt evacuation.

Table 3 summarizes the 51 fields and discoveries in the Subsalt province that are considered to be commercial. Two key structural styles create the traps. First, the Keathley–Walker fold belt extends across the southern part of the province (Figures 5, 6, 13, 14). Traps for 15 fields are contractional folds (Figure 11; e.g., St. Malo, Figure 13; Leon, Figure 14; Table 3). Second, the wide variation in salt styles creates two kinds of general traps—those detached

Table 7. Wells That Penetrated Lower Cretaceous Strata, Northern Deep-Water Gulf of Mexico: Exploration Target, Age at Total Depth, Thickness of Top Cretaceous–Paleogene Deposit (After Denne et al., 2013), Well Status

Well Number in Figure 19	Location Abbreviation	Field, Well Name	Exploration Target	Approximate Top Cretaceous Erosion (m [ft]), or Thickness of KPg Deposit (After Denne et al., 2013)	Status	Oldest Cretaceous Strata Penetrated
27	AC 557	Baha 2	Perdido fold belt	204 (669)	Dry hole	Hauterivian
28	AT 182–1S	Sturgis	MS Fan fold belt	24 (79)	Noncommercial	Aptian
29	AT 187	Sierra	Under salt (overturned)	NA	Dry hole	Aptian
30	KC 875–1	Lucius	Keathley–Walker fold belt	27 (88)	Producing	Barremian
31	KC 875–2	Lucius	Keathley–Walker fold belt	23 (75)	Producing	Barremian
32	KC 919–1	Hadrian	Keathley–Walker fold belt	5 (16)	Producing	Albian

Abbreviations: AC = Alaminos Canyon; AT = Atwater Valley; KC = Keathley Canyon; KPg = top Cretaceous–Paleogene; MS = Mississippi; NA = not available.

from the salt and those attached to the salt (Mount et al., 2006, 2007; Weimer et al., 2006; Pilcher et al., 2011). Detached traps underlie the allochthonous salt and formed prior to the emplacement of the shallow Neogene salt. Trap styles include four-way closures created from (1) turtle structures (five fields; Figure 11; Table 3; see figure 77 in Weimer et al., 2017d, this issue) and (2) one fault-bounded field (Mica field, Table 3). One accumulation with a stratigraphic trap is present at Raton–Raton South–Gemini complex (Figure 11; Table 3). In contrast, fields with attached traps have three-way closure against salt or salt weld, which also acts as the updip seal (27 fields; Figure 11; Kaskida, Figure 14; K2–K2 North, Genghis Kahn, Figure 15; Table 3).

Reservoirs become younger from west to east (Figure 9). To the west and south, reservoirs are upper Paleocene–lower Eocene, that is, the downdip equivalent of the prolific updip Wilcox Formation in onshore Texas (Zarra, 2007a); 21 fields have reservoirs of this age. In contrast, to the east, 29 fields have reservoirs that are primarily Miocene, and one field includes lower Pliocene reservoirs.

Reservoirs primarily consist of amalgamated channel-fill and sheet sandstones (lobes) deposited in both unconfined and confined basins and slope fairways. The upper Paleocene–lower Eocene Wilcox Formation was deposited in a largely unconfined, base-of-slope setting (Zarra, 2007a). Curiously, the Wilcox strata thin over the crest of the structures that were created by the Early Cretaceous salt emplacement (North Platte, Figure 13; Figure 14).

In contrast, for the fields with Miocene–lower Pliocene reservoirs, sands were deposited in intraslope basins, either adjacent to or against the shallow-salt features. With ongoing deformation, the salt was emplaced later and overrides the reservoir (e.g., Kaskida, Figure 14; K2 North and Genghis Khan, Figure 15; Mars and Ursa fields, Meckel et al., 2002).

It is worth noting that if the shallow allochthonous salt were not present, many of these detached structures probably would have been drilled 10 to 15 yr earlier, because many of the structures are not particularly complex (Figures 6, 13, 14). However, this is not true in the attached traps that developed during the emplacement of shallow-salt bodies. For these fields, salt is part of the trap and seal (Figure 15).

Fold Belt Province

The northern deep-water Gulf of Mexico holds three subregional fold belts: (from west to east) Perdido, Keathley–Walker, and the Mississippi Fan (Figures 3, 5). (The Keathley–Walker fold belt completely underlies the salt and is included above in the Subsalt province.) These fold belts have different structural styles, timing of deformation, ages of potential

Table 8. Wells That Penetrated Upper Cretaceous Strata, Northern Deep-Water Gulf of Mexico: Exploration Target, Age at Total Depth, Thickness of Top Cretaceous–Paleogene Deposit (After Denne et al., 2013), Well Status

Well Number in Figure 19	Location Abbreviation	Field, Well Name	Exploration Target	Approximate Top Cretaceous Erosion (m [ft]), or Thickness of KPg Deposit (After Denne et al., 2013)	Status	Oldest Cretaceous Strata Penetrated
33	AT 63	Telemark	MS Fan fold belt	>40 (131)	Producing	TDed in KPg deposit
34	AT 398	Bonsai	MS Fan fold belt	>15 (49)	Dry hole	TDed in KPg deposit
35	AT 428	Palamino	MS Fan fold belt	>20 (66)	Dry hole	TDed in KPg deposit
36	GB 840	Vienna	Salt feature	>15 (49)	Dry hole	TDed in KPg deposit
37	GB 989	Salida	Keathley–Walker fold belt	>2 (6)	Dry hole	TDed in KPg deposit
38	GC 639	Tahiti West	Overturned subsalt feature	>40 (131)	Dry hole	TDed in KPg deposit
39	GC 653	Shenzi	MS Fan fold belt	90 (295)	Producing	Turonian
40	GC 826	Mad Dog	MS Fan fold belt	>18 (59)	Producing	TDed in KPg deposit
41	GC 847	Turtle Lake	MS Fan fold belt	>55 (180)	Dry hole	TDed in KPg deposit
42	GC 866	Puma	Overturned salt carapace	39 (128)	Dry hole	Campanian/Salt
43	KC 102	Tiber	Keathley–Walker fold belt	90 (295)	Appraisal	Albian (?)
44	KC 596–1	Bass	Keathley–Walker fold belt	100 (328)	Dry hole	Campanian
45	KC 681	Sardinia	Keathley–Walker fold belt	>30 (98)	Dry hole	TDed in KPg deposit
46	KC 774	Ponza	Keathley–Walker fold belt	85 (279)	Dry hole	Santonian
47	KC 919–2	Hadrian	Keathley–Walker fold belt	>20 (66)	Producing	TDed in KPg deposit
48	MC 84	Horn	Salt diapir	27 (88)	Producing	Cenomanian
49	MC 379	Chin Music	Overturned salt carapace	46 (151)	Dry Hole	TDed in Campanian
50	MC 876	Callisto	MS Fan fold belt	–	Produced 2007–2015	TDed in KPg deposit (logs didn't reach the deposit)
51	VK 915	Dorado	Salt feature	>13 (43)	Producing	TDed in KPg deposit
52	VK 826	Neptune	Salt feature	60 (197)	Producing	Tded in Cenomanian/Anhydrite
53	WR 52–1	Shenandoah	Keathley–Walker fold belt	>30 (98)	Appraisal	TDed in KPg deposit
54	WR 95	Yucatan	Keathley–Walker fold belt	>9 (29)	Appraisal	TDed in KPg deposit
55	WR 155	Atlas Deep	Keathley–Walker fold belt	>9 (29)	Dry hole	TDed in KPg deposit
56	WR 316	Lewis	Keathley–Walker fold belt	14 (46)	Dry hole	TDed in KPg deposit
57	WR 584–1	Julia	Keathley–Walker fold belt	>21 (69)	Appraisal	TDed in KPg deposit
58	WR 969	Logan	Keathley–Walker fold belt	155 (508)	Appraisal	Hauterivian*

* Logan penetrated a shallower Cretaceous section that overlies allochthonous salt. Well total depth (TDed) in Paleocene.

Abbreviations: AT = Atwater Valley; GB = Garden Banks; GC = Green Canyon; KC = Keathley Canyon; KPg = top Cretaceous–Paleogene; MC = Mississippi Canyon; VK = Viosca Knoll; WR = Walker Ridge.

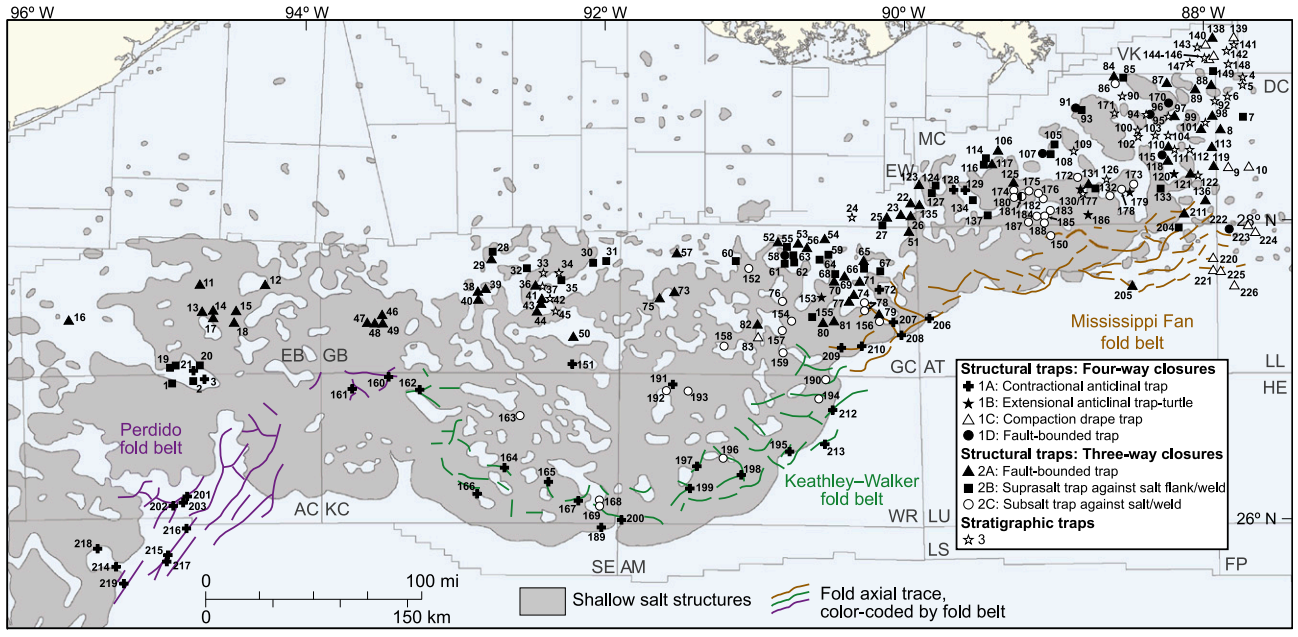

Figure 11. Regional map showing the relationship of kinds of trap styles in the northern Gulf of Mexico to the tectonic provinces. Eight kinds of traps are recognized (see Tables 2–5 for fields and Figure 5A for the name of each field). For trap classification, see figure 3 in Weimer et al. (2017d, this issue) and figure 5 in Bouroullec et al. (2017a, this issue). Abbreviations for protraction areas: AC = Alaminos Canyon; AM = Amery Terrace; AT = Atwater Valley; DC = DeSoto Canyon; EB = East Breaks; EW = Ewing Bank; FP = Florida Plain; GB = Garden Banks; GC = Green Canyon; HE = Henderson; KC = Keathley Canyon; LL = Lloyd Ridge; LS = Lund South; LU = Lund; MC = Mississippi Canyon; SE = Sigsbee Escarpment; VK = Viosca Knoll; WR = Walker Ridge.

reservoirs, and natures of salt. Discoveries have been made in both the Perdido and Mississippi Fan fold belts (Table 4).

The Perdido fold belt is characterized by northeast-trending folds, with minor faulting along their flanks (Figures 3, 16, 17; Trudgill et al., 1999; Camerlo and Benson, 2006; Zarra, 2007a). The northeastern part extends below the allochthonous salt. These folds are cored with allochthonous Upper Jurassic salt (D. Worrall, 2012, personal communication; Figures 8, 16). The fold belt formed primarily during the latest Oligocene, although there was minor growth during the Eocene. Traps in the Great White and Tobago producing fields are four-way closures; at Silvertip field, the trap is a dipping three-way closure that is slightly fault bounded (Eikrem et al., 2010). All fields have a stratigraphic component to their traps. At the Great White field, the reservoirs are deep-water Wilcox (upper Paleocene–lower Eocene) and deep-water Frio (Oligocene; Figures 5, 8; Zarra, 2007b; Eikrem et al., 2010); at Tobago field, the Wilcox forms the reservoir. In the Silvertip field, the reservoirs are Oligocene (Figures 5, 8; Eikrem et al., 2010). These three fields produce from the Perdido SPAR facility in 2438 m (8045 ft) water depth—the world record for SPAR (Figure 2). Tobago and Silvertip fields produce via subsea tieback to the SPAR. Tobago produces from the deepest water depth from tiebacks (9636 ft [2937 m]). Note that most of the Perdido fold belt rests in the Mexican deep water to the southwest, where Pemex has made six discoveries during the past 4 yr (Figures 5, 17; Cratos, Exploratus, Maximino, Maximino-DL, Supremus, Trion; Colmenares, 2014).

The Mississippi Fan fold belt developed primarily during the middle to late Miocene and consists of slightly asymmetric folds with primary vergence to the north (Figures 5, 12; Morris and Weimer, 2004a, b; see figure 20 in Bouroullec and Weimer, 2017, this issue; figures 3, 4 in Bouroullec et al., 2017b, this issue). This fold belt is cored by the Lower Cretaceous allochthonous salt layer that developed from the Middle Jurassic autochthonous salt layer (Figures 8, 12; Moore et al., 2001). Traps for the five western fields are four-way closures (Atlantis, Mad Dog, Neptune, Parmer, Shenzi; Figure 11). For the three eastern fields (Bass Lite, Merganser, Q), traps are combined three-way closures. For the seven fields (except Bass Lite), the reservoirs are lower to middle

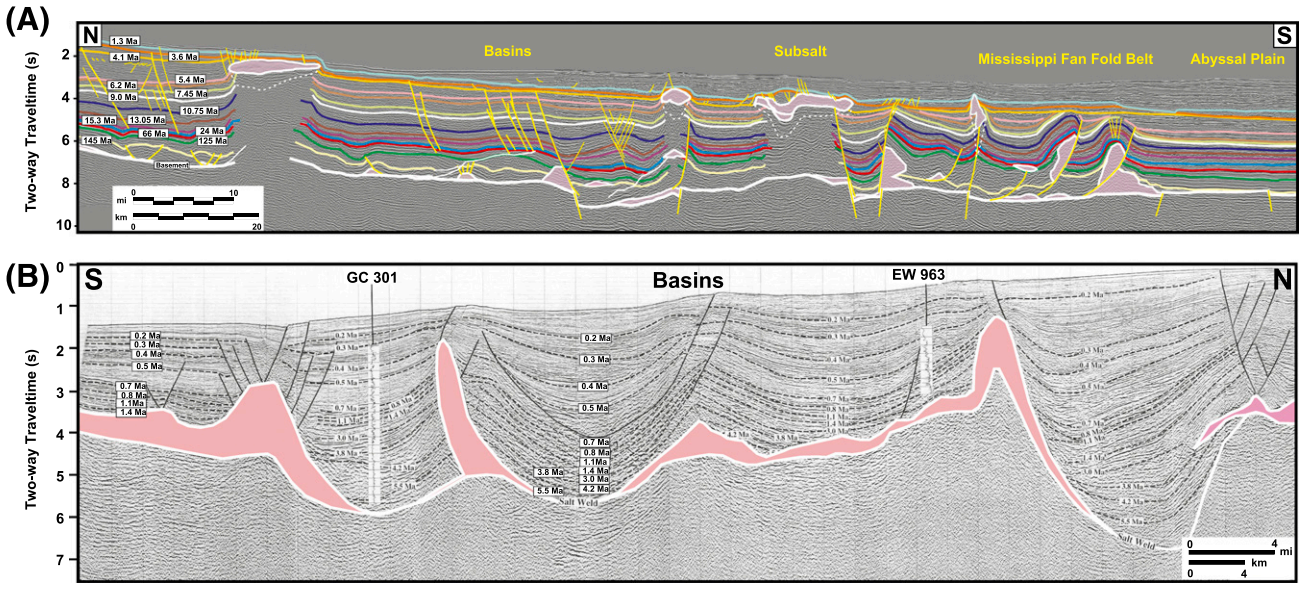

Figure 12. Regional seismic profiles across the Basins province. (A) Interpreted profile in eastern Mississippi Canyon and northern Atwater Valley across the Basins province (undeformed strata), Subsalt province (isolated shallow and deep salt structures), Fold Belt province (eastern part of the salt-cored Mississippi Fan fold belt), and Abyssal Plain province (south of fold belt). After Bouroullec et al. (2004). Reproduced with permission of the Gulf Coast Association of Geological Societies. (B) Interpreted profile from eastern Green Canyon (Basins province) across counterregional and reverse faults, faults, and shallow-salt structures. Prominent weld surface is shown. See Figure 5B for location of profiles. After McBride et al. (1998b). Reproduced with permission of AAPG.

Miocene sands that were deposited in an unconfined, base-of-slope setting (Mander et al., 2012; Walker et al., 2012). Bass Lite produces from an upper Pleistocene channel-fill sand.

Finally, the Cascade and Chinook fields are part of the Keathley–Walker fold belt system (discussed above) but rest outside of the Subsalt province (Figures 5, 18). Traps are four-way closures that are cut by faults near their crest. Reservoirs are Wilcox sandstone (Figure 10; Table 4). The Cascade field is produced by an FPSO, and Chinook is produced by a subsea tieback.

Abyssal Plain Province

The Abyssal Plain province (Table 5) rests outboard (south) of the Subsalt, Fold Belt, and Basins provinces (Figures 4, 6A). The boundary of the Subsalt province is abrupt and is marked by the edge of the Sigsbee Escarpment. This province lies directly basinward of the Fold Belt province. To the east, the boundary is transitional with the Basins province. The Abyssal Plain province can simplistically be subdivided into two parts: areas underlain by Louann salt and areas that are salt free. The basinward edges of the original depositional salt (autochthonous Louann) and allochthonous salt (Early Cretaceous emplacement) are present in the northern part of the Abyssal Plain province (Hudec et al., 2013). Structures consist of deformed salt or elevated basement blocks (Post et al., 2001).

Seven fields have been discovered in the province (Table 5). All reservoirs are upper Miocene and were deposited in channel fill or levees. Six fields have four-way closure that developed from compactional drape (Weimer et al., 2017d, this issue). All fields produced by subsea tieback to the Independence Hub in southeastern Mississippi Canyon, until abandoned (Figure 2; Table 5).

What distinguishes this province from the others is the lack of bathymetric expression of the structures. Significantly, fewer wells have been drilled in this area than in the rest of the northern deep-water Gulf of Mexico, so less is known about the details of the stratigraphy.

OTHER PETROLEUM SYSTEMS FACTORS

Source Rocks

The source rocks in the northern deep-water Gulf of Mexico are found at great subsurface depths, commonly

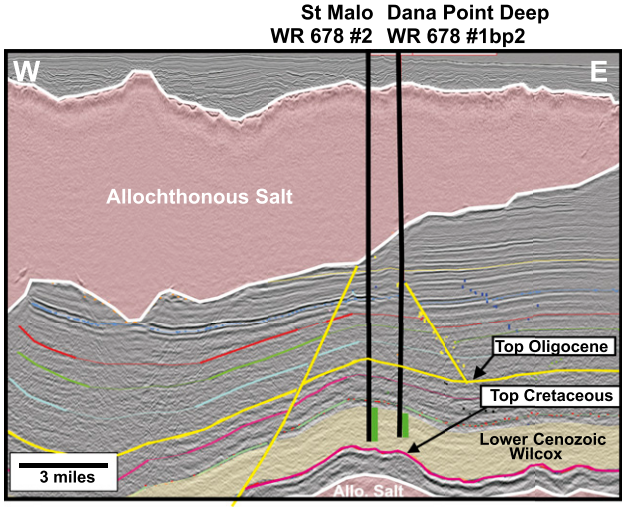

Figure 13. Interpreted seismic profile across St. Malo (Walker Ridge [WR] 678) and Dana Point (WR 678) in WR protraction area. The two wells underlie the shallow allochthonous (Allo.) salt sheet. The field consists of a deep Wilcox Formation reservoir in a four-way closure. This was the first subsalt discovery in the lower Wilcox Formation. Note the thinning of the Wilcox Formation across the crest of the fold, indicating the bathymetric expressions of the folds during the late Paleocene–early Eocene. Green (in online version) bars correspond to reservoir. See Figure 5B for location of profiles. After Lewis et al. (2007). Reproduced with permission of the Gulf Coast Section SEPM Foundation, and any other use requires their permission.

overlain by more than 13,000 m (30,000 ft) of strata. Consequently, only 26 wells have penetrated the source rocks, primarily around the northeastern margin and shallow structural features (Figure 19; Tables 6–8; Weimer et al., 2016a). Thus, the relatively few penetrations mean that the regional distribution of source rocks is interpreted based on primarily the oil composition and biomarker data from reservoirs or by seeps on the slope (Wenger et al., 1994; Cole et al., 2001a, b; Colling et al., 2001; Hood et al., 2002; Jacques and Clegg, 2002).

Two source intervals are interpreted as coeval to upslope shallow-marine–equivalent strata: (1) Oxfordian shallow marine limestones and marls (Smackover equivalent), found primarily to the northeast, and (2) Tithonian shales (Cotton Valley equivalent), which is areally widespread. A third possible source interval, Lower Cretaceous, is interpreted to be present by some authors (Teerman et al., 2010). The areal distribution of these source rocks is shown in Figure 19. Oxfordian source rocks have type I kerogens (Godo, in press), and Tithonian source rocks have type II and type IIS kerogens; they were deposited during the early post-rift history (Cole et al., 2001b). The Lower Cretaceous interval is considered a type II kerogen. One area in the northern slope has oils that are produced from a mixture of these source intervals (Figure 19). Wireline characteristics for these source rocks are shown in Weimer et al. (2016a), and their approximate thicknesses are in Table 6.

Evolution of Exploration Plays and Results

An important part of the continuing exploration success in the northern deep-water Gulf of Mexico is that exploration play concepts have evolved through time, which has resulted in substantial reserve growth. Five major exploration plays (Figure 20), related to the four tectonic provinces (Zarra, 2007a; Figure 5), have been developed during the past 25 yr: the flex trend, minibasins, fold belt, subsalt, and Mesozoic plays. Also shown in Figure 20 are the number of discoveries per year and the timing and transition of the exploration plays. For example, in 1975, Cognac field was the first discovery in greater than 200 m (660 ft) water depth (Figure 20); 2001 was the year for the largest number of discoveries, with no discoveries in 1978, 1979, and 1992. The Macondo incident in April 2010 led to an increase

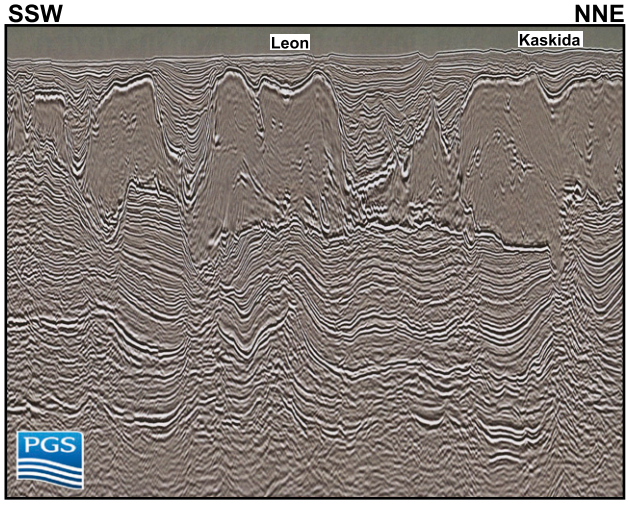

Figure 14. Seismic profile across the Kaskida (Keathley Canyon [KC] 292) and Leon (KC 642) discoveries in KC in the Subsalt province. Kaskida discovery consists of a three-way closure against a salt feeder. Leon discovery consists of a four-way closure below salt. See Figure 5B for location of profile. Reprinted with permission of PGS. Data are proprietary to MKI.

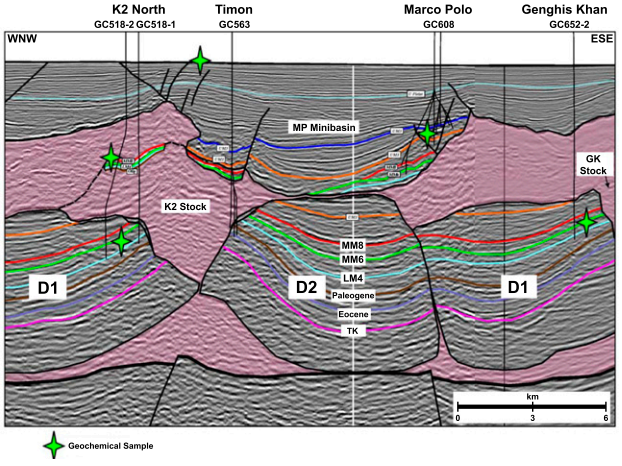

Figure 15. Regional seismic profile across the K2 North, Timon, Marco Polo (MP), and Gengis Khan (GK) fields in the Subsalt province of southern Green Canyon (GC). Note the subsalt truncation traps for the three subsalt fields. See Figure 5B for location of profile. After Mount et al. (2006). Republished by permission of the Gulf Coast Association of Geological Societies, whose permission is required for further publication use. Horizon abbreviations: LM4 = lower Miocene 4; MM6 = middle Miocene 6; MM8 = middle Miocene 8; TK = top Cretaceous.

in regulatory action and a subsequent decrease in discoveries.

The first two deep-water exploration plays—flex trend and minibasins—occurred in the Basins province (Figure 5). In the early to mid–1980s, exploration companies started drilling in greater than 1500 ft (457 m) water depth, focused on drilling in the flex trend, which is the upper slope basinward of the present shelf edge. Discoveries generally had small reserves in reservoirs comprising channel-fill sediments and thin beds in levees. Because of the relatively small reserves and improving drilling technology, exploration activity then moved into the deep water of the middle slope, where larger fields were discovered, such as Mars (800 million BOE), Ursa (500 million BOE), and Mensa (1.2 tcf), all notable fields for their pioneering development.

The third exploration play was in the deep-water fold belts. One exploration well was drilled in this Mississippi Fan fold belt (albeit 8 yr earlier) before the first discovery (Neptune: AT 575; Figures 5; 10B, C; 11) in 1995. In the Perdido fold belt, three wells were drilled before the first commercial discovery (Great White: Alaminos Canyon 857; Figures 5; 10B, C; 11) in 2002.

The fourth exploration play was the subsalt play; subsalt discoveries were initially made on the shelf, and then slowly exploration moved to the middle to lower slope during the 1990s, with more exploration wells drilled since 2000. Initial discoveries were made in areas where the salt partially overhung the prospects. Later discoveries were made where the shallow allochthonous salt extended across the entire prospect field. Finally, the Mesozoic play saw its first exploration success in 2004; since then, there have been three additional discoveries as well as several noncommercial discoveries and dry holes (Tables 6–8). Five exploration wells were drilled before the first commercial discovery was made in 2009 (Rojas, 2015).

The continued evolution in exploration plays has had a major effect on sustained reserve growth by year (Figure 21) and cumulatively (Figure 22). Reserves grew at the highest rates between 1995 and 2001 and have continued to grow more slowly since that time. One challenge in compiling these data is that the sizes of the subsalt fields have not been announced.

The exploration results summarized in Figures 20–22 indicate several important aspects of the deep-water play for the northern deep-water Gulf of Mexico; by analogy, these findings are also important

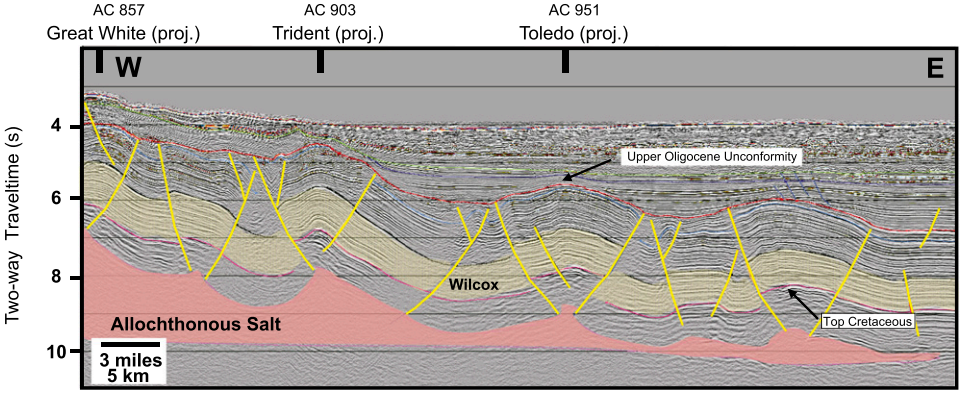

Figure 16. Regional seismic profile across the Perdido fold belt showing the box folds that decrease in height from west to east (left to right). Fold 4 is closest to the Great White and Trident discoveries. See Figure 5B for location of profile. After Zarra (2007a). Reproduced with permission of the Gulf Coast Section SEPM Foundation, and any other use requires their permission. AC = Alaminos Canyon; proj. = projected.

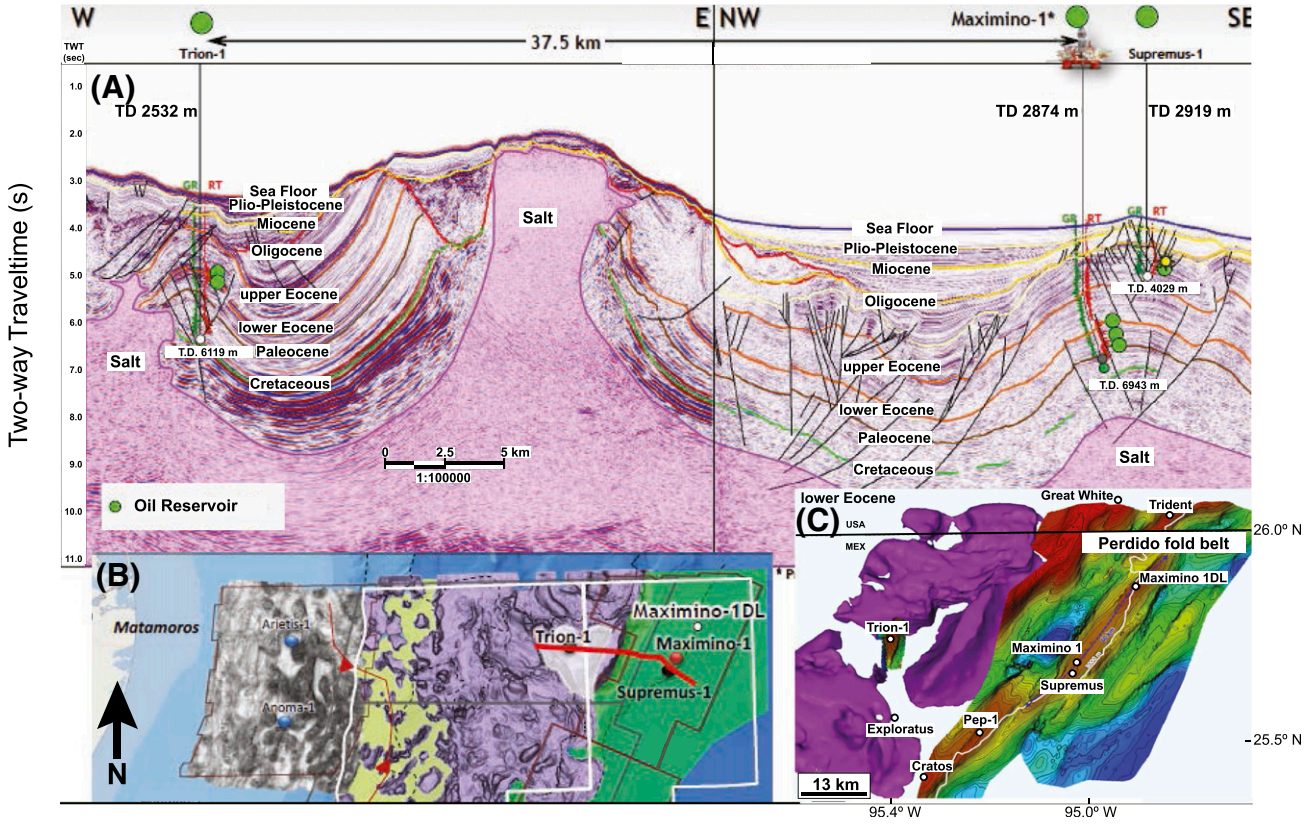

Figure 17. (A) Regional seismic profile across the Trion and Perdido fold belt structures in the northwestern deep-water Gulf of Mexico. Locations of Trion, Maximino, and Supremus wells are shown. (B) Map showing location of the seismic profile in (A). From west to east, light blue = shelf; gray = upper slope; light green = middle slope; purple = lower slope with shallow allochthonous salt; white = Trion structure; green and light blue = undifferentiated abyssal plain. (C) Lower Eocene structure contour map of Perdido fold belt and Trion structure. Depth gradient is red (shallow) to blue (deep). Purple = lower slope with shallow allochthonous salt. After Colmenares (2014). Reprinted with permission of AAPG. 1DL = 1 delineation; GR = gamma ray; MEX = Mexico; Plio = Pliocene; RT = resistivity; TD = total depth. Note: A color version can be seen in the online version.

for many global deep-water basins. First, because drilling technology and seismic imaging have improved, new plays have developed. Second, because new drilling provinces have opened, reserve growth has remained high. Finally, exploration continues today in all of these provinces. The economics of drilling and development discoveries in each province vary considerably. Where development infrastructure exists in a province (middle to upper slope), smaller companies can economically develop fields with smaller reserves (Table 2).

Field Sizes

The sizes of the reserves of the 50 largest fields and discoveries in the northern deep-water Gulf of Mexico are shown in Figure 23. Note that only 24 fields have reserves larger than 300 million BOE, and 38 fields have more than 200 million BOE in reserves; the remaining 186 fields are less than 200 million BOE. The average reserve size for fields in the northern deep-water Gulf of Mexico is 77 million BOE (Beaubouef, 2015). A common theme in many fields is that although there are reservoir-quality sands present in multiple depositional sequences, commonly only some of the sands are charged. Thus, many structures could potentially hold considerably more petroleum if they were fully charged.

Reservoir Quality

When companies decide whether to develop a discovery, one challenge is determining the overall reservoir quality. In many cases, the reservoirs are so

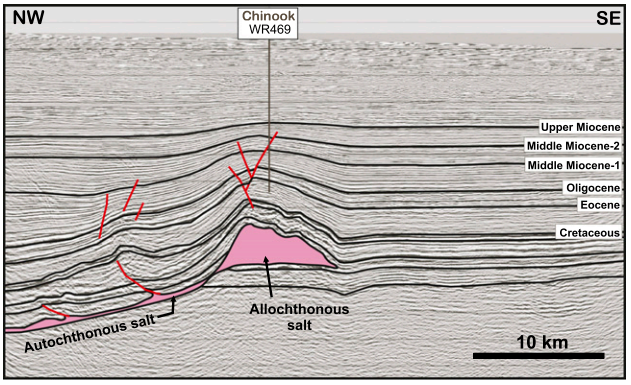

Figure 18. Regional seismic profile across the Chinook field in the Keathley–Walker fold belt. Fold is underlain by Lower Cretaceous allochthonous salt. Note the thinning of the Wilcox Formation across the crest of the fold, indicting the bathymetric expressions of the folds during the late Paleocene–early Eocene. See Figure 5B for location of profile. Modified from Mount et al. (2007). Reproduced with permission of the Gulf Coast Section SEPM Foundation, and any other use requires their permission. WR = Walker Ridge.

deep below the sea floor that predictive models have inaccurate results. For proprietary reasons, companies do not publish the details of reservoir quality until plays have matured and fields have been producing for some time. However, the little publicly available information, reviewed below, indicates that overall reservoir quality is loosely correlated with reservoir age, specifically for fields with reservoirs from the Upper Jurassic (Figure 10A), upper Paleocene–lower Eocene (Figure 10A), or Neogene (Figure 10B–I).

Neogene Reservoirs

The Neogene fields were the first reservoirs discovered and developed in the northern deep-water Gulf of Mexico (Figures 10B–I; 21). In the Basins province, the Miocene and Pliocene sands have relatively high porosity and permeability resulting from less compaction and diagenesis and, locally, lower geothermal gradients. Taylor et al. (2010) noted that the reservoir sands fall within a relatively narrow range in grain size (80–120 μm), are moderately sorted, have variable compositions but similar mechanical properties (within local areas), and are typically overpressured. Overpressure develops in the shallow subsurface, helping to preserve porosity and permeability by decreased rates of compaction. In addition, low geothermal gradients in the region contribute to the decreased rates in diagenesis; today, the reservoir temperatures are less than 80°C (176°F) and thus are not adversely affected by quartz and other kinds of cementation. From the sea floor to 4500-m (14,764-ft) subsurface depth, mechanical compaction, as a function of effective vertical stress, is the main control on sand porosity.

For Miocene reservoir quality in the Subsalt province, Taylor et al. (2010) discussed the effect of allochthonous salt on the subsalt's geothermal gradient and rates of diagenesis. Because the overlying salt is highly conductive, it draws heat away from the sediment below, thus decreasing the sediment's geothermal gradient. To reach this conclusion, Taylor et al. (2010) compared the reservoir quality from two subsalt wells at the same subsurface depth—Tahiti (Green Canyon 640) and Poseidon (Mississippi Canyon 727). Taylor et al. (2010) found that the Tahiti reservoir was approximately 30°C (86°F) cooler than the regional geothermal gradient, whereas the Poseidon reservoir was 40°C (104°F) higher than Tahiti, closer to the measured geothermal gradient. The Tahiti reservoir may also have been affected by its close proximity to the salt feeder that forms the field's trap (Figure 15). Poseidon's higher reservoir temperature enhanced development of quartz overgrowths, effectively causing reservoir quality to degrade significantly. Taylor et al. (2010) concluded that the timing of emplacement, thickness of salt, burial depth of the reservoir, and vertical separation are likely important factors in controlling the magnitude of thermal suppression on quartz cementation.

Upper Paleocene–Lower Eocene Reservoirs

The reservoir quality of the upper Paleocene–lower Eocene deep-water Wilcox reservoirs is, in general, considerably lower than the Neogene sands. To date, six fields are producing from the Wilcox in pairs: Great White–Tobago, Cascade–Chinook, and Jack–St. Malo (Figure 10A; Tables 3, 4). Eikrem et al. (2010) summarized the reservoir quality of the deep-water Wilcox in the Great White field, a suprasalt field, with average porosity values in the shallower producing reservoir sandstones of 25%–30% and permeabilities of 50–250 md. Deeper, nonproducing reservoir sands have lower porosities (<15%) and permeabilities (average of 2 md). In contrast, the subsalt fields have lower porosity and permeability values in the Wilcox reservoirs than those of the Great White field. The following

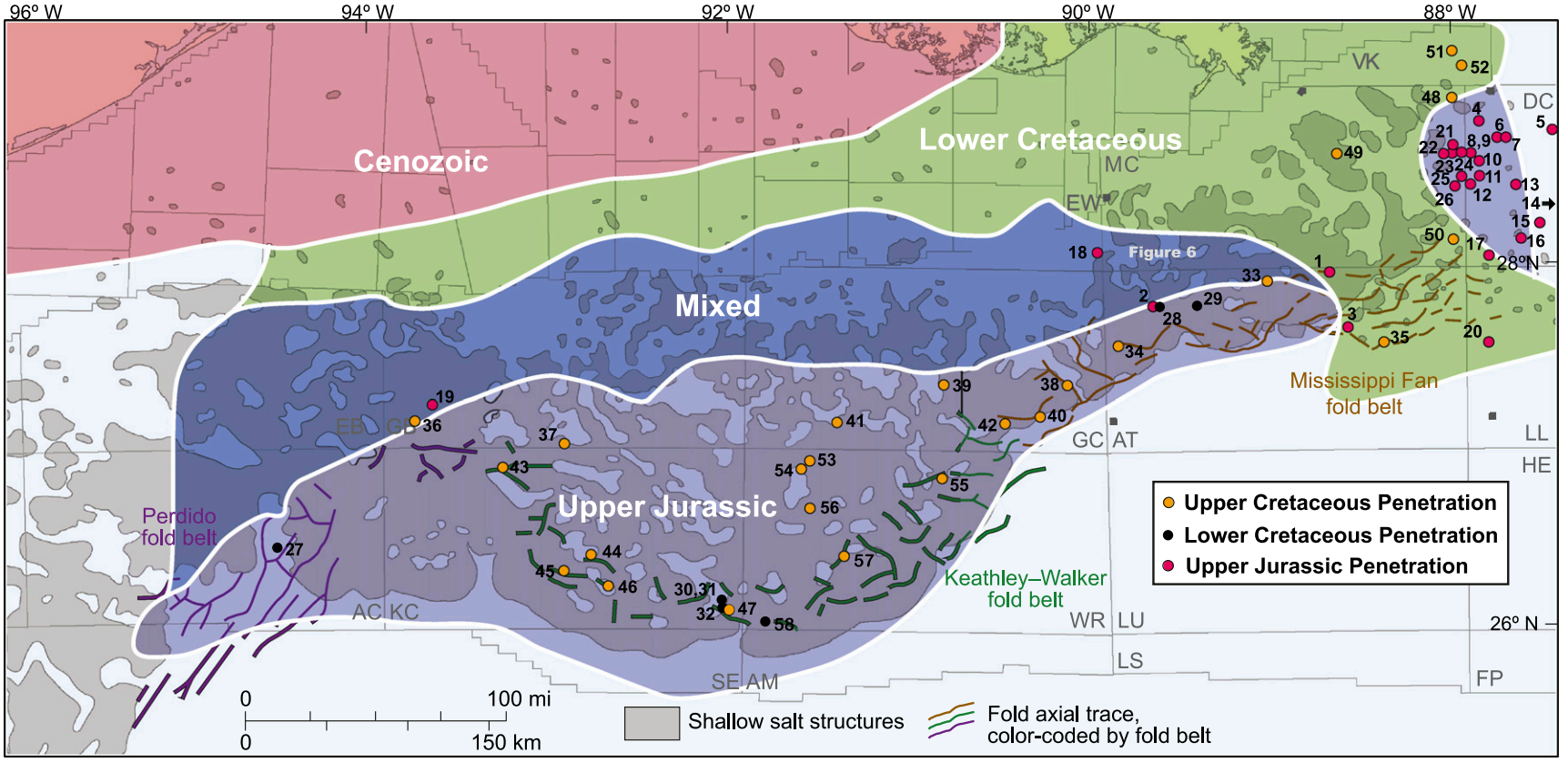

Figure 19. Map showing the distribution of different ages of source rocks and the Upper Cretaceous Chicxulub deposit (after Denne et al., 2013) are shown by numbered circles (see Tables 6–8). Note that well 14 is present east of the figure. Modified and reprinted with permission of John Zumberge and GeoMark Research. Abbreviations for protraction areas: AC = Alaminos Canyon; AM = Amery Terrace; DC = DeSoto Canyon; EB = East Breaks; EW = Ewing Bank; FP = Florida Plain; GB = Garden Banks; GC = Green Canyon; HE = Henderson; KC = Keathley Canyon; LL = Lloyd Ridge; LS = Lund South; LU = Lund; MC = Mississippi Canyon; SE = Sigsbee Escarpment; VK = Viosca Knoll; WR = Walker Ridge.

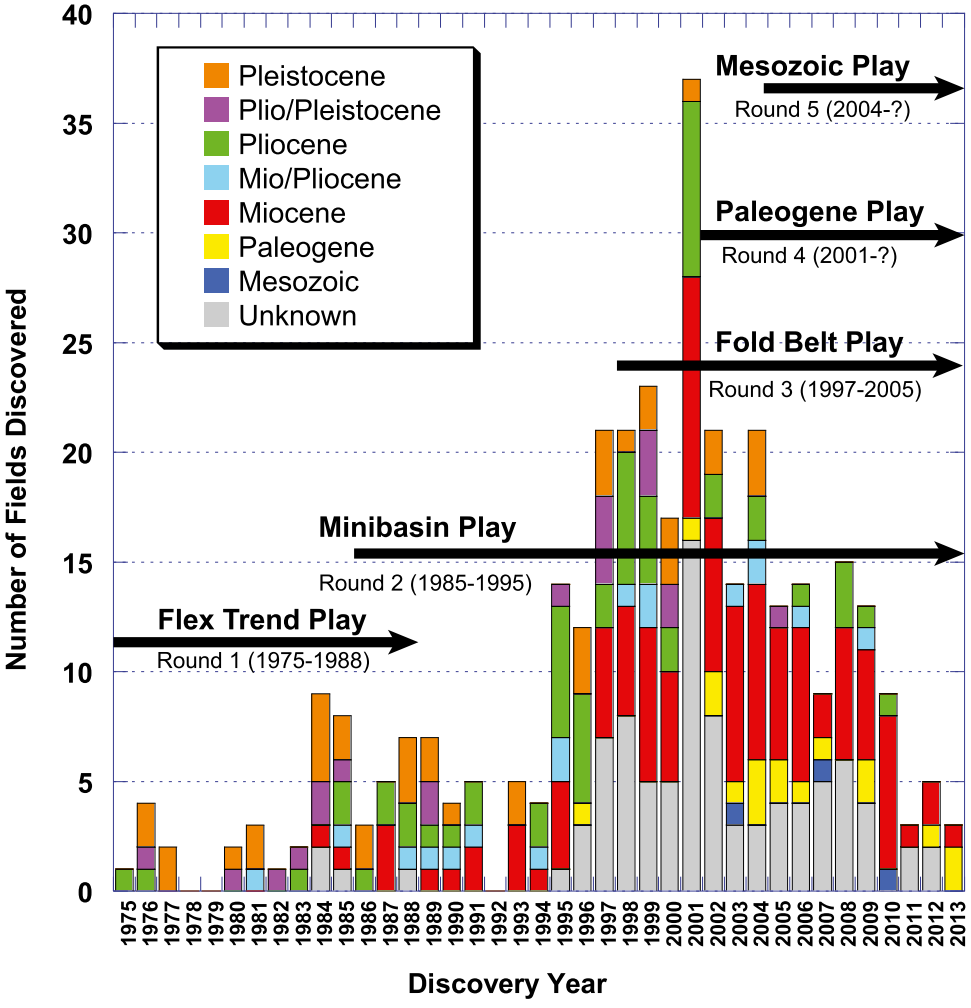

Figure 20. Graph shows the number of discoveries in the northern Gulf of Mexico by year for water depths greater than 200 m (650 ft), the ages of the reservoirs, and the timing of five major exploration plays. Mio = Miocene; Plio = Pliocene.

summary of the subsalt deep-water Wilcox reservoirs is based on several presentations (Zarra, 2007a; Cearley, 2011; Kane and Ponton, 2012; Sullivan et al., 2014; Marchand et al., 2015).

The main factors in controlling the porosity and permeability are the depositional elements, composition and mineralogy of the sandstones, basic sedimentology of the units, and depth of burial. Channel-fill strata have the highest permeability values, with average values of 40 and up to 400 md for maximum values. Channel-lobe transition sands average 17 md, and permeability values decrease to the lobes' fringes. Silt content is higher in the Wilcox than in the Neogene reservoirs. Channel-fill reservoir sands have 20% silt content, increasing to 55% in the lobe fringe. The presence of silt affects permeability much more than porosity; a decrease of 2% to 3% in porosity has a more significant effect in permeability reduction. In addition, the Paleogene sands have greater amounts of ductile grains (20%) than most Miocene sands (5%). Finally, trunk channels have fewer ductile grains, and the amounts tend to increase in the lobe deposits.

As the depths of the reservoirs increase, the amount of quartz cementation is also an important factor. In general, deeper wells have higher bottomhole temperatures, and they may have more cementation. In some cases, the effects of higher temperature can be mitigated by proximity to adjacent or overlying salt bodies, which tend to draw off some excess heat.

Sullivan et al. (2014) noted that porosity and permeability values are dependent on reservoir elements and depth, and they identified three groupings. First, the channel-fill reservoirs of the Wilcox 1A unit, the youngest sandstone unit of Zarra (2007a), have the best porosity and permeability, up to 400 md. Second, the slightly deeper Wilcox 2 channel-fill reservoirs have porosity values that are lower than the channel fill of Unit 1A and slightly lower

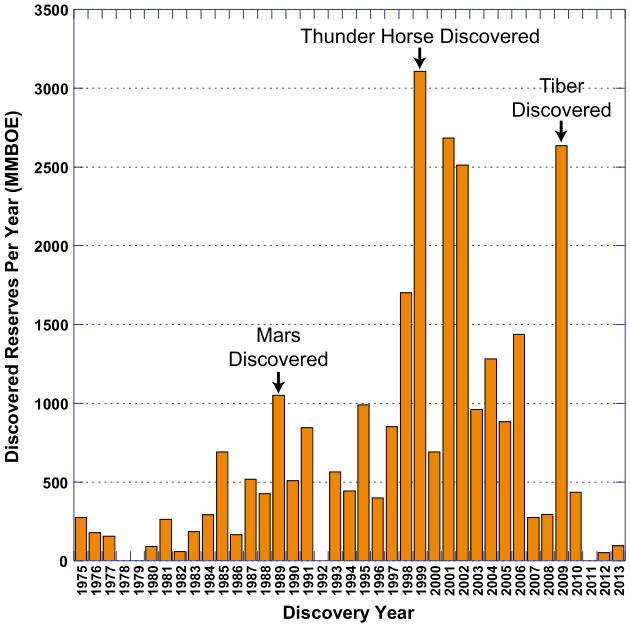

Figure 21. Graph shows the volume of reserves in the northern Gulf of Mexico discovered by year for water depths greater than 200 m (650 ft). Largest discoveries include Mars (1989, Basins province), Thunder Horse (1999, Miocene Subsalt province), and Tiber (2009, Eocene Subsalt province).

permeability. Third, Wilcox 1A lobes have lower permeability and porosity values because of the increased presence of turbidites with linked debrites (transitional flow deposits) throughout the section, especially in the middle to outer lobes. Kane and Ponton (2012) noted that an individual transitional flow deposit is typically 1 to 10 cm thick, with some thicker amalgamated bedsets up to 3 m (10 ft); however, only the turbidite part of the sand has effective porosity and permeability. As a consequence, the potential reservoir is possibly 50%–70% of the deposit.

Cearley (2011) compared the reservoir quality of representative suprasalt Miocene and subsalt Wilcox wells, noting five significant differences. (1) Net reservoir thicknesses range from 150 ft net pay for Miocene to 700 ft net pay for Wilcox. (2) Average permeability values range from 500 (Miocene) to 15 md (Wilcox). (3) The permeability × thickness values are 75,000 and 10,500 md ft, respectively. (4) Initial subsurface pressure may be the same for both at 20,000 psi; however, once production begins, drawdown pressures are less than 1000 psi for Miocene versus greater than 3000 psi for Wilcox. (5) Finally, initial production rates for the Miocene are greater than 20,000 versus 10,000 BOPD for the Wilcox.

Upper Jurassic Reservoirs

Reservoir quality in the Upper Jurassic (Oxfordian) Norphlet eolian reservoirs in the northeastern deep-water Gulf of Mexico (Figure 10A) is also of concern for field development. Based on core analyses from three wells, Douglas (2010) identified seven lithofacies in the Norphlet, two of which form the reservoir facies—grain-flow deposits and wind ripples. Based on the depth and age of the reservoirs, diagenetic models would have suggested low effective porosity and permeability. However, the Norphlet reservoirs in the deep-water Gulf of Mexico have a unique diagenetic history where chlorite grain coats have developed authigenically around the individual sandstone grains (Douglas, 2010; Godo, in press). The presence of the chlorite inhibited the development of authigenic quartz and microquartz, both of which occlude porosity and permeability, keeping pore throats open by preventing quartz from nucleating onto sand-grain surfaces. Similar petrographic relationships have been described in the Norphlet fields both onshore and in the shallow shelf of the northern Gulf of Mexico (Ajdukiewicz et al., 2010; Taylor et al., 2010), although more chlorite is present

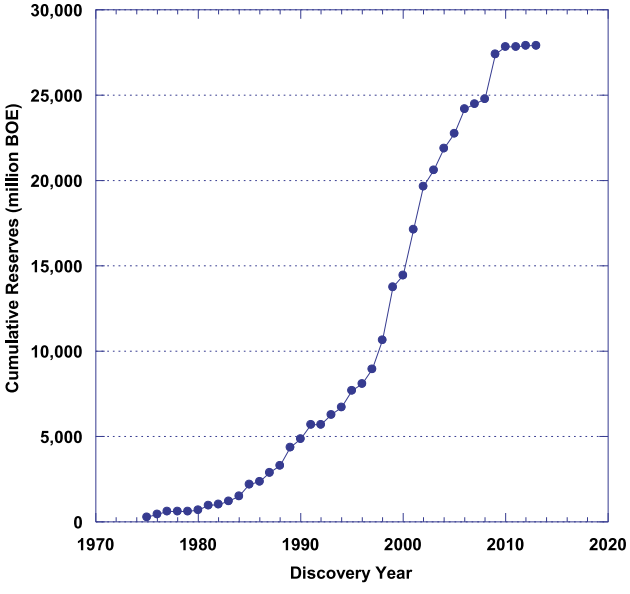

Figure 22. Graph shows the cumulative addition of reserves by year for water depths greater than 600 ft (183 ft) in the northern Gulf of Mexico.

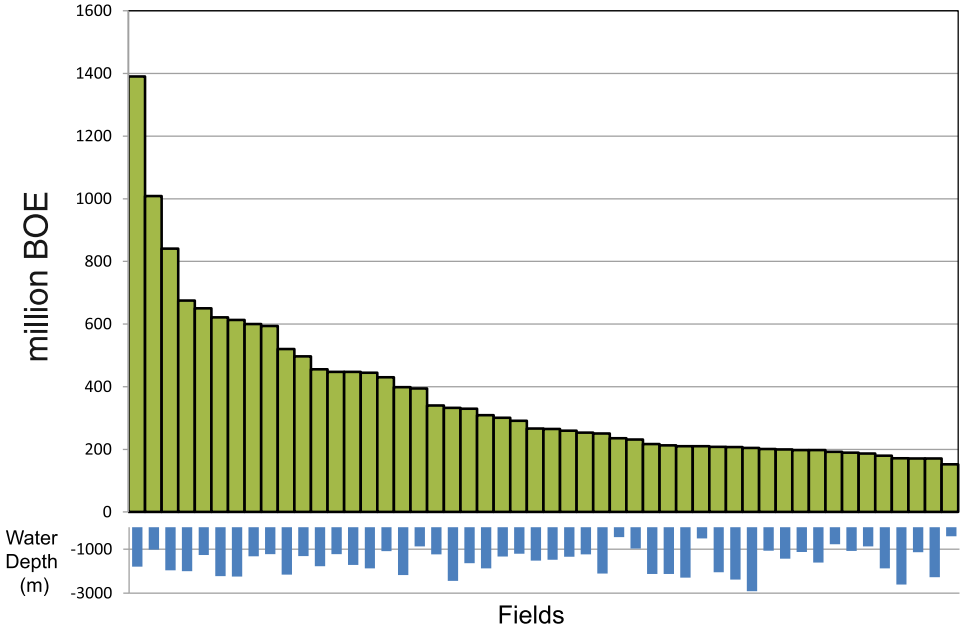

Figure 23. Graph showing the distribution of the largest 50 fields by reserves in the northern deep-water Gulf of Mexico. Lower graph shows the water depth of each discovery. Note that only 16 fields are 300 million BOE or larger. Figure is provided by IHS.

in the shallow water fields, and they consequently have lower porosity values.

STUDY AREA—THIS ISSUE

The study area for this theme issue is located in the northeastern, central, and southern Mississippi Canyon; the northern Atwater Valley; and the easternmost parts of the DeSoto Canyon and Lloyd Ridge protraction areas (Figures 1, 24). Historically, a significant part of the early petroleum exploration in the northern deep-water Gulf of Mexico occurred in this area. This area contains 86 fields and discoveries (Weimer et al., 2017d, this issue), including several of the larger fields in the northern deep-water Gulf of Mexico (Mars, Thunder Horse, Ursa, Appomattox, Thunder Horse North, Tubular Bells, Princess, Sturgis, Vicksburg).

The study area includes parts of all four of the discrete geologic-exploration provinces summarized above—Basins, Subsalt, Fold Belt (Mississippi Fan fold belt), and Abyssal Plain (Figures 5, 24). Water depths range from 437 to 2745 m (1500 to 9000 ft) (Figure 1). In the southern Mississippi Canyon and northernmost Atwater Valley protraction areas, the continental slope has a highly irregular bathymetry, caused by extensive shallow-salt deformation. Bathymetric highs are caused by shallow allochthonous salt, and the intervening low areas form the intraslope basins.

DATABASE

The database for this issue consists of a regional seismic data set, more-detailed seismic data sets, wire-line logs, and biostratigraphy. For the regional study, approximately 12,165 mi (19,550 km) of two-dimensional regional seismic data were interpreted (see figure 3 in Bouroullec and Weimer, 2017, this issue). These data are 24- and 48-fold and were collected in the 1980s. Using newer seismic data with better acquisition and processing parameters would certainly lead to a more robust interpretation, especially for the subsalt structures and Mesozoic stratigraphy. Nonetheless, we believe that the older seismic data still provide valuable insights in the evolution of the geology of the area.

Of the more than 600 wells in the area, we studied 120 exploration wells that were all straight holes. Synthetic seismograms and time-based logs were generated for all 120 wells. We also studied the biostratigraphy from 115 wells, combining data from private sources and the Minerals Management Service (now Bureau of Ocean Energy Management). The biostratigraphic data include foraminifera, calcareous nannoplankton, and high-resolution foraminifera studies. These data allowed us to establish the age dates for the sequence stratigraphic framework.

Finally, for the detailed study of the Mensa and Thunder Horse minibasins (Figure 24), we interpreted three-dimensional (3-D) seismic data, wire-line logs, and biostratigraphic data from six wells. The 3-D

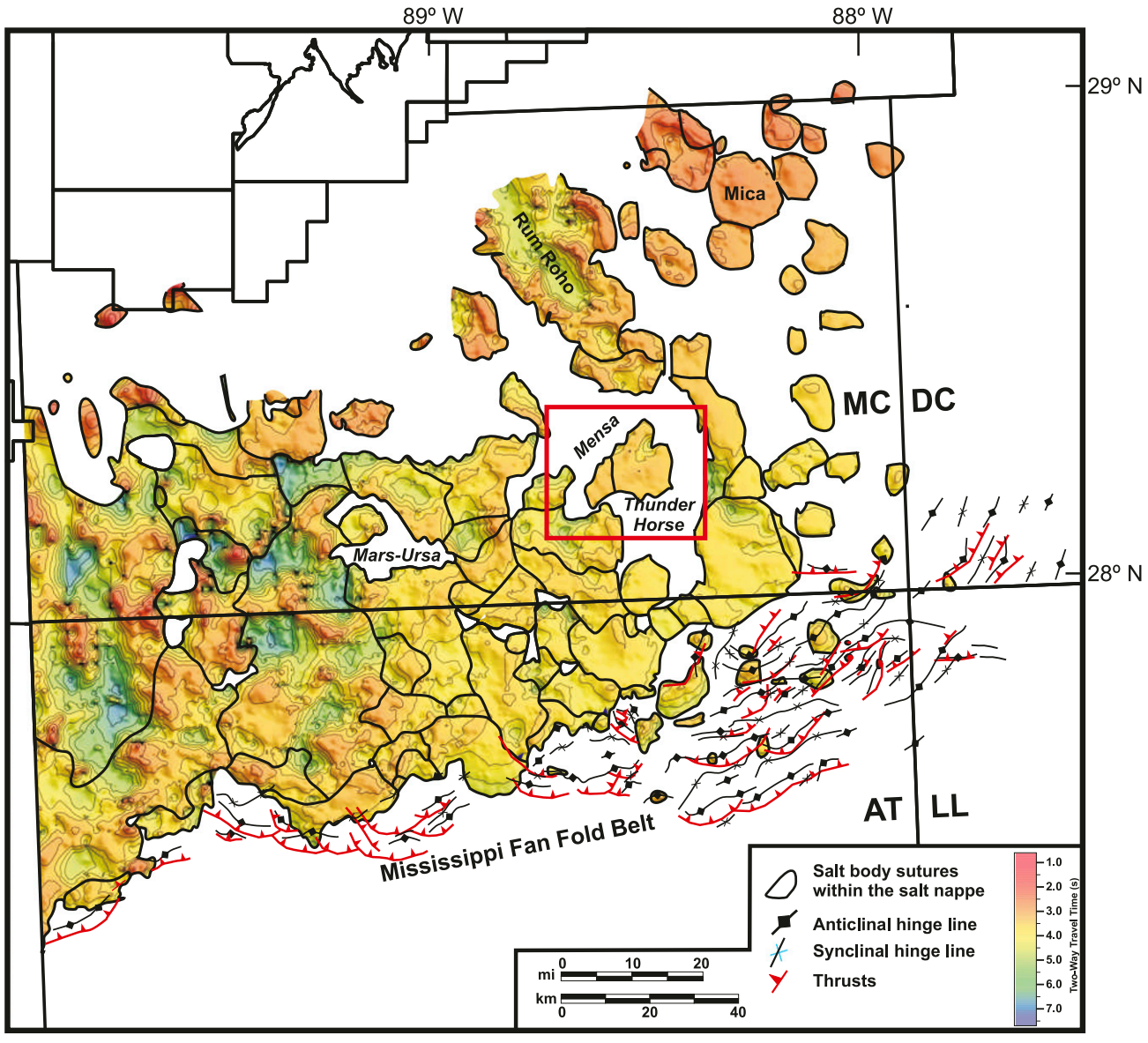

Figure 24. Map showing the outline of the study area in Mississippi Canyon (MC), northern Atwater Valley (AT), westernmost DeSoto Canyon (DC), and western Lloyd Ridge (LL) protraction areas, northern deep-water Gulf of Mexico. Top of Neogene allochthonous salt is shown in two-way traveltime. The Neogene salt consists of a large nappe (Sigsbee Escarpment) in the central and western parts of the area and isolated salt bodies or complexes in the northern, eastern, and four-corners areas. Salt sutures within the salt nappe are shown by the heavy solid line. Red (in online version) box shows the outline of the three-dimensional study area.

seismic data set consists of post-stack time-migrated, minimum-phase, 32-bit seismic data. The data set is 378 mi^2 (979 km^2) in area: 21 mi (34 km) in the east–west direction and 18 mi (29 km) in the north–south direction.

OBJECTIVES OF THESE PAPERS

The following seven papers in this *AAPG Bulletin* theme issue summarize the petroleum systems of the Mississippi Canyon and Atwater Valley protraction areas, northern deep-water Gulf of Mexico (Figures 1, 5, 24). The papers illustrate how we used integrated stratigraphic and structural studies to analyze the petroleum systems and timing of petroleum generation in the area. The latter analyses can only be evaluated once a considerable amount of regional and local geologic interpretation has been done.

Two groups of papers describe different aspects of the area. The first four papers address the

subregional setting in terms of its structural geology, linked tectonics and stratigraphic evolution, and petroleum systems.

1. Weimer et al. (2017d) document the general setting of 86 fields and discoveries, including seismic reflection expression, wire-line logs, and a brief summary of the reservoir. Fields produce from structural (four kinds of traps), combined structural-stratigraphic (three kinds of traps), and stratigraphic traps. A total of 86 fields and discoveries are evaluated: 19 comprise structures with four-way closures, 50 have three-way closures, and 17 are stratigraphic traps. Four of these discoveries are in Upper Jurassic eolian reservoirs; the remainder are in Neogene deep-water reservoirs. Importantly, the purpose of this field atlas is to provide the basis for the following three papers, such that the origins of the fields can be described in terms of the timing of development of their traps, reservoirs, seals, and charging.
2. Bouroullec and Weimer (2017) document the complexity of the regional structural setting. A complex, multilayer allochthonous salt system is present with three periods of shallow-salt emplacement (Barremian, late Cretaceous, and middle Miocene to present). Four kinds of salt systems are present: basement controlled, stepped counterregional, roho, and fold-belt related. A detailed study of the Neogene allochthonous salt systems is used to build conceptual kinematic models.
3. Bouroullec et al. (2017b) describe the structural evolution of the study area, which consists of a complex geological history influenced by basement structures, multiple stages of salt movement, gravitational gliding, and strike-slip movements. Basement structures were the primary control on early salt kinematics, affecting gravity-driven slope deformation and resulting in a wide variety of structural styles. Salt from the autochthonous and two Cretaceous allochthonous salt layers was expelled vertically and basinward during the Neogene, feeding the younger allochthonous salt systems. The autochthonous and early allochthonous salt layers were used as detachments for many of the large Neogene extensional structures (growth faults and turtles) and contractional structures (anticlines and thrust faults), whereas the Neogene allochthonous salt system accommodated suprasalt minibasins associated with counterregional and roho salt systems. These three allochthonous salt layers were successively loaded by gravity-flow sediments, resulting in the formation of deep (above autochthonous or early allochthonous salt layers) and shallow (supra-Neogene allochthonous salt) minibasins and local development of extensive salt welds. Northwest–southeast-oriented strike-slip structures, active during the Neogene, are present in the salt province within the study area. They are related to basin-wide heterogeneities in the original and subsequent salt distribution and are controlled by differential basinward movements of adjacent suprasalt minibasins.
4. Bouroullec et al. (2017a) analyze the tectono-stratigraphic evolution of the area at 11 discrete intervals between 24 Ma and present. Four external stratigraphic forms—troughs, bowls, wedges, and sheets—are identified and integrated with the results of the structural study to understand the changing shape of suprasalt basins during the Neogene. The analyses show how the allochthonous salt systems evolved over time and how they affected sedimentation patterns and the evolution of the individual basins.

   Most of the fields in the study area are contained within sheetlike or wedge-shaped stratigraphic intervals and have four-way or three-way trapping configurations. These findings indicate the profound effect of mobile salt on the petroleum geology of the region.

The final three papers describe the geology and evolution of the Mensa and Thunder Horse fields in adjacent minibasins. The fields are significant because Thunder Horse and Mensa are two of the largest oil and gas fields, respectively, in the northern deep-water Gulf of Mexico.

First, Weimer et al. (2017a) summarize the stratigraphic evolution of the middle to late Miocene in the two basins. The Thunder Horse reservoir sands were deposited in amalgamated sheet and amalgamated channel-fill units within a major paleobathymetric low. Later turtle formation created the trap for the field and a paleobathymetric high. Channelized sands were diverted around and deposited on the flanks of the turtle. At 9.0 Ma, Mensa's sheet-sand reservoir represents a different setting; sands were deposited near the

crest of the Mensa turtle, which had subtle bathymetric expression.

Second, Weimer et al. (2017b) document the linked structural evolution of the two basins from the Early Cretaceous through the late Miocene. Structural features and associated minibasins evolved during several discrete intervals. From 99 to 24 Ma (latest Early Cretaceous through latest Oligocene), an extensive allochthonous salt canopy was present within the Mensa and Thunder Horse minibasins. During this interval, sediments loaded the salt, forming thin wedge- and sheet-form deposits in the Mensa area and a thick, northwest-trending trough in the Thunder Horse area. A secondary allochthonous salt system extruded at the Top Cretaceous level, as evinced by remnant salt bodies. Salt withdrawal from these allochthonous salt systems provided accommodation for bowl- and trough-shaped external stratigraphic forms during the Miocene. High sedimentation rates produced salt evacuation from these allochthonous salt systems and initiated diapirism that formed the Neogene allochthonous salt level. The prominent turtle structures in the two minibasins, critical to the formation of traps to the two major fields, developed at slightly different times: Thunder Horse at 14.35 and Mensa at 11.4 Ma.

Finally, Weimer et al. (2017c) analyze the petroleum systems to explain the distribution of fluids in the Mensa (gas) and Thunder Horse (oil) fields. They conclude that the original allochthonous salt underlying the Mensa minibasin was thicker than in the Thunder Horse area, providing more accommodation for sediments to accumulate. Consequently, the Thunder Horse turtle structure formed 1–2 m.y. before the Mensa structure, and source rocks matured earlier. Today, the source rocks below Mensa are in the dry-gas window, whereas the source rocks underlying Thunder Horse are in the wet-gas generation window.

In summary, these eight papers allow the reader the opportunity to view and analyze different aspects of the petroleum systems of one important part of a deep-water basin in the northern deep-water Gulf of Mexico. Although each paper can be read separately, we suggest that they be read in the order of presentation to follow the petroleum systems logic. Our hope is that these papers can be used as an analog for many other deep-water basins in the world.

REFERENCES CITED

Ajdukiewicz, J. M., P. H. Nicholson, and W. L. Esch, 2010, Prediction of deep reservoir quality using early diagenetic process models in the Jurassic Norphlet Formation, Gulf of Mexico: AAPG Bulletin, v. 94, no. 8, p. 1189–1227, doi:10.1306/04211009152.

Beaubouef, B., 2015, Gulf E&P remains active despite falling oil prices: Offshore Magazine, accessed October 26, 2016, http://www.offshore-mag.com/1/volume-75/issue-1/gom/gulf-e-p/gulf-e-p-remains-active-despite-falling-oil-prices-full.html.

Bouroullec, R., and P. Weimer, 2017, Geometry and kinematics of Neogene allochthonous salt systems in the Mississippi Canyon, Atwater Valley, western Lloyd Ridge, and western DeSoto Canyon protraction areas, northern deep-water Gulf of Mexico: AAPG Bulletin, v. 101, no. 7, p. 1003–1034, doi:10.1306/09011609186.

Bouroullec, R., P. Weimer, and O. Serrano, 2004, Salt tectonic history of the northeastern deep Gulf of Mexico: Gulf Coast Association of Geological Societies Transactions, v. 54, p. 63–80.

Bouroullec, R., P. Weimer, and O. Serrano, 2017a, Petroleum geology of the Mississippi Canyon, Atwater Valley, western DeSoto Canyon, and western Lloyd Ridge protraction areas, northern deep-water Gulf of Mexico: Traps, reservoirs, and tectono-stratigraphic evolution: AAPG Bulletin, v. 101, no. 7, p. 1073–1108, doi:10.1306/09011610093.

Bouroullec, R., P. Weimer, and O. Serrano, 2017b, Regional structural setting and evolution of the Mississippi Canyon, Atwater Valley, western Lloyd Ridge, and western DeSoto Canyon protraction areas, northern deep-water Gulf of Mexico: AAPG Bulletin, v. 101, no. 7, p. 1035–1071, doi:10.1306/09011609187.

Camerlo, R. H., and E. F. Benson, 2006, Geometric and seismic interpretation of the Perdido fold belt: Northwestern deep-water Gulf of Mexico: AAPG Bulletin, v. 90, no. 3, p. 363–386, doi:10.1306/10120505003.

Cearley, J., 2011, The discovery of the lower Tertiary trend in the deepwater Gulf of Mexico: Discovery thinking talk, AAPG Annual Convention and Exhibition, accessed May 2, 2017, http://www.aapg.org/videos/discovery-thinking/articleid/37031/james-cearley-the-discovery-of-the-lower-tertiary-trend-in-the-deepwater-gulf-of-mexico.

Cole, G. A., A. Yu, F. Peel, J. DeVay, B. Bernard, J. Zumberge, and S. Brown, 2001a, Constraining source and charge risk in deepwater areas: World Oil, v. 2001, no. 10, p. 69–77.

Cole, G. A., A. Yu, F. Peel, C. H. Taylor, R. Requejo, J. DeVay, J. Brooks, B. Bernard, J. Zumberge, and S. Brown, 2001b, The deep water Gulf of Mexico petroleum system: Insights from piston coring, defining seepage, anomalies, and background, *in* R. H. Fillon, N. C. Rosen, P. Weimer, A. Lowrie, H. Pettingill, R. L. Phair, H. H. Roberts, and B. van Hoorn, eds., Petroleum systems of deep-water basins: Global and Gulf of Mexico experience: Gulf Coast Section SEPM Foundation 21st Annual Bob F.

Perkins Research Conference, Houston, Texas, December 2–5, 2001, p. 315–342, doi:10.5724/gcs.01.21.0315.
Colling, E. L., R. J. Alexander, and R. L. Phair, 2001, Regional mapping and maturity modeling for the northern deep water Gulf of Mexico, *in* R. H. Fillon, N. C. Rosen, P. Weimer, A. Lowrie, H. Pettingill, R. L. Phair, H. H. Roberts, and B. van Hoorn, eds., Petroleum systems of deep-water basins: Global and Gulf of Mexico experience: Gulf Coast Section SEPM Foundation 21st Annual Bob F. Perkins Research Conference, Houston, Texas, December 2–5, 2001, p. 87–110, doi:10.5724/gcs.01.21.0087.
Colmenares, M., 2014, The Perdido and the southwestern Gulf of Mexico: AAPG Search and Discovery article 30331, accessed October 26, 2016, http://www.searchanddiscovery.com/documents/2014/30331colmenares/ndx_colmenares.pdf.
Day-Stirrat, R. J., P. B. Flemings, Y. You, A. C. Aplin, and B. A. van der Pluijm, 2012, The fabric of consolidation in Gulf of Mexico mudstones: Marine Geology, v. 295–298, p. 77–85, doi:10.1016/j.margeo.2011.12.003.
Denne, R. A., E. Scott, D. Eickhoff, J. Kaiser, R. J. Hill, and J. M. Spaw, 2013, Massive Cretaceous-Paleogene boundary deposit, deep-water Gulf of Mexico: New evidence for widespread Chicxulub-induced slope failure: Geology, v. 41, p. 983–986, doi:10.1130/G34503.1.
Douglas, S. W., 2010, The Jurassic Norphlet Formation of the deepwater eastern Gulf of Mexico: A sedimentologic investigation of eolian facies, their reservoir characteristics, and their depositional history, master's thesis, Baylor University, Waco, Texas, 59 p.
Eikrem, V., R. Li, M. Medeiros, B. J. McKee, E. E. Shumilak, B. L. Boswell, and R. Mohan, 2010, Perdido development project: Great White WM12 Reservoir and Silvertip M. Frio Field, development plans and comparison of recent well results with pre-drill models: Offshore Technology Conference, Houston, Texas, May 3–6, 2010, 10 p.
Galloway, W. E., 2008, Depositional evolution of the Gulf of Mexico sedimentary basin, *in* A. D. Miall, ed., The sedimentary basins of the United States and Canada: Sedimentary Basins of the World 5, p. 505–549.
Galloway, W. E., P. E. Ganey-Curry, X. Li, and R. T. Buffler, 2000, Cenozoic depositional history of the Gulf of Mexico basin: AAPG Bulletin, v. 84, no. 11, p. 1743–1774.
Galloway, W. E., T. L. Whiteaker, and P. E. Ganey-Curry, 2011, History of Cenozoic North American drainage basin evolution, sediment yield, and accumulation in the Gulf of Mexico basin: Geosphere, v. 7, p. 938–973, doi:10.1130/GES00647.1.
Gibson, R., 2012, A methodology to incorporate salt evolution in three-dimensional basin models: Application to regional modeling of the Gulf of Mexico, *in* K. E. Peters, D. J. Curry, and M. Kacewicz, eds., Basin modeling: New horizons in research and applications: AAPG Hedberg Series 4, p. 103–118.
Godo, T., in press, The Appomattox Field Norphlet eolian sand dune reservoirs in the deep water Gulf of Mexico, *in* R. Merrill and C. Sternbach, eds., Giant oil fields of the decade 2000–2010: AAPG Memoir 113, doi:10.1306/13572000M1133680.
Godo, T. J., E. Chuparova, and D. E. McKinney, 2011, Norphlet eolian sand fairway established in the deep water Gulf of Mexico (abs.): AAPG Annual Convention and Exhibition, Houston, Texas, April 10–13, 2011, accessed October 26, 2016, http://www.searchanddiscovery.com/abstracts/html/2011/annual/abstracts/Godo.html.
Hood, K. C., L. M. Wenger, O. P. Gross, and S. C. Harrison, 2002, Hydrocarbon systems analysis of the northern Gulf of Mexico: Delineation of hydrocarbon migration pathways using seeps and seismic imaging, *in* D. Schumacher and L. A. LeSchack, eds., Application of geochemistry, magnetics and remoter sensing: AAPG Studies in Geology 48, p. 25–40.
Horn, B., 2011, Identifying new exploration fairways in the Gulf of Mexico: Deepwater Tuscaloosa/Woodbine play: Gulf Coast Association of Geological Societies Transactions, v. 61, p. 245–256.
Hudec, M. R., M. P. A. Jackson, and F. J. Peel, 2013, Influence of deep Louann structure on the evolution of the northern Gulf of Mexico: AAPG Bulletin, v. 97, no. 10, p. 1711–1735, doi:10.1306/04011312074.
Jacques, J. M., and H. Clegg, 2002, Late Jurassic source rock distribution and quality in the Gulf of Mexico: Inferences from plate tectonic modeling: Gulf Coast Association of Geological Societies Transactions, v. 52, p. 429–440.
Kane, I. A., and A. S. M. Ponton, 2012, Submarine and transitional flow deposits in the Paleogene Gulf of Mexico: Geology, v. 40, p. 1119–1122, doi:10.1130/G33410.1.
Lewis, J., S. Clinch, D. Meyer, M. Richards, C. Skirius, R. Stokes, and L. Zarra, 2007, Exploration and appraisal challenges in the Gulf of Mexico deep-water Wilcox: Part I—Exploration overview, reservoir quality, and seismic imaging, *in* L. Kennan, J. Pindell, and N. C. Rosen, eds., The Paleogene of the Gulf of Mexico and Caribbean Basins: Processes, events, and petroleum systems: Gulf Coast Section SEPM Foundation Bob F. Perkins 27th Annual Research Conference, Houston, Texas, December 2–5, 2007, p. 398–414, doi:10.5724/gcs.07.27.0398.
Magoon, L. B., T. L. Huston, and H. E. Cook, 2001, Pimenta-Tamabra(!)—A giant supercharged petroleum system in the southern Gulf of Mexico, onshore and offshore Mexico, *in* C. Bartolini, R. T. Buffler, and A. Cantu-Chapa, eds., The western Gulf of Mexico basin: Tectonics, sedimentary basins, and petroleum systems: AAPG Memoir 75, p. 83–125.
Mander, J., J. d'Ablaing, J. Howie, K. Wells, R. Ramazanova, D. Shepherd, and C. Lee, 2012, 21st century Atlantis—Incremental knowledge from a staged-approach to development, illustrated by a complex deep-water field, *in* N. Rosen, P. Weimer, S. M. Coutes dos Anjos, S. Henrickson, E. Marques, M. Mayall, R. Fillon, et al., eds., New understanding of the petroleum systems of continental margins of the world: 32nd Annual Gulf Coast Section SEPM Foundation Bob F. Perkins Research Conference, Houston, Texas, December 2–5, 2012, p. 65–95, doi:10.5724/gcs.12.32.0065.
Marchand, A. M. E., G. Apps, W. Li, and J. R. Rozien, 2015, Depositional processes and impact on reservoir quality in

deepwater Paleogene reservoirs, US Gulf of Mexico: AAPG Bulletin, v. 99, no. 9, p. 1635–1648, doi:10.1306/04091514189.

McBride, B. C., M. G. Rowan, and P. Weimer, 1998a, The evolution of allochthonous salt systems, northern Green Canyon and Ewing Bank (offshore Louisiana), northern Gulf of Mexico: AAPG Bulletin, v. 82, no. 5B, p. 1013–1036.

McBride, B. C., P. Weimer, and M. G. Rowan, 1998b, The effect of allochthonous salt on the petroleum systems of northern Green Canyon and Ewing Bank (offshore Louisiana), northern Gulf of Mexico: AAPG Bulletin, v. 82, no. 5B, p. 1083–1121.

Meckel, L. D. III, G. A. Ugueto, D. H. Lynch, B. M. Hewett, E. J. Bocage, C. D. Winker, and B. J. O'Neill, 2002, Genetic stratigraphy, stratigraphic architecture, and reservoir stacking patterns of the upper Miocene–lower Pliocene Greater Mars-Ursa intraslope basins, Mississippi Canyon, Gulf of Mexico, *in* J. M. Armentrout, ed., Sequence stratigraphic models for exploration and production: Gulf Coast Section SEPM Foundation Bob F. Perkins 22nd Annual Research Conference, Houston, Texas, December 8–11, 2002, p. 113–147, doi:10.5724/gcs.02.22.0113.

Mitra, S., J. A. Duran Gonzalez, J. G. Hernandez, S. H. Garcia, and S. Banerjeee, 2006, Structural geometry and evolution of the Ku, Zaap, and Maloob structures, Campeche Bay, Mexico: AAPG Bulletin, v. 90, no. 10, p. 1565–1584, doi:10.1306/04240605101.

Moore, M. G., G. M. Apps, and F. J. Peel, 2001, The petroleum systems of the western Atwater Foldbelt in the ultra deep water Gulf of Mexico, *in* R. H. Fillon, N. C. Rosen, P. Weimer, A. Lowrie, H. W. Pettingill, R. L. Phair, H. H. Roberts, and B. van Hoorn, eds., Petroleum systems of deep-water basins: Global and Gulf of Mexico experience: Gulf Coast Section SEPM Foundation 21st Annual Bob F. Perkins Research Conference, Houston, Texas, December 2–5, 2001, p. 369–380, doi:10.5724/gcs.01.21.0369.

Morris, P. L., and P. Weimer, 2004a, Structural geology of the Mississippi Fan Foldbelt, northern deep-water Gulf of Mexico, Part 1: Geometry and restorations: Gulf Coast Association of Geological Societies Transactions, v. 54, p. 461–481.

Morris, P. L., and P. Weimer, 2004b, Structural geology of the Mississippi Fan Foldbelt, northern deep-water Gulf of Mexico, Part 2: Growth history and evolution: Gulf Coast Association of Geological Societies Transactions, v. 54, p. 483–501.

Mount, V., K. Dull, and S. Mentemeier, 2007, Structural style and evolution in the Paleogene play, deepwater Gulf of Mexico, *in* L. Kennan, J. Pindell, and N. C. Rosen, eds., The Paleogene of the Gulf of Mexico and Caribbean Basins: Processes, events, and petroleum systems: Gulf Coast Section SEPM Foundation Bob F. Perkins 27th Annual Research Conference, Houston, Texas, December 2–5, 2007, p. 54–80, doi:10.5724/gcs.07.27.0054.

Mount, V. S., A. Rodriguez, A. Chauoche, S. G. Crews, P. Gamwell, and P. Montoya, 2006, Petroleum system observations and interpretation in the vicinity of the K2/K2North, Genghis Khan, and Marco Polo fields, Green Canyon, Gulf of Mexico: Gulf Coast Association of Geological Societies Transactions, v. 56, p. 613–625.

Offshore Technology, 2015, Cascade and Chinook subsea development, Gulf of Mexico, United States of America, accessed October 26, 2016, http://www.offshore-technology.com/projects/cascadechinook/.

Pilcher, R. S., B. Kilsdonk, and J. Trude, 2011, Primary basins and their boundaries in the deep-water Gulf of Mexico: Origin, trap type, and petroleum system implications: AAPG Bulletin, v. 95, no. 2, p. 219–240, doi:10.1306/06301010004.

Pilcher, R. S., R. T. Murphy, and J. M. Ciosek, 2014, Jurassic raft tectonics in the northeastern Gulf of Mexico: Interpretation, v. 2, p. SM39–SM55.

Post, P., P. F. Harrison, G. H. Whittle, and J. D. Hunt, 2001, Mesozoic ultra-deep water potential of the U.S. Gulf of Mexico—Conceptual play development and analysis, *in* R. H. Fillon, N. C. Rosen, P. Weimer, A. Lowrie, H. W. Pettingill, R. L. Phair, H. H. Roberts, and B. van Hoorn, eds., Petroleum systems of deep-water basins: Global and Gulf of Mexico experience: Gulf Coast Section SEPM Foundation 21st Annual Bob F. Perkins Research Conference, Houston, Texas, December 2–5, 2001, p. 35–68, doi:10.5724/gcs.01.21.0035.

Radovich, B. J., C. D. Connors, and J. Moon, 2007, Deep imaging of the Paleogene, Miocene structure and stratigraphy of the western Gulf of Mexico using 2D prestack depth migration of mega-regional onshore to deep water, long-offset seismic data, *in* L. Kennan, J. Pindell, and N. C. Rosen, eds., The Paleogene of the Gulf of Mexico and Caribbean Basins: Processes, events, and petroleum systems: Gulf Coast Section SEPM Foundation Bob F. Perkins 27th Annual Research Conference, Houston, Texas, December 2–5, 2007, p. 307–322, doi:10.5724/gcs.07.27.0307.

Ricoy, V., 2005, 3D seismic characterization of the Cantarell Field, Campeche Basin, Mexico, Ph.D. dissertation, Cardiff University, Cardiff, United Kingdom, 418 p.

Rojas, P., 2015, The road to Shell's Appomattox discovery (abs.): Gulf Coast Association of Geological Societies and Gulf Coast Section of SEPM 65th Annual Convention, Houston, Texas, September 20–22, 2015, accessed October 26, 2016, http://www.searchanddiscovery.com/abstracts/html/2015/90219gcags/abstracts/139.html.

Sanford, J. C., 2015, The Cretaceous-Paleogene boundary deposit in the Gulf of Mexico: Oceanic response to the Chicxulub impact, master's thesis, The University of Texas at Austin, Austin, Texas, 130 p.

Scott, E., R. Denne, J. Kaiser, and D. Eickhoff, 2012, Immediate and postevent effects of the K/Pg boundary, Chicxulub impact on the northern Gulf of Mexico, *in* N. Rosen, P. Weimer, S. M. Coutes dos Anjos, S. Henrickson, E. Marques, M. Mayall and R. Fillon, et al., eds., New understanding of the petroleum systems of continental margins of the world: 32nd Annual Gulf Coast Section SEPM Foundation Bob F. Perkins

Research Conference, Houston, Texas, December 2–5, 2012, p. 96–109, doi:10.5724/gcs.12.32.0096.

Scott, E., R. Denne, J. Kaiser, and D. Eickhoff, 2014, Impact on sedimentation into the north-central deepwater Gulf of Mexico as a result of the Chicxulub event: Gulf Coast Association of Geological Societies Journal, v. 3, p. 41–50.

Story, C., 1998, Norphlet geology and 3-D geophysics of Fairway Field Mobile Bay, Alabama, *in* J. L. Allen, T. S. Brown, C. J. John, and C. F. Lobo, eds., 3-D seismic case histories from the Gulf Coast Basin: Gulf Coast Association of Geological Societies Special Publication, p. 123–129.

Stover, S. C., S. Ge, P. Weimer, and B. C. McBride, 2001, The effects of salt evolution, structural development, and fault propagation on Cenozoic oil migration: A two-dimensional fluid flow study along a mega-regional transect in the northern Gulf of Mexico: AAPG Bulletin, v. 85, no. 11, p. 1945–1966.

Sullivan, M., J. Clark, B. Power, T. Dunn, A. Fildani, J. Couvault, L. Zarra, and B. Carson, 2014, Relationship between reservoir quality, facies, and depositional environment: Working towards predictive model for the deepwater Wilcox (abs.): AAPG Annual Convention and Exhibition, Houston, Texas, April 6–9, 2014, accessed October 26, 2016, http://www.searchanddiscovery.com/abstracts/html/2014/90189ace/abstracts/1837768.html.

Taylor, T. R., M. R. Giles, L. A. Haton, T. N. Diggs, N. R. Braunsdorf, G. V. Birbiglia, M. Kittridge, C. I. Macaulay, and I. S. Espejo, 2010, Sandstone diagenesis and reservoir quality prediction: Models, myth, and reality: AAPG Bulletin, v. 94, no. 8, p. 1093–1132, doi:10.1306/04211009123.

Teerman, S. C., R. W. Howe, R. Hwang, and R. Lytton, 2010, A deepwater Gulf of Mexico source rock penetration: Applications to Mesozoic source rocks an depositional systems (abs.): AAPG Annual Convention and Exhibition, New Orleans, Louisiana, April 11–14, 2010, accessed October 26, 2016, http://www.searchanddiscovery.com/pdfz/abstracts/pdf/2010/annual/abstracts/ndx_teerman.pdf.html.

Trudgill, B. D., M. G. Rowan, J. C. Fiduk, P. Weimer, P. E. Gale, B. E. Korn, R. L. Phair et al., 1999, The Perdido Foldbelt: Northwestern deep-water Gulf of Mexico: Part 1: Structural geology, evolution, and regional implications: AAPG Bulletin, v. 83, no. 1, p. 88–113.

Walker, C., P. Belvedere, J. Petersen, S. Warrior, and A. Cunningham, 2012, Straining at the leash: Understanding the full potential of the deep water, sub-salt Mad Dog field from appraisal through early production, *in* N. Rosen, P. Weimer, S. M. Coutes dos Anjos, S. Henrickson, E. Marques, M. Mayall and R. Fillon, et al., eds., New understanding of the petroleum systems of continental margins of the world: 32nd Annual Gulf Coast Section SEPM Foundation Bob F. Perkins Research Conference, Houston, Texas, December 2–5, 2012, p. 25–64, doi:10.5724/gcs.12.32.0025.

Weimer, P., R. Bouroullec, T. G. Lapinski, A. A. van den Berg, R. Cepeda, J. G. Roesink, and M. Leibovitz, 2017a, Sequence stratigraphic evolution of the Mensa and Thunder Horse intraslope basins, northern deep-water Gulf of Mexico—Lower Cretaceous through upper Miocene (8.2 Ma): A case study: AAPG Bulletin, v. 101, no. 7, p. 1109–1143, doi:10.1306/09011608160.

Weimer, P., R. Bouroullec, and G. Tari, 2006, Petroleum traps in deepwater settings, *in* P. Weimer, R. Slatt, R. Bouroullec, R. Fillon, H. Pettingill, M. Pranter, and G. Tari, eds., Introduction to the petroleum geology of deepwater settings: AAPG Studies in Geology 57, p. 15-1–15-90.

Weimer, P., R. Bouroullec, A. A. van den Berg, T. G. Lapinski, J. G. Roesink, and J. Adson, 2017b, Structural setting and evolution of the Mensa and Thunder Horse intraslope basins, northern deep-water Gulf of Mexico: A case study: AAPG Bulletin, v. 101, no. 7, p. 1145–1172, doi:10.1306/09011609112.

Weimer, P., R. Denne, E. Zimmerman, S. Cumella, W. Gutterman, T. Payeur, B. Snyder, H. Hirsh, and D. Bettinger, 2016a, Variations in borehole log expression of the KPg boundary Chicxulub deposit, northern deep-water Gulf of Mexico: Preliminary results: Gulf Coast Association of Geological Societies Transactions, v. 66, p. 583–600.

Weimer, P., R. Denne, E. Zimmerman, S. Cumella, B. Snyder, H. Hirsh, D. Bettinger, W. Gutterman, and T. Payeur, 2016b, Litho- and biostratigraphic evolution of the Upper Jurassic through top Cretaceous section, northern deep-water Gulf of Mexico: Preliminary results: Gulf Coast Association of Geological Societies Transactions, v. 66, p. 569–582.

Weimer, P., V. Matt, R. Bouroullec, A. A. van den Berg, T. G. Lapinski, J. G. Roesink, and J. Adson, 2017c, Three-dimensional petroleum systems modeling of the Mensa and Thunder Horse intraslope basins, northern deep-water Gulf of Mexico: A case study: AAPG Bulletin, v. 101, no. 7, p. 1173–1201, doi:10.1306/09011608153.

Weimer, P., and H. W. Pettingill, 2007, Deep-water exploration and production: A global overview, *in* T. Nilsen, R. D. Shew, G. S. Steffens, and J. Studlick, eds., Atlas of deep-water outcrops of the world: AAPG Studies in Geology 56, 29 p.

Weimer, P., E. Zimmerman, H. Hersh, B. Snyder, M. Leibovitz, K. Schwendeman, B. Hankins et al., 2017d, Atlas of fields and discoveries, central Mississippi Canyon, Atwater Valley, northwestern Lloyd Ridge, and western DeSoto Canyon protraction areas, northern deep-water Gulf of Mexico: AAPG Bulletin, v. 101, no. 7, p. 995–1002, doi:10.1306/bltnfieldatlas070815.

Wenger, L. M., L. R. Goodoff, O. P. Gross, S. C. Harrison, and K. C. Hood, 1994, Northern Gulf of Mexico: An integrated approach to source, maturation, and migration, *in* N. Scheidermann, P. Cruz, and R. Sanchez, eds., Geologic aspects of petroleum systems: First Joint AAPG/Asociación Mexicana de Geólogos Petroleros Hedberg Research Conference, Mexico City, Mexico, October 2–6, 1994, 5 p.

Worrall, D. M., M. W. Bourque, and D. R. Steele, 2001, Exploration in deep water basins…where next? *in* R. H. Fillon, N. C. Rosen, P. Weimer, A. Lowrie, H. W. Pettingill, R. L. Phair, H. H. Roberts, and B. van Hoorn, eds., Petroleum systems of deep-water basins: Global and Gulf of Mexico experience: Gulf Coast Section SEPM Foundation Bob F. Perkins 21st Annual Research Conference, Houston, Texas, December 2–5, 2001, p. 273, doi:10.5724/gcs.01.21.0273.

Yen, T., 2016, Oil production in federal Gulf of Mexico projected to reach record high in 2017, accessed October 25, 2016, http://www.eia.gov/todayinenergy/detail.php?id=25012.

Zarra, L., 2007a, Chronostratigraphic framework for the Wilcox Formation (upper Paleocene–lower Eocene) in the deep-water Gulf of Mexico: Biostratigraphy, sequences, and depositional systems, *in* L. Kennan, J. Pindell, and N. C. Rosen, eds., The Paleogene of the Gulf of Mexico and Caribbean Basins: Processes, events, and petroleum systems: Gulf Coast Section SEPM Foundation Bob F. Perkins 27th Annual Research Conference, Houston, Texas, December 2–5, 2007, p. 81–141, doi:10.5724/gcs.07.27.0081.

Zarra, L., 2007b, Oligocene stratigraphy and depositional systems on the deepwater Gulf of Mexico (abs.): AAPG Annual Convention and Exhibition, Long Beach, California, April 1–4, 2007, accessed October 26, 2016, http://www.searchanddiscovery.com/abstracts/html/2007/annual/abstracts/lbZarra.htm.